BODY MONITORING USING GARMENT-FRIENDLY WEARABLE SENSORS

A Dissertation

Presented to the Faculty of the Graduate School

of Cornell University

In Partial Fulfillment of the Requirements for the Degree of

Doctor of Philosophy

by

Jeyeon Jo

August 2023

BODY MONITORING USING GARMENT-FRIENDLY WEARABLE SENSORS

Jeyeon Jo, Ph. D.

Cornell University 2023

Smart garments have evolved beyond their traditional functions to serve as wearable digital interfaces. The core of these garments lies in the ability to sense changes in the wearer's body and provide relevant feedback, taking advantage of their close and extensive contact with the human body surface. These garment-friendly sensors aim to support healthcare, entertainment, and lifestyle needs. However, current smart garments still face limitations such as the presence of rigid electronic components, susceptibility to moisture, lack of breathability, and rigid electric insulation or connections prone to deformations. These limitations can hinder wearability, durability, convenience in maintenance, system stability, and safety of the wearable interfaces.

To address these limitations, this dissertation highlights three wearable sensor applications utilizing stretchable fiber optics and passive RFID (radiofrequency identification) tags. A respiration sensor used a stretchable fiber optic enclosed by machine embroidery. This sensor tracked changes in thoracic and abdominal circumferences accompanied by breathing behaviors. The machine embroidery secured the optical fiber onto the textile, allowing transition in shapes while providing protection against abrasions. The sensor demonstrated satisfactory results in human tests and maintained sensitivity after multiple machine washes. Another wearable

device discussed is a stretchable fiber optic-based insole that monitors plantar pressure. The insole contained a two-dimensional array of soft fibers embedded in a flexible foam. When compressed by the foot, the fibers deformed, leading to decreased light transmittance. Human participant tests showed that the fiber optic insole, coupled with a neural network model, satisfactorily predicted the gait parameters. Furthermore, the system exhibited potential for providing real-time feedback on abnormal gait patterns, such as toe walking in children with autism spectrum disorder (ASD). Lastly, the dissertation introduces the use of passive RFID tag pairs attached to eyeglasses, enabling battery-free head orientation sensing. The signal strength from each tag became different when the person rotated the head in yaw. The system not only correlated well with head movements but also showed potential for measuring rotations in all three axes, which can be utilized in human-computer interactions, including virtual/augmented reality applications for children.

BIOGRAPHICAL SKETCH

Jeyeon Jo was born in 1990 and raised in Seoul, South Korea. From 2008 to 2017, he attended Seoul National University, where he received his B.S. and M.S. degrees in Textiles, Merchandising, and Fashion Design, with a concentration in fashion design. He also served two years of military service in the Republic of Korea Air Force from 2011 to 2013. His master's thesis focused on the clothing acculturation of North Korean female defectors in South Korea, supervised by Professor Jisoo Ha. In 2017, he relocated to Mongolia International University in Ulaanbaatar, Mongolia, where he taught fashion design courses for two years. Jeyeon began pursuing a doctoral degree at Cornell University in Ithaca, New York, under the guidance of Professor Heeju T. Park. His research revolved around functional apparel design, utilizing emerging technologies such as soft wearable sensors and 3D body scanning. His academic achievements at Cornell were recognized through fellowships, including the Roberta G. 1957 and the John B. 1956 De Vries Graduate Student Award, as well as the Human Service Studies Graduate Fellowship. He expresses his gratitude for his time at Cornell, which provided him with valuable opportunities to learn, gain experience, and explore inspiring research topics in wearable solutions.

To my family

ACKNOWLEDGMENTS

I thank God for always guiding me to places I never expected and didn't deserve, for His name's sake. I thank Him for being my rock, my shield, and my stronghold.

I thank my family for making me smile. I deeply thank my wife Nalea for her endless love and support. I express my love to you – my best friend, my other half. I thank my daughters, Daniella and Cayla, for coming into our lives as a gift and making this time so much more special.

I express my sincere gratitude to my advisor, Professor Heeju Park, for inviting me to Cornell and providing countless knowledge, wisdom, encouragement, and support. I will strive to follow your path as an educator, researcher, advisor, and father.

I greatly appreciate my committee members, Professor Robert Shepherd, Professor Edwin Kan, and Professor Tamer Uyar, for sharing sparkling research ideas and offering valuable guidance with great patience. It was the dream team I had never expected to have in my life.

I thank all the members of the Performance Apparel Design Lab for being wonderful, reliable, and trustworthy colleagues. I hope our story continues wherever we may be.

I thank the professors and colleagues across the campus for their encouragement and support. Additionally, I greatly appreciate the members of the Korean Church at Cornell for their overflowing love for my family.

Lastly, I would like to thank the parents on both sides of the family for their unwavering support, love, and prayers. Thank you for being pillars and shelters we can rely on in times of trouble and happiness. I could have never completed this without any of you.

TABLE OF CONTENTS

LIST OF FIGURES

LIST OF TABLES

CHAPTER 1

INTRODUCTION

Smart garment refers to clothing and accessories with responsive capabilities enabled through embedded electronic, to provide additional functionalities beyond the traditional roles of outfit [1]. Also widely known as wearable technologies, this advanced form of garment systems often contains sensors, actuators, power sources, and microcontroller modules [2]. The upsurge of smart garments has been not only revolutionizing the runway scene, but also creating new and innovative product categories through the body-conformal or miniature sensors integrated into clothing to collect biometric or motion signals, or actuators generating localized sensual feedback on the target body location [3,4].

While smart garments and the ideas of integrating technologies into daily outfits have gained a significant popularity in recent years, the concept of wearing electronics appeared in the late 19th century. The increasing interest in electricity invented 'electric corset', with the belief that the electric shock can help people to regain strength and virility [5]. The modern version of smart garment emerged with the 'WearComp' series and the 'shoe computer' used for gambling in 1970s [6,7]. In the 1990s, prominent Industry players in electronics and fashion such as Philips, Levi's and Nike introduced commercial soft goods products such as outdoor jackets with embedded MP3 players, speakers, and even mobile phones [8]. Though they were not successful in terms of sales at that time, they projected the future of wearables actualized in the 2010s by iconic project such as Project Jacquard of Google and Levi's and smart shirt of Hexoskin, in accordance with the advances in smartphone ecosystem and machine learning [9]. Companies such as Sensoria and Ralph Lauren also introduced sensor-embedded shirts and socks, providing insights regarding the

physical performances including heart rate, gait pattern, and fatigue levels [10]. The state-of-the-art of the field is exploring the shape change materials to assist the musculoskeletal or physiological needs, wireless energy transfer or energy harvesting to remove the batteries, and advanced conformal sensors in accordance with machine learning techniques to offer users more accurate and meaningful insights [11–14].

Key market segments in the current smart garment industry include but are not limited to healthcare, entertainment, and lifestyle [15]. Smart clothing accelerates the telemedicine industry through the daily health tracking capabilities. Biometric sensors embedded in clothing can monitor vital signs and daily activities to send real-time feedback to the medical professionals and caregivers, especially when any anomalies are detected [16,17]. Biometric information is not only beneficial to those under medical attention but also healthy population with interest to improve and optimize the athletic techniques and prevent injuries. Those working in harsh environments like military personnel are actively adopting smart gear systems, to enhance safety and performance by integrating their vital signs and field information and providing exoskeletal assistance [18]. The entertainment and gaming industry utilizes the smart clothing system as a platform to collect inputs and generate haptic feedback in varied human-computer interaction scenarios, which can be maximized within virtual or augmented reality [19]. Lastly, the fashion and lifestyle sectors are increasingly incorporating electronics into soft goods to create interactive, personalized, and aesthetically appealing experiences [20,21].

Integrating electronic components while ensuring wearability and comfort poses a significant challenge in the development of smart clothing systems. The human body moves in numerous ways, and the skin is sensitive to external discomforts, while most electronics are rigid [22]. Furthermore, sensors that collect bio-signals or actuators generating tactile feedback often need to maintain a stable contact with the skin, which

is often not favorable in terms of user comfort [23]. Durability is also a concern as garments experience numerous impacts, including pressure, friction, stretching, and machine washing, which can affect the embedded electronics [24]. Managing power sources is another important issue, because large batteries can be cumbersome, and the performance of energy harvesting is often inconsistent. Creating stable electric connections on textiles in mass manufacturing environments is challenging, and the increasing volume of personal data collection raises concerns about privacy and security [25].

The current dissertation, with a focus on on-body sensors, aims to discuss the areas to improve in smart garment applications and introduce three different wearable sensors as attempts to overcome some of the existing challenges. Chapter 2 opens the discussion with a brief overview of the present and future of textile-based wearable sensors. The following chapters from 3 through 5 introduce wearable sensor applications using stretchable fiber optic and passive RFID (radiofrequency identification) tag as key technologies to break through the existing obstacles. Chapter 3 presents a wearable strain sensor monitoring respiratory patterns through stretchable fiber optics enclosed by machine embroidery. It featured its compatibility with elastic textiles as well as durability against machine washing. Another stretchable fiber optic application is introduced in Chapter 4, which is a plantar pressure sensor utilizing the soft and flexible nature of the optical fibers. In Chapter 5, passive RFID tag-embedded eyewear displayed a head-orientation monitoring capability. This battery-free device can create immersive experiences in human-computer interaction settings, but primarily aims to alternatively track gaze orientation to diagnose lateral glance of children with a developmental disorder. The last chapter wraps up the introduced discussions and attempts to shed light on the further development of better smart clothing solutions.

REFERENCES

[1] V. Sanchez, C. J. Walsh, R. J. Wood, Advanced Functional Materials 2021, 31, 2008278.

[2] S. Mann, Commun. ACM 1996, 39, 23.

[3] L. M. Castano, A. B. Flatau, Smart Materials and structures 2014, 23, 053001.

[4] J. Shi, S. Liu, L. Zhang, B. Yang, L. Shu, Y. Yang, M. Ren, Y. Wang, J. Chen, W. Chen, Y. Chai, X. Tao, Adv. Mater. 2020, 32, 1901958.

[5] D. Stillings, N. Roth, IEEE Spectrum 1978, 15, 56.

[6] S. Mann, Proceedings of the IEEE 1998, 86, 2123.

[7] E. O. Thorp, in Digest of Papers. Second International Symposium on Wearable Computers (Cat. No.98EX215), IEEE Comput. Soc, Pittsburgh, PA, USA, 1998, pp. 4–8.

[8] S. Marzano, Design Management Review 2005, 16, 23.

[9] M. R. Ebling, IEEE Pervasive Computing 2016, 15, 2.

[10] A. K. Yetisen, H. Qu, A. Manbachi, H. Butt, M. R. Dokmeci, J. P. Hinestroza, M. Skorobogatiy, A. Khademhosseini, S. H. Yun, ACS Nano 2016, 10, 3042.

[11] R. Granberry, K. Eschen, B. Holschuh, J. Abel, Advanced materials technologies 2019, 4, 1900548.

[12] H. D. Yang, M. Cooper, A. Eckert-Erdheim, D. Orzel, C. J. Walsh, IEEE Robotics and Automation Letters 2022, 7, 7439.

[13] Y. Su, T. Yang, X. Zhao, Z. Cai, G. Chen, M. Yao, K. Chen, M. Bick, J. Wang, S. Li, G. Xie, H. Tai, X. Du, Y. Jiang, J. Chen, Nano Energy 2020, 74, 104941.

[14] A. K. Yetisen, J. L. Martinez-Hurtado, B. Ünal, A. Khademhosseini, H. Butt, Advanced Materials 2018, 30, 1706910.

[15] S. Seyedin, P. Zhang, M. Naebe, S. Qin, J. Chen, X. Wang, J. M. Razal, Mater. Horiz. 2019, 6, 219.

[16] A. Hatamie, S. Angizi, S. Kumar, C. M. Pandey, A. Simchi, M. Willander, B. D. Malhotra, J. Electrochem. Soc. 2020, 167, 037546.

[17] S. Chen, J. Qi, S. Fan, Z. Qiao, J. C. Yeo, C. T. Lim, Adv. Healthcare Mater. 2021, 10, 2100116.

[18] N. A. Choudhry, L. Arnold, A. Rasheed, I. A. Khan, L. Wang, Advanced Engineering Materials 2021, 23, 2100469.
[19] H. Bai, S. Li, R. F. Shepherd, Adv. Funct. Mater. 2021, 31, 2009364.
[20] K. Vega, H. Fuks, Computer 2014, 47, 71.
[21] B. Tian, Y. Fang, J. Liang, K. Zheng, P. Guo, X. Zhang, Y. Wu, Q. Liu, Z. Huang, C. Cao, W. Wu, Small 2022, 18, 2107298.
[22] S. de Mulatier, M. Nasreldin, R. Delattre, M. Ramuz, T. Djenizian, Advanced Materials Technologies 2018, 3, 1700320.
[23] N. Gandhi, C. Khe, D. Chung, Y. M. Chi, G. Cauwenberghs, in 2011 International Conference on Body Sensor Networks, 2011, pp. 107–112.
[24] R. Cao, X. Pu, X. Du, W. Yang, J. Wang, H. Guo, S. Zhao, Z. Yuan, C. Zhang, C. Li, Z. L. Wang, ACS Nano 2018, 12, 5190.
[25] J. Wei, IEEE Consumer Electronics Magazine 2014, 3, 53.

CHAPTER 2

TEXTILE INTERFACE FOR WEARABLE SENSORS

2.1 Introduction

As ubiquitous computing and data-driven decision-making become part of the daily routine in modern society, the primary utility of clothing has evolved from mere necessity to wearable digital interfaces used to communicate with the world. Such hybrid garments, known as "smart clothing," are part of the fastest-growing sectors in the apparel and textile industries. The global smart clothing market is expected to grow into a $2.95-billion market by 2026 with a 14.84% annual growth rate [1]. Key applications include protective clothing for first responders, wearable healthcare products, active sportswear, and fashion products for the general public.

Smart clothing serves the wearer, collects input from the body and/or the surrounding environments and provides feedback. Consequently, one of the most critical components is reliable sensors that becomes compatible with soft materials covering the human body in motion. Textiles, the most widely used interface for the human body, are ideal for use with sensors, more so than other materials. This is especially true as they consider consumers' comfort and convenience as well as production efficiency in the existing garment manufacturing system. Although fibers, yarns, and textiles have become intelligent by equipping sensing capabilities through materials like conductive fiber, conventional textile structures also play a key role in assisting with and accommodating wearable sensors.

This entry offers an in-depth discussions on existing and emerging textile-friendly wearable sensors and fabrication techniques towards their seamless integration. The entry also covers the challenges and limitations of current soft circuits related to conductivity, stretchability, flexibility, chemical and mechanical stability, safety, and

compatibility with the conventional cut-and-sew garment construction process. The project to be discussed helps the reader understand future directions for the enhanced adoption of textile-friendly wearable sensors on the human body.

2.2 Fibers, Yarns, and Textiles as Wearable Sensors

Circuits conventionally consist of rigid components to achieve maximal functionality in terms of conductivity, durability, complexity, and reliability. Soft conductive materials are often less functional in the listed features above, but they can serve areas where stiff and inelastic materials cannot perform properly, such as the human body surface. Textile-based wearable sensors are breaking through this tradeoff between electrical performance and mechanical conformity for smart clothing applications. From fiber production to textile finishing, any stage of textile fabrication can involve the use of materials with sensing capabilities. Electrical conductivity is one of the most widely used bases of sensors, which fibers with metals, carbon-based materials, and intrinsically conductive polymers can equip [2]. Figure 2.1a and b show commercially available conductive fibers: stainless-steel staple fibers and a silicone-rubber filament filled with carbon nanotubes, respectively. They can function as sensors or as part of the sensor system as they are, or they can be further processed to become a more durable form, such as yarn or felt. Highly conductive metals for conventional circuits such as copper or silver can form a fiber, but they often display brittleness and stiffness, making them an inadequate textile component. An alternative approach is to apply a conductive coating, which can add sensing capabilities while benefitting from the mechanical properties of the base fiber. Light transmitting optical fiber is able to introduce changes in light properties using inputs from the human body. Elastomer-based stretchable fiber optics are capable of tracking dynamic changes on textiles and body surfaces by overcoming the brittle nature of conventional

fiber optics made of glass (Figure 2.1c).

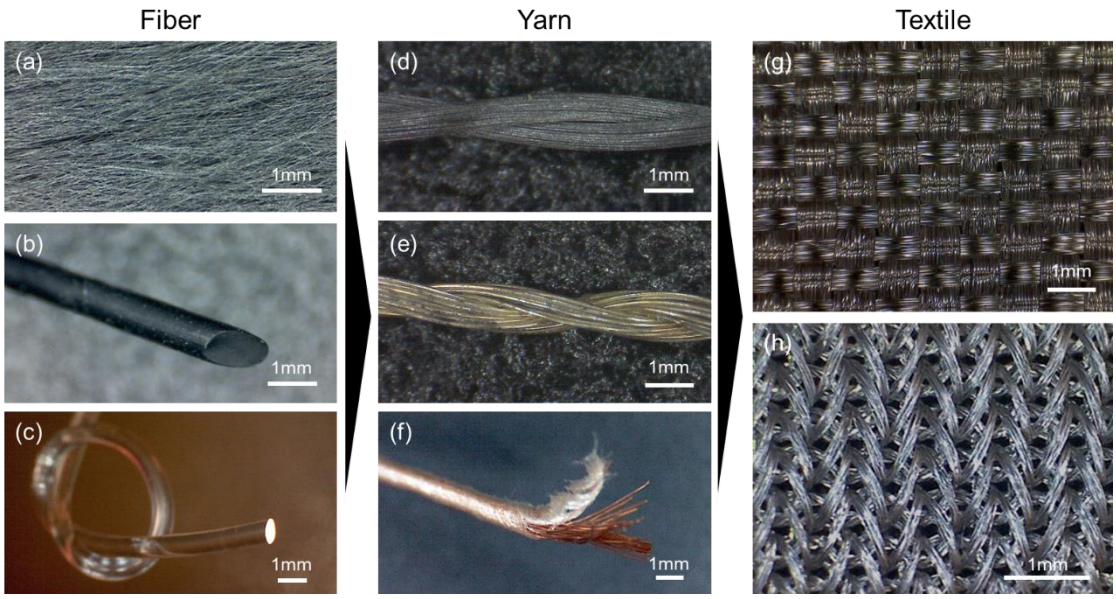

Figure 2.1 Commercially available materials with sensing capabilities. (a) stainless-steel fiber, (b) silicone-rubber cord with carbon nanotubes, (c) extensible optical fiber, (d) stainless-steel yarn, (e) silver-coated nylon thread, (f) copper wires wrapped by natural silk, (g) woven conductive textile), (h) knitted conductive textile.

Spinning converts strands of fibers into a yarn with better mechanical resilience. Figure 2.1d and e show two commercially available conductive yarns made of stainless-steel fibers and silver-coated nylon, respectively. Yarn fabrication often grants additional functionality, such as flexibility, stretchability, and protection that a single fiber lacks. The yarn in Figure 2.1f consists of thin and insulated copper wires as the core, with white natural silk wrapping the core, providing protection against mechanical stress and enhanced tactile sensation. Wrapping multiple fibers with different properties in sequence on a single yarn can create a sensor with a layered structure, such as a triboelectric strain sensing yarn. Conductive yarns or threads are often less soft compared to the yarns/threads normally used for garment construction. Furthermore, in the case of fibers coated by conductive or insulating materials, the thin coating can peel off when passed through a sewing machine to be stitched or when

washed multiple times. One of the common solutions when stitching is using the conductive threads for the bobbin side, not for the machine side, to avoid tensions and abrasions, but adjusting the fine tension in the textile/garment fabrication machines is inevitable for securing the sensor performance.

Once a fiber or a yarn with proper mechanical properties and sensing capabilities is ready, conventional textile fabrication techniques can embed it into textile structures. Weaving and knitting are able to create the most versatile textiles (Figure 2.1g and h), but other structures such as felt, braid, embroidery, and lace can introduce unique functionality to fit the design goal of the sensor. Printing conductive ink on the textile is also a quick and convenient way to fabricate a soft printed circuit on the textile surface, but durability and stability against washings and abrasions have to be examined, as with coated fibers.

2.3 Sensing principles

Mechanical sensors

Mechanical sensors convert mechanical deformations into signal changes. Resistive sensor monitors change the electrical resistance of soft conductive materials. The length and cross-section area determine the resistance of a conductive material, and geometrical changes incurred by external loads such as strain, compression, or bending result in the sensor response. A study showed a resistive strain sensor made of a conductive yarn in various knit structures, where strain decreases the resistance (Figure 2.2a). When a strain was applied to the knitted textiles, the connections between the conductive yarns increased and the overall resistance decreased, while the amount of change depended on the type of the knit structure (Figure 2.2b). Conductive ink printed on a textile often leads to resistance to the strain-sensing capability as stretching the textile generates cracks on the conductive printing, which will increase

the overall resistance. Signal changes in resistive sensors are sometimes not linear and/or have hysteresis issues as resistive sensors rely on the mechanical changes in microstructure, which is hardly controllable. For example, as Figure 2.2b shows, it is almost impossible to control the movement of every fiber/yarn in a knit textile, and the knit stitches might not actively return to their original state after the first few stretches.

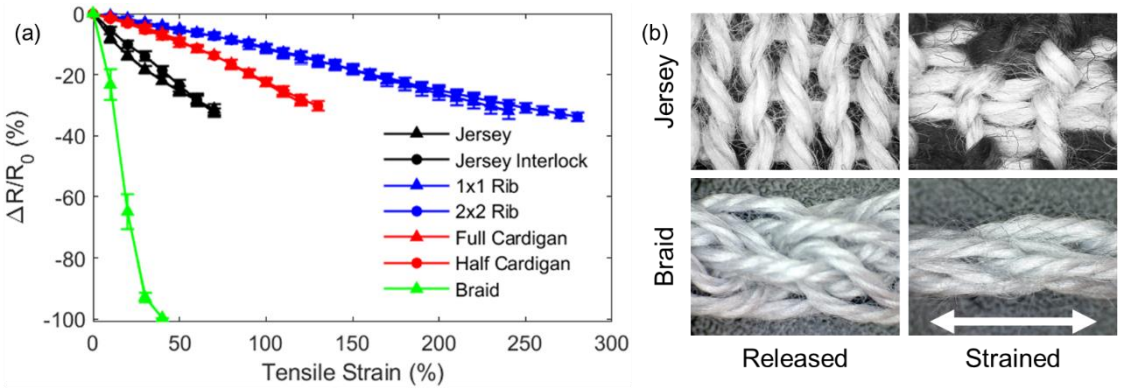

Figure 2.2 Knitted strain sensor. (a) Resistance by strain and knit structure, (b) Contact area by strain.

Capacitive sensors take advantage of the changes in electrical capacitance. Textile-based capacitive sensors often rely on the softness of the same structure as a simple capacitor, where two electrodes are separated by a dielectric layer. The thickness of the dielectric layer (i.e., the distance between the two conductive plates) is responsible for the capacitance changes, so external force such as foot pressure compressing the layers and pushing one plate to the other is a typical measurand of capacitive sensors. Another popular use of the capacitive sensor is touch-input sensing. The human body works as one of the conductive plates, so when the skin touches the insulated surface of a textile-based electrode, it increases the output capacitance. Capacitance touch sensors often require a mere touch without mechanical deformations, yet pressing the dielectric layer can compose another trigger in addition to the simple touches. Whereas resistive and capacitive sensors need a power source, piezoelectric and

triboelectric sensors generate changes in the electric charge. Piezoelectricity utilizes mechanical energy to break the electric balance in a crystalline solid or membrane, such as polyvinylidene fluoride (PVDF), producing a difference in voltage on two conductive plates on each side. On the other hand, triboelectricity involves the exchange of electric charges between two different materials when they come into contact with each other. A piezoelectric sensor is more stable, reliable, and accurate with high-frequency inputs compared to a triboelectric sensor, which is known to be temporary, unpredictable, and relatively easy to fabricate. Both types of sensors can measure various subtle movements throughout the body and harvest electric energy, but piezoelectric sensors concentrate on pressures while triboelectric sensors focus on friction.

Electrical sensors

The human body is a sophisticated system with electrical components generating or conducting biopotentials, whenever it initiates activities in the muscles, brain, and heart [3]. Therefore, textile-based wearable electrical sensors aim to monitor the subtle changes in biosignals non-invasively. Conventional electrodes take advantage of hydrogel to achieve stable skin–electrode contact and low contact impedance, but the wet sensors are uncomfortable, irritating to the skin, less durable, and unstable as the hydrogel dehydrates [4]. Dry sensors have been more common in textile-based electrodes, which use conductive yarns/textiles and/or conductive polymer-based printing on textiles. As dry sensors are susceptible to body movement, textile friction, and skin moisture conditions, high conductivity and low skin contact impedance to minimize noise are key parameters for creating a high-performance textile-based electrode for electrical sensors.

Electromagnetic Sensors

Electromagnetic waves traveling through the tissue carry valuable information on an individual's health status, such as heartbeat and respiratory patterns [5]. Infrared waves generated and emitted by the body are also worth tracking, as the active transmission of electromagnetic waves onto the skin to collect the reflected waves allows in-depth monitoring. The design and fabrication of wearable antennas are key processes for creating a stable and comfortable electromagnetic sensor system. Trade-offs between the stretchability/flexibility and radio efficiency, complex surface curvatures and power absorption of the human body, and potential health hazards have to be carefully considered. Embroidery and stitching of conductive threads, laser-cut conductive textiles, and conductive printing can fabricate the antenna on textiles. A previous study [6] confirmed that the performance of an embroidered radiofrequency identification (RFID) antenna was very similar to a commercial RFID tag.

Passive RFID tags embedded in garment tags have helped with inventory monitoring in the fashion industry. Considering the unique merits of their battery-free operation, lightweight and simple circuit structure, washability, and low cost, RFID tags have promising potential to be developed as wearable sensors. A passive RFID tag harvests electromagnetic waves from the reader to send backscattered signals without any battery. The characteristics of the electromagnetic waves, including the received signal strength indicator (RSSI), phase, and/or doppler, can deliver valuable information about the wearer's body movements (Figure 2.3a) [7] as well as subtle vital signs like heartbeats and breaths of human beings.

Light, electromagnetic waves with optical frequencies are another popular medium conveying biofluid information, as the cells in the blood have a different light absorption spectrum. Light-emitting diodes (LEDs) can directly project lights onto the skin, but optical fibers with flexibility and low light attenuation can deliver light to

optimal regions throughout the body (Figure 2.3b).

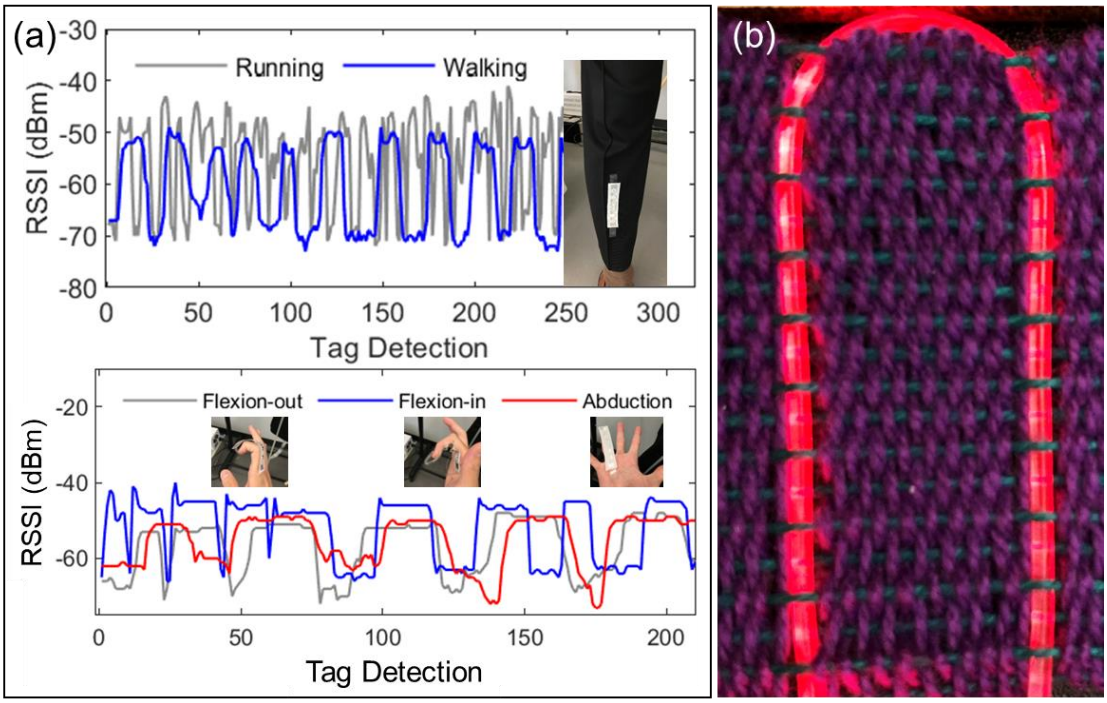

Figure 2.3 Electromagnetic sensors. (a) RSSI change of the passive RFID tags by human body movements, (b) Woven stretchable fiber optic with red visible light.

Chemical Sensors

Wearable chemical sensors contribute to the safety of workers in chemically hazardous environments and health status monitoring for medical diagnoses [8]. Chemical sensors often employ electrochemical approaches. For instance, a probe, such as a screen-printed enzyme, reacts to biofluid, making changes in the current while another electrode stays as a reference. Therefore, it is crucial to develop a sensor with the mechanical resiliency of a textile-based probe against deformations from body movements, frictions, and washings, requiring easy or minimum receptor regeneration, and biocompatibility with the skin [9], along with stable electrical connections.

2.4 Textile Structure Accommodating Wearable Sensors

Wearable sensors need physical accommodations to be worn on the body, particularly when they are not fabricated directly on a textile. Even fiber or yarn-based sensors need to be integrated into another textile, as attaching them directly onto the skin has issues regarding stability and durability. Furthermore, most sensors cannot perform alone; a microcontroller, a power source, and/or relevant circuitry with lots of electric connections are necessary to support the sensor for continuous monitoring. Wiring connects a wearable sensor at the location of interest with other supportive units somewhere on the garment, such as the hem, pocket, or cuff, and requires insulation to prevent potential shorts along with additional protection from external stress. Textiles can assist the whole wearable sensor system as a physical platform where the components reside under protection.

Various textile construction techniques, including weaving, knitting, embroidery, piping, and appliqué, can accommodate the sensors and accompanying units, such as channels, pockets, and internal rooms. Wearable sensors rely on human anatomy in terms of the location, shape, and dimension to maximize the performance, so freedom to decide the shape of the accommodating structure is important. For example, a strain sensor monitoring respiratory patterns may have to be placed on the chest and/or abdomen horizontally to allow for changes in chest circumference. Moreover, textile structures enclosing a mechanical sensor may affect the amount of mechanical deformation, which offers an additional opportunity to optimize the sensing capability during textile fabrication. Embroidering and stitching the sensors and wires directly onto the textile do not restrict the shape or length of the sensor-enclosing structure on a basis textile, but they can provide only limited protection and are not appropriate for a circuit board or battery. Knitting has great potential to create a seamless internal room where a wearable sensor system can be inserted, particularly when double layers

join to form any shape. A pilot study introduced a knitted pocket and channels in which a microcontroller and wirings are integrated (Figure 2.4). The pocket is useful for detachable parts like a microcontroller and battery when protecting them from the laundry, recharging the battery, or updating the software. The channel with rooms can shape a wire or a string-type sensor into a serpentine pattern to achieve stretchability, stability, comfort, and optimal sensitivity.

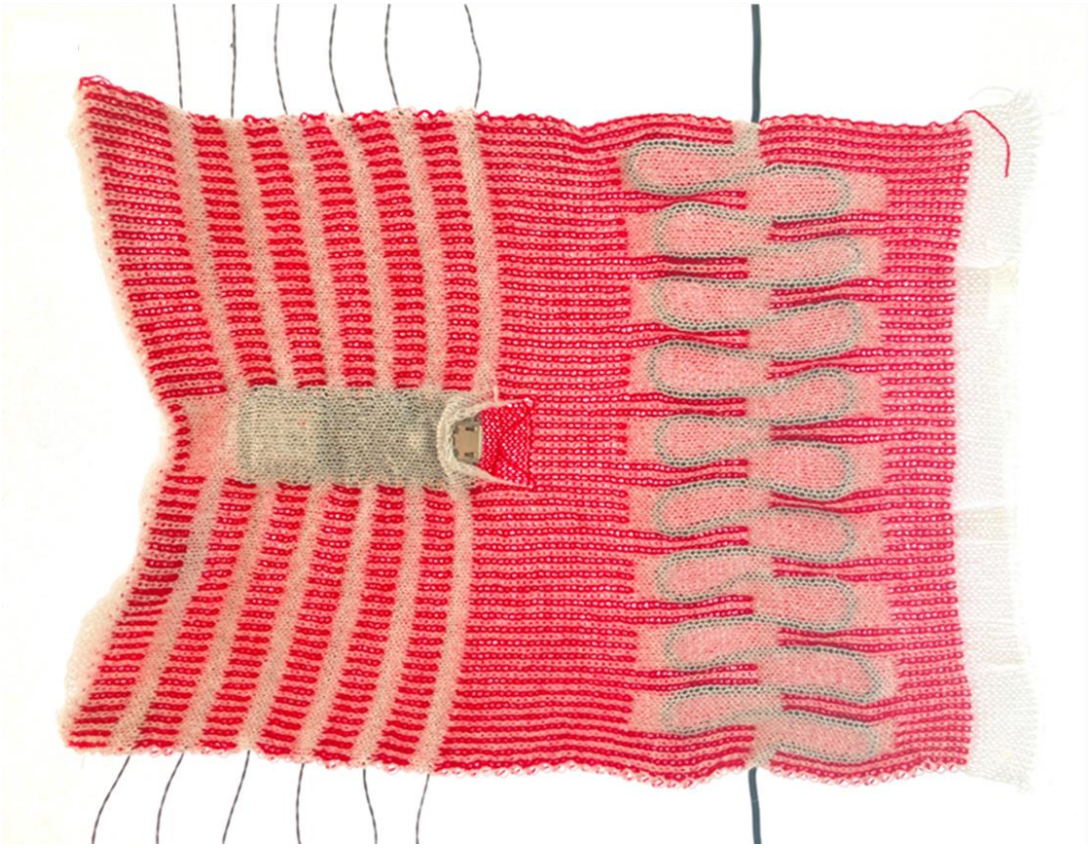

Figure 2.4 Knit structures for wearable sensor systems. a knitted channel and pocket for a microcontroller and electrodes (left) and a knitted channel with rooms for a wire in a serpentine pattern.

2.5 Challenges and Opportunities

Electromagnetic Field and Radiofrequency Radiation

The literature [10] indicates that health and safety concerns related to electromagnetic

fields generated from wearable electronics are one of the perceived risks among consumers. In contrast, the World Health Organization (WHO) states that no substantive relationships have been identified between health issues and low frequency electric fields that the public encounter at the general level. The US National Cancer Institute also confirmed that there is no definitive evidence that electromagnetic fields or radiofrequency radiation generated by consumer electronics causes cancer, including Wi-Fi [11]. Wearable technology devices only need extremely low power levels to operate and, thus, expose the users to very low levels of radiofrequency radiation, according to the Centers for Disease Control and Prevention (CDC) of the US [12]. Table 2.1 reports the electric field, electromagnetic field, and radiofrequency radiation of consumer appliances, microcontrollers, and soft circuit systems including sensors and LEDs measured at their typical distance in use [13] in an ordinary home environment, along with the safety limits (International Commission on Non-Ionizing Radiation Protection [14, 15]. The measured values from home appliances were much lower than the standard, and the microcontroller-based interactive systems, representing wearable sensors, showed even smaller values. A metallic layer between the sensor and the skin can shield the user from hazardous high-frequency electromagnetic fields such as X-rays and the harmless but unwanted radiation from wearable sensors. As the potential negative effect of electromagnetic fields on human health, such as breast cancer, has been sporadically proposed, conducting long-term and thoroughly designed epidemiologic research following fast-evolving wearable technologies remains a challenge.

Table 2.1 Electromagnetic field (EMF), electric field, (EF), and radiofrequency power density (RF) of home appliances and wearable devices at their typical distance of use. Measured continuously for 60 seconds.

	Distance	**EMF**	**EF**	**RF**

	(cm)	(mG)	(V/m)	(mW/m^2)
ICNIRP Standard*	NA	2,000	4,167	10,000
TV	200	0.28	8.09	3.69
Wi-Fi router	200	0.28	1.12	3.65
Microwave	75	8.37	65.64	158.50
Desktop monitor	50	0.30	208.87	7.62
Laptop	30	0.30	2.06	2.55
Refrigerator	30	0.90	0.98	6.48
Hairdryer	10	11.91	134.46	2.79
Electric blanket	0	88.64	99.24	2.51
Smartphone	0	0.31	2.25	36.67
Interactive soft circuit with 10 LEDs	0	0.21	0.86	1.06
Foot pressure monitoring insole	0	0.30	2.65	3.75
Microcontroller	0	0.29	14.44	7.77
Gesture-sensing glove (including a microcontroller and 10 flex sensors)	0	0.30	4.87	8.90

*EF and EMF in 60Hz, RF in 2.4GHz. All for whole-body exposure among the general public.

Moisture and Laundry

Textile-based wearable sensors often expose electrodes and circuit components to sweat from the body, water for washing, and humid air. Exposure to moisture can cause shorts in the circuit, degrading the reliability of the sensor, and decaying metallic materials. Insulating textile sensors is challenging, as microlevel movements of fibers and yarns incapacitate conventional insulation methods like conformal coating, treating only the surface. Textile-friendly approaches to adding a moisture-blocking layer include textile structures made of seam-sealing tapes (Figure 2.5a) or

low-melt yarns, but they limit the elasticity of the base textile and require a carefully engineered process to provide an effective level of waterproofness. Flexible printed circuit board (PCB) is one solution for keeping fully integrated electronic components waterproof, yet its rigid, inextensible, and unbreathable characteristics are not ideal for textile-based systems. Stretchable fiber optic sensors have an advantage over sensors using electrical properties in this sense, because they are chemically and electromagnetically inert while being soft, lightweight, and biocompatible. In the case of microcontrollers and batteries, it is highly recommended to make them detachable, as the water, detergent, heat, and mechanical shocks during laundry can easily damage them. Battery-less systems such as passive RFID tag sensors are free from these issues as they have much more concise structures.

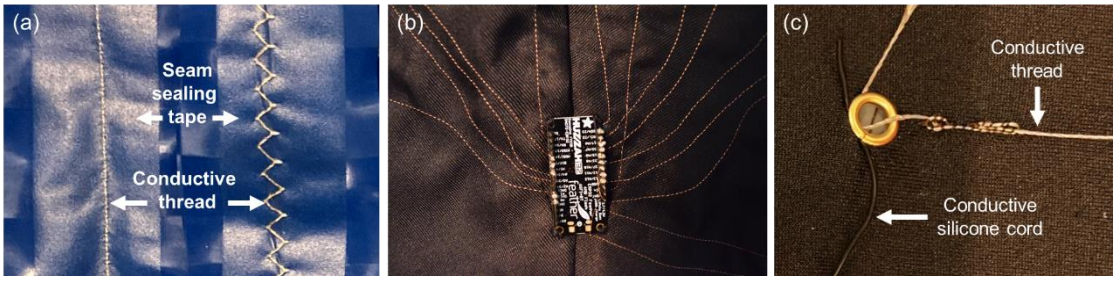

Figure 2.5 Textile-friendly approaches for soft circuits. (a) stitched conductive threads on which seam sealing tape blocks the external moisture, (b) stitched and soldered copper wires, and (c) electric connection using metallic eyelet.

Electric Connection and Heat

Creating stable electric connections is a challenging part of textile-based wearable sensor systems. Most fibers, yarns, and textiles are not suitable for soldering, so their electric connection with hard electric components like microcontrollers often relies on conductive epoxies. However, connections based on conductive epoxies rarely endure more than 25 washes [16]. Thin copper wire (≥36 AWG) stitches (Figure 2.5b) or low-melt solder paste have been explored, but both expose the base textile to high

temperatures for soldering (>700°C, less than 5 seconds) or to reflow the low-melt solder paste (>143°C, 6 minutes) [17]. Alternative solutions include creating mechanical joints using metal eyelets (Figure 2.5c) or metal snap buttons to create a stable connection between conductive yarns and textiles. The additional process of insulating the surface of soft circuits including conductive yarns, textiles, and mechanical connections is necessary to minimize the impacts of moisture on thecircuits. Flexible PCB with magnetic connectors is a relatively stable and mass-manufacturing friendly option, but the rigid materiality of these components compared to textiles has room to improve in design and material choice to make it soft and comfortable on the human body as part of one's clothing.

Another challenge in the use of conductive threads for wiring is their relatively higher resistance in generating heat, compared to conventional electrical wires made of copper. Microcontroller-based wearable sensor systems usually do not involve a voltage higher than 5V or a current greater than 40mA, which does not generate much heat. Yet wearable devices with actuators for light, heat, and movement tend to utilize a high voltage and current, so the use of conductive thread for the entire wiring has to be carefully examined to prevent discomfort and burn injuries. A study showed the temperature change of a commercial stainless-steel conductive thread (0.75Ω/cm) 10 seconds after a range of voltage (0~20 V) was applied without limiting current flow, showing that the high voltage quickly generates heat on the thread (Figure 2.6). The temperature stayed below 50oC when the voltage was within the common range of microcontroller-base systems (0-5V), but it increased rapidly and reached up to 163.1^{o}C at 20V. Humans begin to feel pain at 44^{o}C [18]. An object with a surface temperature around 49^{o}C, touching human skin, can cause thermal blisters within 12 minutes [19]. One-minute skin contact to a surface temperature of 55^{o}C can cause a second-degree burn injury [20]. Therefore, conductive threads used in smart clothing

systems powered by more than 5V, requires 1) safety features in the circuit design to limit current and an increase in temperature of conductive thread, and 2) insulation that covers conductive threads.

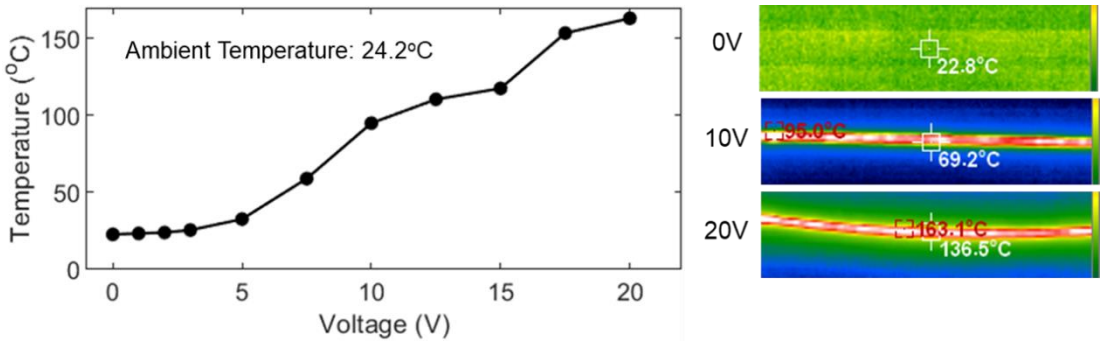

Figure 2.6 Temperature of a stainless-steel thread by voltage, measured at 10 seconds after the voltage is loaded.

REFERENCES

[1] Technavio, “Smart Connected Clothing Market Size to Grow by USD 2.95 Billion| Technology Innovation Leading to Product Premiumization to boost market growth| Technavio,” can be found under https://www.yahoo.com/now/smart-connected-clothing-market-size-100000271.html, n.d.

[2] S. Liu, K. Ma, B. Yang, H. Li, X. Tao, Adv. Funct. Mater. 2021, 31, 2007254.

[3] M. Lin, H. Hu, S. Zhou, S. Xu, Nat Rev Mater 2022, DOI 10.1038/s41578-022-00427-y.

[4] D. Pani, A. Achilli, A. Bonfiglio, Advanced Materials Technologies 2018, 3, 1800008.

[5] P. Sharma, X. Hui, J. Zhou, T. B. Conroy, E. C. Kan, npj Digit. Med. 2020, 3, 98.

[6] P. H. Gordon, R. Chen, H. Park, E. C. Kan, 2017, DOI 10.48550/arXiv.1710.02237.

[7] J. Jo, H. Park, in 2021 International Symposium on Wearable Computers, ACM, Virtual USA, 2021, pp. 141–143.

[8] M. Tessarolo, I. Gualandi, B. Fraboni, Advanced Materials Technologies 2018, 3, 1700310.

[9] A. J. Bandodkar, J. Wang, Trends in Biotechnology 2014, 32, 363.

[10] N. Ju, K.-H. Lee, Fash Text 2020, 7, 21.

[11] NCI, “Electromagnetic Fields and Cancer,” can be found under https://www.cancer.gov/about-cancer/causes-prevention/risk/radiation/electromagnetic-fields-fact-sheet, 2019.

[12] CDC, “Wearable Computers and Wearable Technology,” can be found under https://www.cdc.gov/nceh/radiation/wearable.html, 2015.

[13] T. Behrens, C. Terschüren, W. T. Kaune, W. Hoffmann, J Expo Sci Environ Epidemiol 2004, 14, 144.

[14] International Commission on Non-Ionizing Radiation Protection (ICNIRP), Health Physics 2010, 99, 818.

[15] International Commission on Non-Ionizing Radiation Protection (ICNIRP), Health Physics 2020, 118, 483.

[16] N. Dabby, A. Aleksov, E. Lewallen, S. Oster, R. Fygenson, B. Lathrop, M. Bynum, M. Samady, S. Klein, S. Girouard, in Proceedings of the 2017 ACM International Symposium on Wearable Computers, ACM, Maui Hawaii, 2017, pp. 38–41.

[17] Md. T. I. Molla, S. Goodman, N. Schleif, M. E. Berglund, C. Zacharias, C. Compton, L. E. Dunne, Proceedings of the 2017 ACM International Symposium on Wearable Computers 2017, 18.

[18] A. M. Stoll, L. C. Greene, Journal of Applied Physiology 1959, 14, 373.

[19] C. Williamson, J. R. Scholtz, Journal of Investigative Dermatology 1949, 12, 41.

[20] A. R. Moritz, F. C. Henriques, Am J Pathol 1947, 23, 695.

CHAPTER 3

MACHINE EMBROIDERY ENCLOSURE FOR STRETCHABLE FIBER OPTIC RESPIRATION SENSOR

3.1 Introduction

The respiratory pattern is one of the major indicators of the physiological and emotional status of a person [1,2]. From chronic respiratory diseases and of the severe acute respiratory syndrome (SARS) of the recent pandemic to heart failure, an assessment of the respiratory pattern can contribute to accurate medical prediction, diagnosis, and treatment [3,4]. The respiratory rate, tidal volume, absence/duration of the flow, and flow rate are the most popular parameters used to define a pattern, especially abnormal respirations such as apnea, hyperpnea, and/or Cheyne-Stokes respiration [5]. Because the breathing behavior accompanies movements of the ribcage and organs, real-time respiration tracking is also crucial for accurate medical snapshots such as in magnetic resonance imaging (MRI)[6]. Monitoring respiratory patterns is also of significant interest to those pursuing high performance in physical activities like elite sports because a different breathing pattern can improve exercise performance [7]. In a similar sense, professionals conducting important missions under a physically harsh environment like soldiers, astronauts, firefighters, and divers are looking for new or better methods of integrating a respiration monitoring system into their mission arena [8].

The method used to assess pulmonary function involves the measurement of direct/indirect respiratory parameters such as the airflow, chest wall movement, or intrathoracic volume [9]. Spirometry, which directly quantifies the entering and leaving airflow, requires a nose clip or tightly sealed face mask to ensure accurate measurements without air leakage, which introduces discomfort and limits body

movements. The same limitations can be found in devices for monitoring the parameters relevant to the airflow, such as the air temperature, humidity, and airflow pressure, because these have to be placed very close to where the air enters and exits [10–13]. A strain gauge is a common indirect sensor for respiratory inductive plethysmography (RIP). Sensor-embedded tension bands around the thoracic and abdominal circumferences are used to track subtle expansions of the ribcage following the lung volume [14]. Textile-based pressure sensors and accelerometers can also be used to monitor the forward–backward movement of the chest wall, but they are relatively more susceptible to artifacts caused by body motions and additional garment layers on the sensor [13–16]. Various methods have been developed to use an ECG to monitor the shift of the heart axis, respiratory sinus arrhythmia, or muscle electromyogram activities involved in breathing behaviors [17]. Near-field coherent sensing (NCS) overcame the discomfort from skin contact or the snug fit of most ribcage movement-tracking sensors, but the optimal design and integration of a garment-friendly antenna remain as tasks [18]. Non-contact approaches that use computer vision or radio waves to observe the displacement of the chest provide much better comfort to the patient, but the body part of interest always has to remain visible and a long distance from the device makes it harder to recognize the chest movements [19,20]. Indirect sensors that do not cover the face are less obtrusive and therefore more suitable for continuous monitoring during daily life. Among these, the strain measurement approach can be used in most settings from a static lab session in a hospital to sports and exercise in an unstructured environment [21].

A fiber optic strain gauge is one of the promising on-body strain sensors because of its advantages compared to conventional systems based on electrical properties. These include immunity to electromagnetic interference, no risk of shorting or grounding by moisture, a light weight and thin form factor, multiplexing capabilities, and high

compatibility with textile fabrication/maintenance processes [22–26]. In medical environments, optical fiber-based respiration sensors can contribute to accurate results and the real-time monitoring of a patient's condition during MRI with a high magnetic field and/or computed tomography (CT), which often require the patient to hold their breath for ~15 s to remove respiratory artifacts [27–29]. The thin, soft, and lightweight lightguides can easily become a part of textile structures through weaving, knitting, embroidering, or stitching [24,30]. Their chemical inertness is also advantageous, especially when the fiber is subjected to harsh but still plausible conditions for a garment, such as heavy sweating or repetitive washing [22,31,32]. Although a conventional silica-core lightguide is brittle and has a high modulus, making it unsuitable for on-body applications [27,33–35], polymer-based fiber optics are showing stretchability, sensitivity, and compatibility with soft systems such as textiles [24,26,30,36].

The challenges to designing a wearable fiber optic strain gauge for respiration sensing include i) sufficient sensitivity to monitor subtle ribcage movements, ii) the minimization and distribution of the light source and detector, and iii) the prevention of discomfort from the tightness of the strain gauges. The chest circumference expands by up to 4 cm during normal breathing and 8 cm during deep breathing, which is a strain of only 4.6–9.2 % in terms of the underbust girth of a U.S. female and 4.0–8.0 % for a male [37–39]. Therefore, the fiber optic sensor has to have a high gauge factor and linearity in the low strain range (<10 %). A fiber Bragg grating (FBG) allows high sensitivity and multiplexed information from a single fiber, but it often comes with a relatively large and expensive optical interrogator, which is not ideal for most activities [36]. On the other hand, measuring the light intensity or color only requires a small detector, which provides a user with better wearability, as well as high sensitivity [40–42]. Lastly, elongation- or compression-based strain sensing requires a

pre-strain to avoid non-linear signal changes under low strains or higher stress than bending, which will introduce a stronger tension around the body [31,42,43]. Controlling the fiber movement is important to ensure consistency in macro-bending methods, but most applications so far have only secured the fiber using glue or stitches at a few fixed points, which has allowed the rest of the fiber to arbitrarily bend without any control or guidance [24,41,44].

This study reports a wearable strain gauge that uses a stretchable optical fiber, called Optical Lace (OL), to develop durable, washable, and affordable respiratory sensor for the general population engaged in everyday activities. Machine embroidery was used to enclose the OL to control the fiber movements and provide protection from external impacts (Figure 3.1a). The tensile stress on an elastic band changed the shape of the optical fiber from a serpentine pattern to a straight line without tensioning the OL itself, which increased the intensity of the light transmitted in the OL. The enclosure did not affect the stretchability of the basis elastic band, while the sensitivity to strain was adjustable by the embroidery parameters such as the density and tension of the stitches. We embedded two sensors in a compression shirt on the thoracic and abdominal circumferences to accommodate different breathing styles [1,9] and monitored the respiratory rate and respiratory volume. The signal displayed satisfactory correlation coefficients with the respiratory volume (RV) trend from a spirometer in both static and dynamic postures ($0.690 < r^2 < 0.881$), and a neural network model (multilayer perceptron (MLP) regressor) accurately predicted the RV (0.258 L $<$ RMSE < 0.381 L). The respiratory rate (RR) computed by a fast Fourier transform (FFT) also showed low absolute errors between 0.017 and 1.513 breaths per minute (BPM), except under the running condition, which added significantly more motion artifacts. This study also found that the system was resilient to typical adverse scenarios such as abrasions (100,000 rubs) and washings (10 cold washes using a

detergent). Lastly, while the sensor sewn into a compression garment was the main interest of the study, we compared its performance to a belt-type sensor to reveal the best option for consumers.

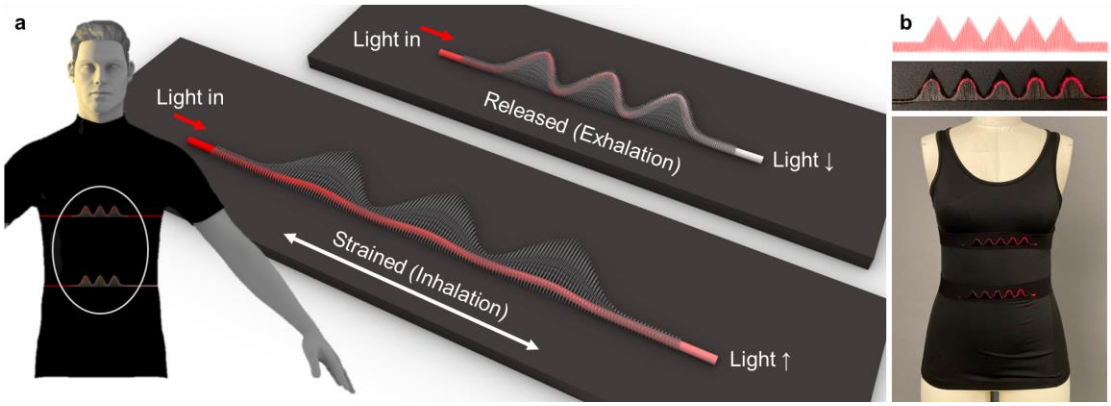

Figure 3.1 Design overview and sample images. a) Sensor design and principle sensing the strain of the textile caused by respiration. b) Embroidery design (top), a close-up image of the fabricated sensor (middle), and the sensors embedded on a compression shirt (bottom).

3.2 Result

System design

The goal of the design was to create a textile-friendly enclosure to i) hold the OL firmly on the elastic band, ii) guide its movements between a serpentine shape and straight line, iii) with no or minimal limitation of the original stretching behavior of the elastic band. Integrating an optical fiber into a textile itself at the initial manufacturing phase (e.g., weaving or knitting) could achieve a durable and seamless installation of the sensor in the textile, but the optical fiber often experiences large light loss as a result of micro-bending in the midst of the woven/knitted yarn [30]. Gluing the entire fiber optic on the textile or enclosing it in a serpentine pattern with another layer of elastic textile or elastomer could restrict the stretchability of the basis

elastic band. Hand embroidery and gluing to create a few anchors on the fiber do not guarantee that the unfixed parts will remain on the textile surface or behave as expected under strain [44].

Therefore, this study adopted machine embroidery consisting of only zigzag stitches as the enclosure for the strain sensing OL. A zigzag stitch is one of the most common and widely used stitching methods for stretchy textiles. It does not produce significant changes in the mechanical properties of the textile under strain [42]. Unlike typical embroidery where many short stitches fill the target area, the embroidery in this study used stitches only at the boundaries of the enclosure (i.e., the needle penetrated the upper/lower edges of the enclosure shape, not in the middle), to create a space underneath the embroidery where the OL could freely move and change its shape under strain (Figure 3.1b). The OL enclosed in the embroidery was longer than the horizontal length of the embroidery, which caused the OL to bend into a serpentine shape with fiber peaks as guided by the five triangular spaces created by the embroidery. Light leaked around the peaks of the curve, which reduced the amount of light arriving on the other side. When the elastic band was strained (i.e., the wearer inhaled and the ribcage expanded), the zigzag stitched enclosure followed the horizontal expansion and straightened the OL, which increased the light intensity.

Respiratory volume measurement by conditions

The normalized light intensity of the raw signals from the OL and the respiratory volume prediction using the MLP model showed good agreement with the ground truth from the spirometer (Figure 3.2). The Pearson correlation coefficient (r^2) was the highest at 0.924 in the setting where the wearers sat and breathed deeply (Std. Error = 0.016, Figure 3.3a). Normal breathing while sitting had an r^2 value of 0.887 (Std. Error = 0.024). When the wearers walked and ran on the treadmill, because of the motion

artifacts, the coefficient was not as good as those for the stable postures (walk: r^2 = 0.844, Std. Error = 0.045; run: r^2 = 0.872, Std. Error = 0.024). The root-mean-square error (RMSE) values of the predictions in terms of the actual respiratory volume were 0.258 L (sitting and breathing normally), 0.381 L (sitting and breathing deeply), 0.338 L (walking), and 0.367 L (running). The raw signal also showed a satisfactory correlation across the tasks (normal breathing: r^2 = 0.880, deep breathing: r^2 = 0.896, walk: r^2 = 0.816, run: r^2 = 0.691). The results were still sufficient to demonstrate the positive correlation between the sensor reading and ground truth, considering most of the previous studies faced challenges in finding a high correlation between their sensor reading and the respiratory volume when the wearer was engaged in active body movements [18,45–47].

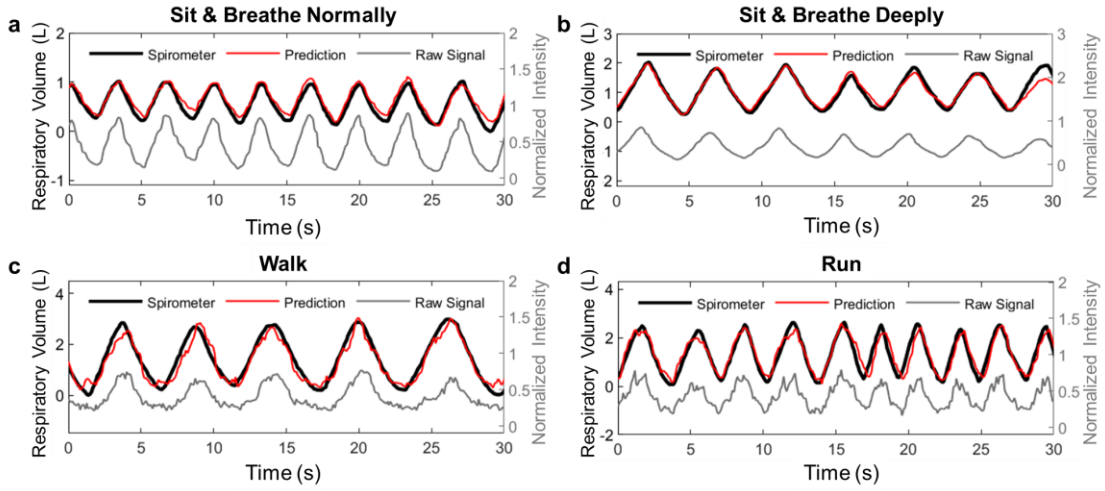

Figure 3.2 Respiratory volume prediction results using raw signal readings as inputs for the MLP model and the ground truth from a commercial spirometer. a) Sit and breathe normally. b) Sit and breathe deeply. c) Walk on a treadmill. d) Run on a treadmill.

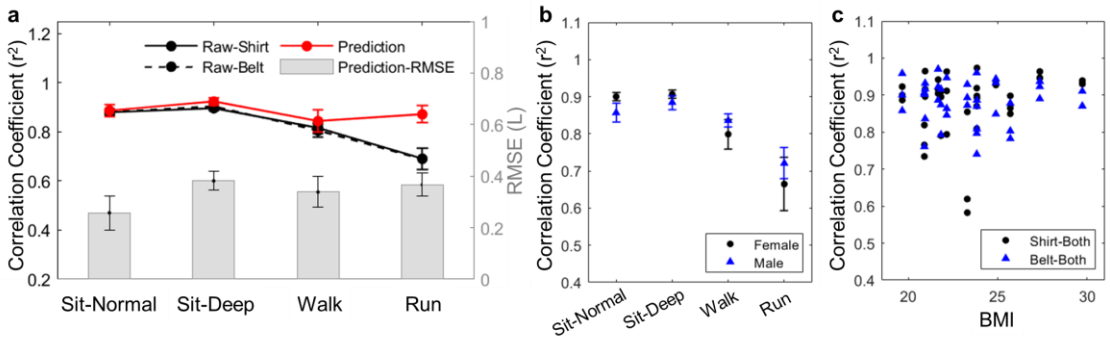

Figure 3.3 Respiratory volume measurement. a) Pearson correlation coefficients between sensor type and the ground truth. 'Both' was the sum of the sensors on the chest and waist, and 'Prediction' was based on the signals from the shirt and MLP model. b) Correlation coefficient comparison by sex and posture, in case of using 'Shirt-Both'. c) Correlation coefficient distribution by BMI and sensor type, in case of sitting-breathing normally.

There was no significant difference between the shirt-type sensor and belt-type, but as a single sensor, the belt on the upper chest showed fine performance overall. Meanwhile, the sex or body mass index (BMI) did not produce any significant bias in the results (Figures 3.3b and 3.3c).

Respiratory rate measurement by conditions

The stretchable optical fiber enclosed by machine embroidery accurately monitored the respiratory rate when the wearer was sitting (absolute $error_{deep\text{-}shirt}$ = 0.017 ± 0.002 BPM, Figure 3.4a) or walking (absolute $error_{shirt}$ = 1.024 ± 0.555 BPM). However, the error was significantly high when the wearer ran (absolute $error_{shirt}$ = 9.35 ± 5.003 BPM, absolute $error_{belt}$ = 23.86 ± 6.999 BPM) as a result of the increased motion artifacts. This study used the frequency with the highest amplitude in the FFT result as the RR. Thus, when the noise caused by consistent running motions increased, it sometimes replaced the RR. Figure 3.4b shows the second-highest peak around 180 BPM, which was from the running motion. The signal-noise-ratio (SNR) also showed

the amount of noise from the motion artifact (Figure 3.4c). While the signal was robust compared to the noise in sitting postures (SNR > 14.6 dB), active body movements added significant noise (SNR_{walk} > 7.122 dB, SNR_{run} > 4.106 dB). There was no noticeable difference between the shirt- and belt-type sensors, but the absolute error for respiratory rate monitoring during running was higher when using the belt.

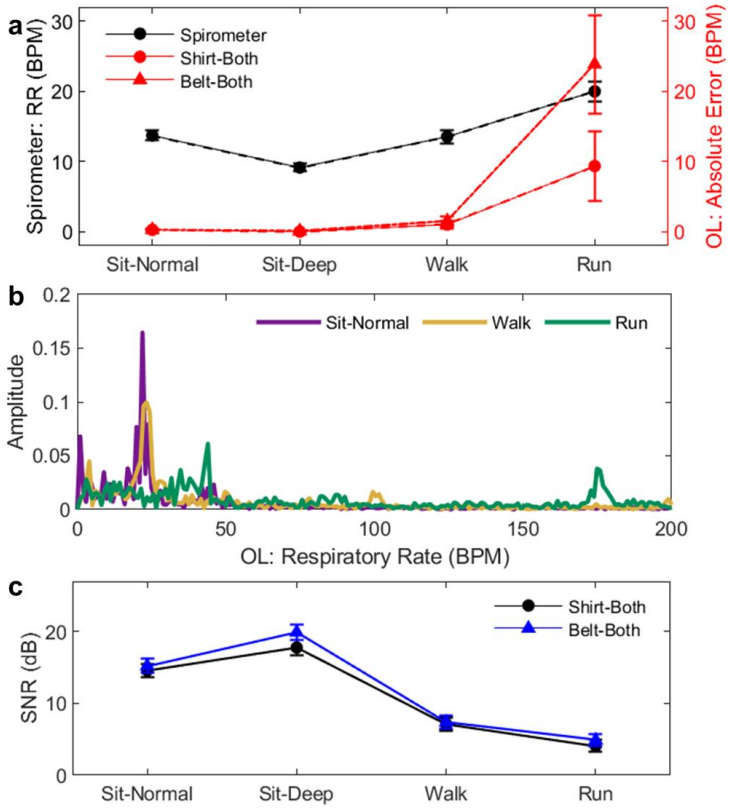

Figure 3.4 Respiratory rate measurement. a) Respiratory rate from a commercial spirometer and absolute error from the sensor by posture and sensor type. b) FFT result of the signals from the shirt-type sensor by posture. c) Signal-to-noise ratio by posture and type of sensor.

Sensitivity adjustment

The light source and straight-line length of the OL predetermined the level of maximum light intensity on the side of the light detector. Therefore, the sensitivity to

strain depended on the methods used to decrease the light transmittance when the sensor was free of tension. The embroidery enclosure determined the condition of the OL when released. Thus, the parameters of the embroidery could be used to adjust the strain sensitivity of the sensor. The embroidery shape, number of curves, stitch tightness/density, thread type, and other factors could be adjusted to achieve the optimal sensitivity for a given application. Figure 3.5 shows the gauge factor ($GF = \frac{|\Delta V/V|}{\gamma}$, where V is the analog input level indicating the intensity of light and γ is the strain) between the released status and fully strained status based on the embroidery parameters.

Because the light leakage around the curve depended on the curve angle (Figure 3.8), the shape of the embroidery, which caused the fiber to curve, affected the GF, as shown in Figure 3.5a. When the width and height of the shape were the same, a triangle-shaped enclosure, which could create the sharpest curve angle (>0.92 rad), showed the highest sensitivity, followed by the square (>1.57 rad) and round shapes (with different but larger angles than the triangle). The number of spaces accommodating the extra length of OL determined the number of curves. More curves resulted in greater light leakage, along with larger changes in the light intensity when the OL was straightened (Figure 3.5b). The stitch spacing, which refers to the distance between two adjacent peaks in zigzag stitches, had a negative relationship with the gauge factor (Figure 3.5c). A smaller spacing (i.e., denser stitches) loaded more compression from the thread on the soft optical fiber. It reduced the light transmittance but led to a greater increase in light intensity when the textile was under tension. The number of layers of water-soluble stabilizers determined the tightness of the embroidery. Less or no stabilizer created tighter stitches, which resulted in a bigger difference between the released status and strained status (Figure 3.5d).

The gauge factor observed in the lab tests (~5) exceeded that of most carbon nanotube (CNT)-filled elastomeric strain gauges [48–50], but fell short of the gauge factors exhibited by highly sensitive systems based on carbon black (CB) [51,52], graphene [53,54], silver nanowires (AgNW) [55,56], or liquid metal [57]. In comparison to strain gauges employed for wearable respiration monitoring, which typically range from 0.9 to 522 [58–60], the current system's performance lies in the low-to-middle range. When compared to polymer-based optical waveguides, the gauge factor is similar to or lower than other strain gauges [31,42,61], yet higher than FBG-based strain gauges [62,63] and the reported sensitivity of fiber-optic-based respiratory sensors [44,64]. Overall, the number of rooms was the most significant factor in gauge factor. However, it is also important to optimize the other parameters to maximize the sensitivity, because only a limited number of rooms can be fabricated within the relatively flat side of the front torso.

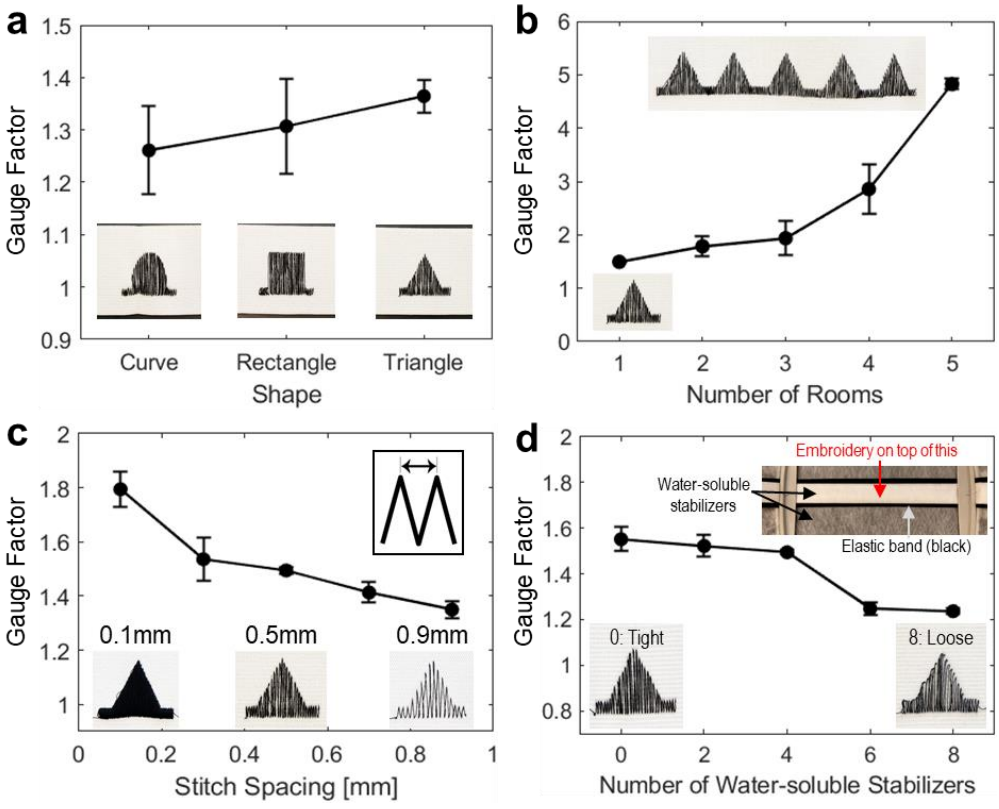

Figure 3.5 Gauge factor by embroidery parameter adjustment. a) Embroidery shape. b) Number of the enclosing rooms deciding the number of curves of OL. c) Stitch spacing that decides the density of stitches. d) Number of water-soluble stabilizers between the embroidery and the elastic band, deciding the tightness of the embroidery.

Reliability and durability

The reliability and durability of the current sensor using OL and machine embroidery were demonstrated through tensile, abrasion, and washing tests to simulate potential adverse scenarios to which a textile-based respiratory sensor could be subjected over its lifespan. An extension-controlled cyclic tensile test confirmed the consistency in signal changes for up to 500 cycles of strain (Figure 3.6a). The low drift implied that respiratory volume monitoring using this current sensor is promising (Figure 3.6b). The signal trends by strain were consistent under different tensile extension speeds, which showed the capability of the sensor to accurately detect an abnormal breathing pattern such as apnea, hypopnea, and/or hyperpnea (Figure 3.6c). Meanwhile, the sensor had a consistent signal level under 60 s of strain loading (Figure 3.6d), which could be useful for monitoring breath-holding behaviors.[65] Because strain sensors for respiratory monitoring need to be tightly fitted to the torso, the effect of abrasion on the signal was examined, assuming that the sensor would be worn as innerwear. The signal noise caused by abrasion with a pressure of 9 kPa was not significant (Figure 3.6e), especially when considering that common garment layers will not create much pressure on the innerwear.

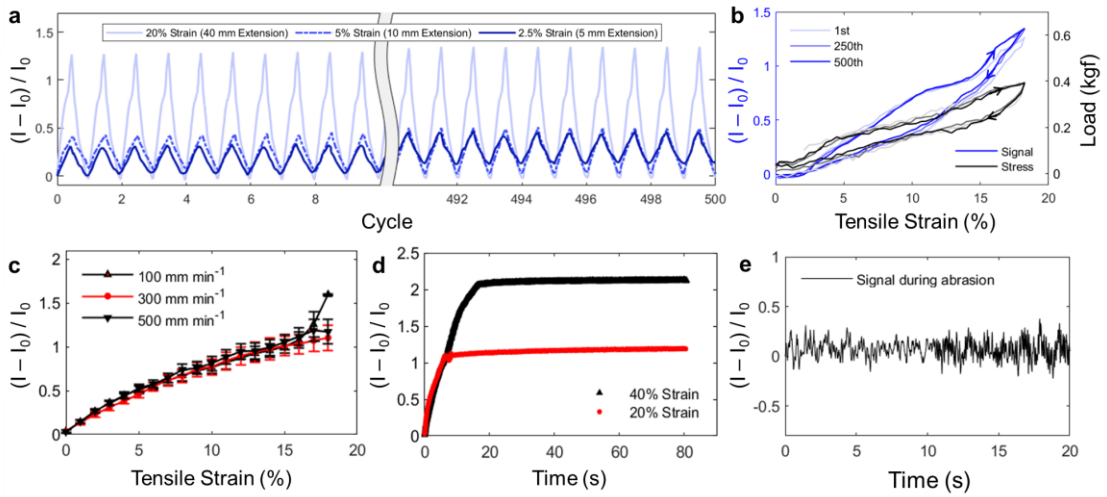

Figure 3.6 Reliability tests. a) Cyclic tensile test by extension length. b) Light intensity changes during the 500 cycles of extension-controlled tensile test. c) Light signal changes under different extension speeds. d) Consistent light intensity under tensile loadings. e) Signal noises created by abrasions.

In terms of durability, the embroidery enclosure made of nylon thread suffered only minor damage after 100,000 abrasions. None of the threads and only a few fibers were broken (Figure 3.7a). The tensile tests showed that even though the sensitivity decreased under strains larger than 10%, the sensor still functioned, and the gauge factor was sufficient to monitor respiration (Figure 3.7b). However, the other two types of common embroidery threads, polyester, and rayon, could not withstand more than 5,000 abrasions (Figure 3.9). Ten cold machine washes using detergent did not cause any noticeable changes in the embroidery threads or OL (Figure 3.7c and Figure 3.10). In addition, there was no degradation in the sensitivity to strain over the repetitive washing (Figure 3.7d).

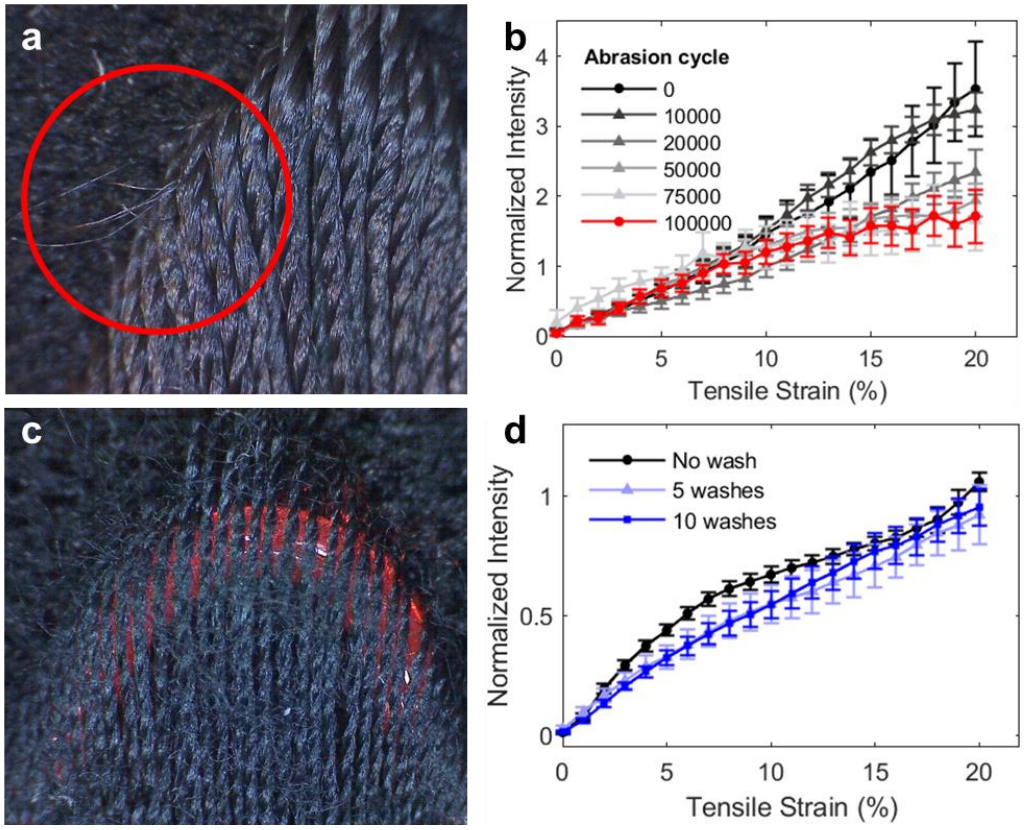

Figure 3.7 Durability tests. a) Sensor after 100,000 abrasion cycles. Only a few fibers were broken in the red-marked circle area. b) Tensile test result over the abrasion cycles. c) Sensor after 10 cold machine washes. d) Tensile test results over the laundry cycles.

3.3 Conclusion

In this study, machine embroidery was used to install a stretchable light guide called OL on an elastic textile to create a wearable respiratory monitoring sensor. The embroidery with enclosed spaces guided the OL to form a serpentine shape when the textile was free of tension (i.e., exhalation), and to react to the ribcage expansion during inhalation by being straightened. The intensity of the light passing through the fiber changed in correspondence to the respiratory volume trend, demonstrating a high correlation even when the wearer was running ($r^2 = 0.872$), with the assistance of a

neural network. The sensor was used to accurately measure the respiratory rates of 13 human participants (absolute error < 1.513 BPM) when the participants were sitting or walking. The machine embroidery used in the current study consisted only of zigzag stitches. Thus, the enclosure did not restrict the original stretchability of the elastic textile. Furthermore, the parameters of the embroidery, including its shape and stitch density/tightness, could be used to adjust the sensitivity of the OL to strain. The sensor was durable and reliable against abrasions, repetitions, and machine washes.

The primary population who could benefit from this sensor would be those with health risks in daily life due to abnormal respiratory symptoms such as hyperventilation and/or hypoventilation. Because this shirt-type sensor could be used with innerwear, the real-time respiratory monitoring results could be shared with the wearer, caregivers, and medical professionals while the patient is continuing their daily routine. Those who put importance on their physical performances would be another major target group, including but not limited to athletes, military personnel, astronauts, and the general public who love sports. This study only investigated RV and RR, but the raw signal could be processed into key health performance indicators according to the interest of the population, to contribute to improvements in physical activities. Because respiration is an indicator of an individual's emotional condition, those interested in their mental health and/or meditation would be able to gain insights using the current sensor by associating the readings with other sources like heartbeats.

The machine embroidery enclosure is easy to fabricate, cost-effective, fast, textile-friendly, and durable enough to launder. Installing a strain sensor on a stretchy textile while preserving its original elasticity and that of the textile is often challenging, but the embroidery consisting of only a zigzag pattern allowed the OL to be embedded on the textile surface while still behaving like a part of the textile. The computerized design and fabrication made the parameter adjustment easy and yielded consistent

results, unlike most manual garment construction techniques. A significant benefit of the OL is its stability against sweat, which contributed to the breathability, softness, and comfort of the final product. The current study did not add any cladding to the OL, but cladding would increase the durability and stability of the OL against abrasion, moisture, and external shock.

While the machine embroidery made of zigzag stitches showed an advantage in terms of elasticity, if the embroidery was large enough, the OL sometimes stuck out between the threads. This rarely occurred during the actual usage for respiratory monitoring and most instances were after machine washing. Extensible stitch types other than zigzag stitches may be able to prevent this issue. The nylon thread used in the abrasion test was thicker than the common thin embroidery threads, but there are thinner options available in the market. While the OL and embroidery enclosure were resistant to water, the other electronic components like the light source, photodetector, and others on the circuit board were still susceptible to moisture. In this study, the light source and photodetector were permanently attached to the OL. In future developments, modular design to create detachable, but also stable and consistent connections between the OL and electronics will be an important task to guarantee the sensor reliability over time and convenience for maintenance. Meanwhile, the belt-type sensors tended to move to the narrowest girth of the torso when they are not tight enough as the wearer moved, which affected the sensor performance. Dotted or thin silicone grippers, mostly used for underwear or waistband to prevent slipping during exercises, can help to reduce the movement of the sensors on the body. The current study predicted the respiratory volume through calibration using the data from a commercial spirometer. Therefore, an easier way to quickly calibrate the respiratory volume should be developed and examined with the current sensor (e.g., a smartphone application predicting respiratory volume through breathing sounds). Lastly, the

current system aimed to monitor everyday activities such as sitting, walking, and running with a limited sampling rate (100 Hz), but for more advanced features to instantly respond to abnormal events such as obstructive or paradoxical breathing behaviors, a more elaborated experiment design and a higher sampling rate will be necessary according to the feature of the target symptoms.

The present research introduced a machine embroidery enclosure that supported the shape transitions of a stretchable light guide as a result of strain. Although we used it to track ribcage movement for respiratory monitoring, its potential is open to most textile-based wearable or robotics applications involving strains. The embroidery enclosing the OL will be able to measure human joint movements or the stretching behaviors of soft systems. Furthermore, the enclosure is not limited to optical fiber, but could be used for any other non-stretchable but soft wearable electronics in the form of a fiber or tube, including sensors, wires, actuators, and/or batteries, to make them flexible and stretchable on textiles.

3.4 Methods

Materials and fabrication

A thermoplastic elastomer manufactured by Crystal Tec, Inc. was used as a thin, soft, and stretchable light guide (n = 1.54, D = 1.2 mm) without cladding [42]. An LED (B07QXR5MZB; BOJACK) and a photodiode (SFH-229; Osram Opto Semiconductors) transmitted/detected a visible red light (~650 nm) compatible with the fiber [31]. The lens of the LED and the photodiode were drilled to create a 1.2 mm-diameter hole to plug in and glue the optical fiber. A 2 kΩ potentiometer was used to adjust the brightness of the LED to an appropriate level, and an I–V converter consisting of an OP-AMP (LM324A; Texas Instruments), a 1 MΩ resistor, and a 4.7 nf capacitor delivered analog signals from the photodiode to the Arduino Nano 33

microcontroller using bluetooth low energy (BLE) (Figure 3.11). A portable battery powered the microcontroller and whole system, and the microcontroller delivered the signals wirelessly to another Arduino Nano 33 BLE connected to a laptop through BLE.

The vector graphic software Inkscape and its add-on package Ink/Stitch supported the design of the embroidery. The dimensions of the embroidery design can be found in Figure 3.12 A piece of elastic (width = 25 mm, thickness = 1.5 mm) on top of six layers of a non-woven water-soluble stabilizer (thickness = 0.16 mm) was loaded onto the embroidery frame holding the textiles tightly. A programmable embroidery machine (Brother PE770) was used to create the embroidery on the elastic band according to the design, using an all-purpose polyester thread (D = 0.06 mm, Dual Duty All Purpose Thread, Coats & Clark). When the machine was doing the embroidery, the fiber optic connection to the LED/photodiode was aligned on the elastic band manually. Thus, the embroidery enclosed the OL without penetrating it. After dissolving the water-soluble stabilizers in warm water, the sensor-embedded elastic band was dried and sewn on the under-chest or waist circumference of a sleeveless compression shirt. The elastic band was made of polyester and rubber, while the compression shirt was a blend of polyester and spandex, both of which were compatible with the polyester thread. There were three shirt sizes per sex, and their measurements can be found in Supplementary Table 3.1. To prevent excessive strain on the sensor during donning/doffing, the shirt was cut in half at the center of the back, and a zipper opening was added. In addition to the shirt-type sensors, belt-type sensors were fabricated by connecting length-adjustable buckles at each end of the elastic band, without sewing it on a shirt.

Uniaxial tensile test

Following ASTM D5035-11 (Standard Test Method for Breaking Force and Elongation of Textile Fabrics, Strip Method) [66], a tensile testing machine (Instron 5566, Instron, Norwood, MA) tested the sensor's sensitivity to the strain of the textile ($\gamma_{textile} = \frac{L - L_0}{L_0}$, where L is the current textile length under the elongating force, and L0 is the original length). The size of the specimen was modified to 25 (width) × 200 (length) × 1.5 (thickness) mm, considering the dimension of the sensor-embedded shirt. A gripper held each end of an elastic band. After preloading 0.1 MPa at a speed of 2 mm min^{-1}, the specimen was elongated to 25 % strain at 300 mm min^{-1}. The end strain and extension speed were modified to examine the effects of the extension speed (100 and 500 mm min^{-1}) and cycles at different strain levels (2.5, 5, and 20 %, 500 mm min^{-1}). The microcontroller collected the signal from the photodiode at 100 Hz.

Human participant test and data processing

The human participant tests were conducted following the protocols approved by the Institutional Review Board (IRB) of Cornell University. A total of 13 healthy adults participated in this study (sex: 7 females and 6 males; age: 36.5 ± 12.1 years, height: 171.6 ± 11.4 cm, weight: 69.6 ± 13.0 kg, BMI: 23.5 ± 2.9). After providing consent, each participant donned a sensor-embedded sleeveless compression shirt in their preferred size, on top of one layer consisting of a t-shirt. The fit of the shirt was adjusted to place the sensors at the under chest and waist levels. In addition, the researcher helped the participant don two belt-type sensors on the upper chest and waist levels (Figure 3.13). The belt for the waist was placed right above or below the sensor embedded in the shirt. The microcontroller and power source were attached to the back of the participant's waist using Velcro. The microcontroller read signals and sent them at 100 Hz to the other microcontroller connected to a laptop through BLE, but the frequency of the received signals varied from 60 to 100 Hz according to the

environment and body movements.

Each participant was asked to perform four tasks: 1) sit comfortably and breathe normally 2) sit comfortably and breathe deeply, 3) walk on a treadmill at a preferred speed, and 4) run on a treadmill at a preferred speed. There were three sessions for each task, and each session took approximately 60 s. To collect the ground truth data, the participants used a hand-held portable spirometer (Spirotel, MIR International, France) connected to a disposable filtered mouthpiece, along with a nose clipper to ensure that air only flowed through the mouth. The filter in the mouthpiece decreased the overall airflow by less than 1.5 cm H_20 L^{-1} s^{-1} at 14 L s^{-1}, and it was necessary to protect the participants during the pandemic [67]. The mouthpiece, filter, and nose clipper were discarded, and the spirometer was sanitized using 3% hydrogen peroxide immediately after each experiment [68]. The spirometer collected the respiratory data at 10 Hz for 60 s.

The light signals from the OLs were normalized within each session and smoothed by averaging over a five-point moving window. The sum of the normalized light intensity from the chest and waist was used as the main signal for each type of sensor: shirt or belt. The frequency with the highest amplitude retrieved from the fast Fourier transform (FFT) for each session (60 s) was used as the respiratory rate of the session. After joining the two datasets (the OLs and spirometer) based on the corresponding timestamps, the correlation coefficient was computed for each session. All the data processing and analysis described so far was done in MATLAB.

The neural network MLP Regressor model from the Scikit-learn library was used in Python [69]. The normalized signal from the shirt (i.e., the sum of the signals from the sensors installed at the chest and waist levels of the shirt) from t-10 to t-1 (about 1 second time window) was provided as the input to reduce the effect of the noise in prediction [70]. The respiratory volume from the spirometer worked as the output after

normalization. Because each participant had a different fit with the pre-manufactured compression garment, the training and testing were done for each participant. Among three sessions for each task, data from two sessions (approximately 120 s) were used to train the model, and the other session (approximately 60 s) was used for the model test. The neural network trained the model until convergence (or max. 1,000 iterations) with the Adam optimizer. The hidden layer size was 64 * 64 * 64, and a rectified linear unit (ReLU) performed as an activation function.

Abrasion test

The abrasion resistance of the embroidery and the strain-sensing capability of the system were examined using the M235 Martindale abrasion tester, according to the modified ASTM D4966-12 Standard Test Method for Abrasion Resistance of Textile Fabrics (Martindale Abrasion Tester Method).[71] The belt-type sensor (OL enclosed by the embroidery on elastic, without being sewn on a shirt) was fabricated using three different threads (the polyester used for all the other tests in this study, rayon, and nylon). The sample size for each thread type was three. The samples were attached to the bottom of the moving textile holder with the OL and embroidery facing downward, instead of clamping the sensor into the holder, to prevent damage to the OL. The moving holder rubbed the sensor surface onto the standard rugged woven textile (D = 13 cm) clamped on the other side. The weight connected to the top of the holder added a pressure of 9 kPa to the rubbing surfaces, and the speed of the abrasion was 47.5 rpm. Because the diameter of the bottom of the holder (5 cm) was shorter than the length of the embroidery (10 cm), the abrasions only affected the center of the sensor (Figure 3.14).

A portable microscope (USB2-MICRO-200X; Plugable Technologies, Redmond, WA) was used to obtain close-up images of the embroidery surface before the

experiment, and after 5000, 10000, 20000, 50000, 75000, and 100000 abrasion cycles. In addition, following the same uniaxial tensile testing protocol except for the specimen dimension (25 × 100 × 1.2 mm) and preload (0.025 MPa), the strain sensitivity was examined every time after taking close-up images.

Machine washing test

Following the AATCC LP1-2018e Laboratory Procedure for Home Laundering: Machine Washing, the washability of the system was tested. The standard normal/cold washing procedure includes 27 °C water, machine washing for 16 min, a final spin at 660 rpm for 5 min, 66 g of 1993 AATCC Standard Reference Detergent, and laundering ballast to meet the total laundry weight level of 1.8 kg. A Vortex M6 (SDL Atlas, Rock Hill, SC) standard washing machine took approximately 40 min for one cycle of washing in total. Four sensor samples embedded on compression shirts were laundered along with the ballast, and each was hung on a hanger and dried for approximately 1 h before going through the next cycle of washing. The strain sensitivity of the samples was tested following the same uniaxial tensile test protocol, before the laundering and after 5 and 10 washes.

3.5 Supporting Information

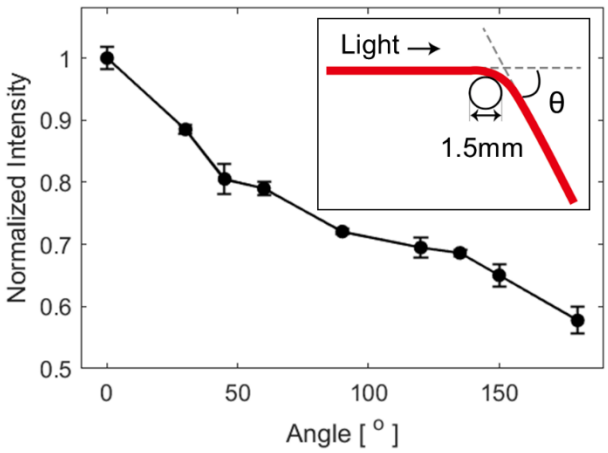

Figure 3.8 Light intensity by the angle of a curve of the OL.

The OL bent around a rod with a diameter of 1.5mm to keep a specific angle. The light intensity normalized based on the straight status of the OL. As the angle increased (the curve became sharp), the light leaked around the curve, and the amount of light arriving on the other side decreased.

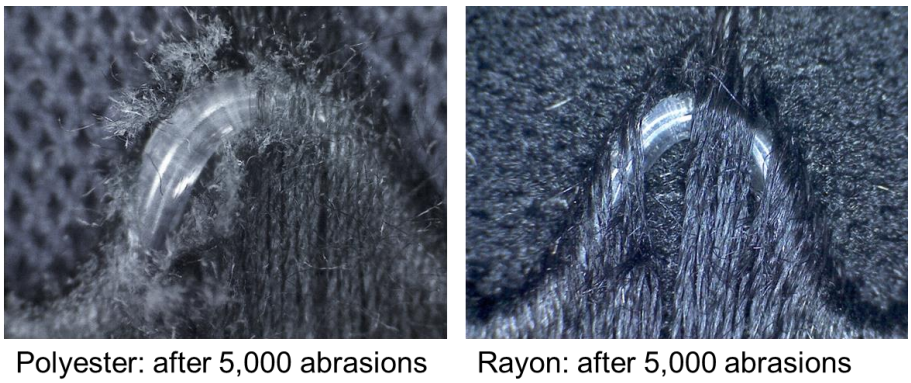

Figure 3.9 Abrasion results of embroideries made of polyester and rayon thread.

Polyester and rayon thread did not show compelling abrasion resistance compared to the nylon thread. A major part of the embroidery was damaged by the rubbings.

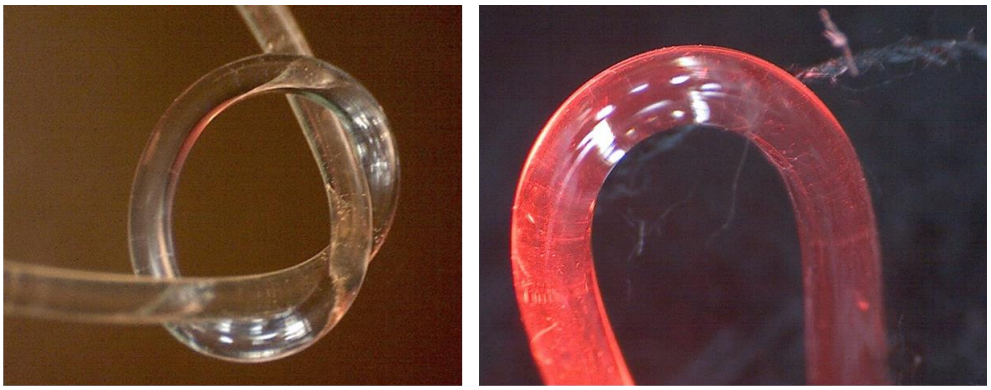

Figure 3.10 OL before and after machine washes.

There was no damage detected after 10 cold machine washes.

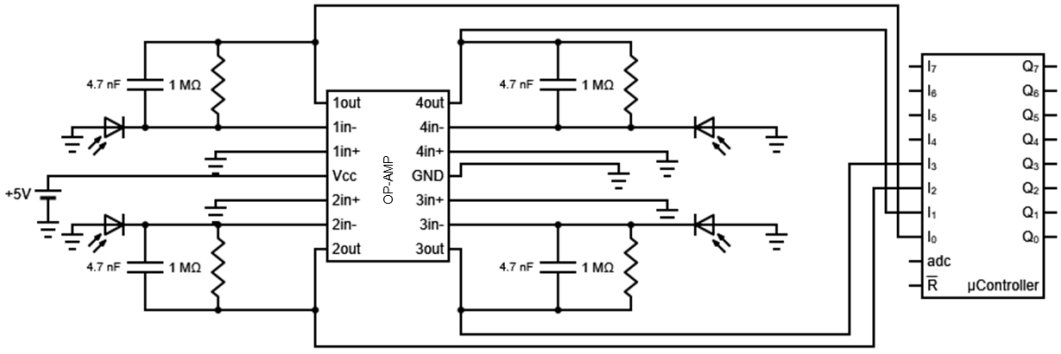

Figure 3.11 Circuit schematic.

The following schematic contains four photodiodes connected to an OP-AMP and a microcontroller, collecting the changes in light intensity from the end of the fiber optic.

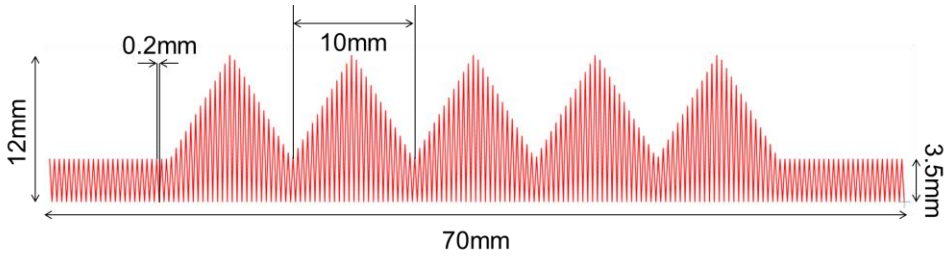

Figure 3.12 Dimension of the embroidery enclosure.

The embroidery enclosed 100mm-OL, 30mm of which created serpentine patterns in the five triangular rooms of the embroidery.

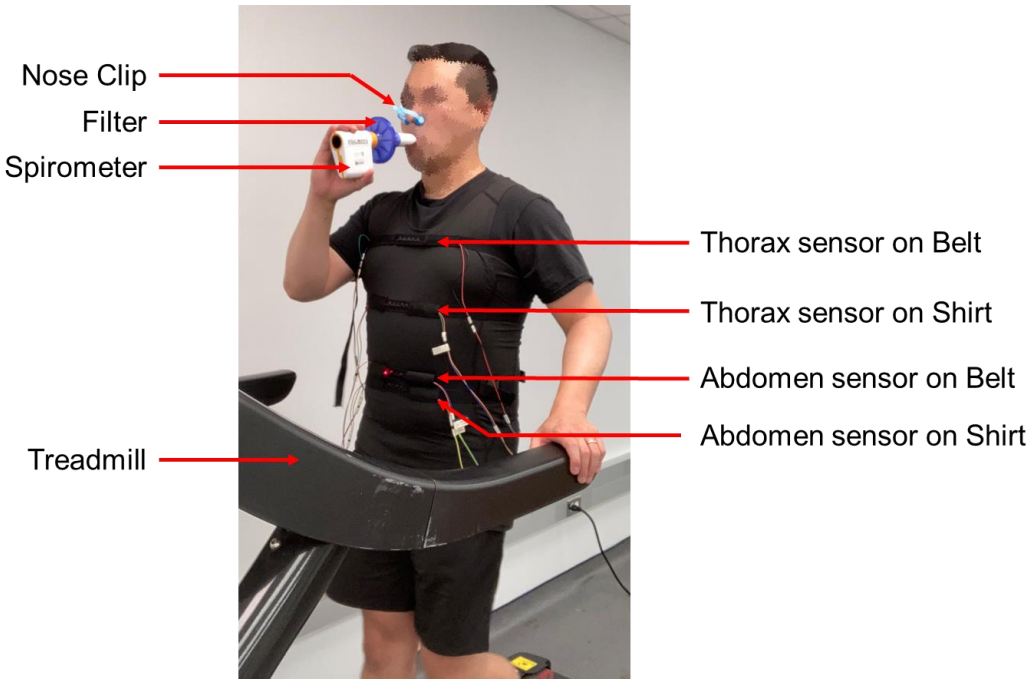

Figure 3.13 Human participant test setting.

Each participant wore a sleeveless compression shirt where two sensors were installed around the chest and waist respectively and wore two sensor-embedded belts additionally. They were asked to hold the spirometer in one hand and hold the rail using the other hand.

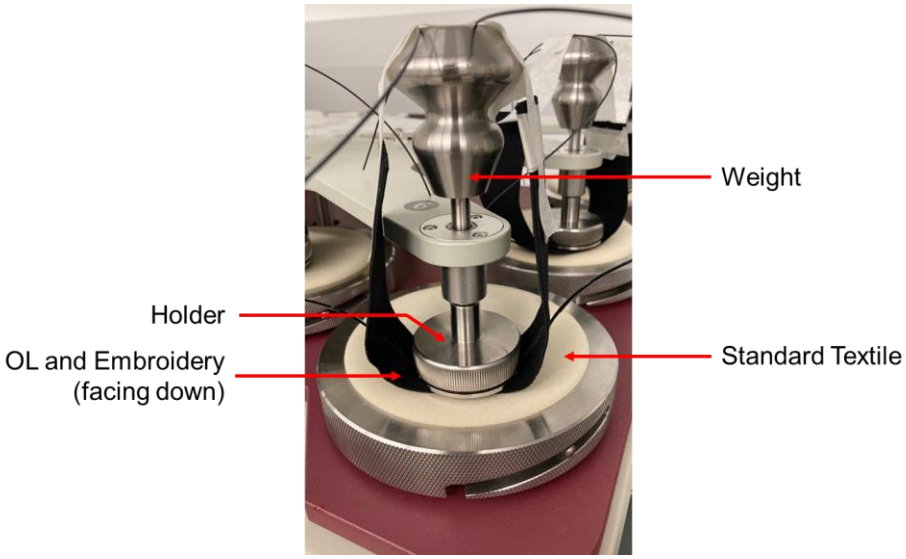

Figure 3.14 Abrasion test setting.

The standard requires clamping the specimen within the holder. However, in this study, the sample was simply attached to the bottom of the holder not to damage the sensor by clamping. The weight gives a pressure of 9kPa on each rubbing side of the textile.

Table 3.1 Size of the compression shirt samples.

(cm)	Female			Male		
Size	**Small**	**Medium**	**Large**	**Small**	**Medium**	**Large**
Chest width	38	41	45	42	46	48
Waist width	34	37	41	35	39	42
Full length	56	58	60	67	68	69

REFERENCES

[1] F. q. AL-Khalidi, R. Saatchi, D. Burke, H. Elphick, S. Tan, Pediatric Pulmonology 2011, 46, 523.

[2] F. A. Boiten, N. H. Frijda, C. J. E. Wientjes, International Journal of Psychophysiology 1994, 17, 103.

[3] N. Yanamala, N. H. Krishna, Q. A. Hathaway, A. Radhakrishnan, S. Sunkara, H. Patel, P. Farjo, B. Patel, P. P. Sengupta, npj Digit. Med. 2021, 4, 95.

[4] H. Chen, S. M. Lundberg, G. Erion, J. H. Kim, S.-I. Lee, npj Digit. Med. 2021, 4, 167.

[5] P. A. Lanfranchi, A. Braghiroli, E. Bosimini, G. Mazzuero, R. Colombo, C. F. Donner, P. Giannuzzi, Circulation 1999, 99, 1435.

[6] S. Yildiz, S. Thyagaraj, N. Jin, X. Zhong, S. Heidari Pahlavian, B. A. Martin, F. Loth, J. Oshinski, K. G. Sabra, Journal of Magnetic Resonance Imaging 2017, 46, 431.

[7] C. M. Spengler, U. Boutellier, Physiology 2000, 15, 101.

[8] K. E. Friedl, Journal of Science and Medicine in Sport 2018, 21, 1147.

[9] W. Porges, E. A. Byrne, Biological Psychology 1992, 93.

[10] J. Dai, H. Zhao, X. Lin, S. Liu, Y. Liu, X. Liu, T. Fei, T. Zhang, ACS Appl. Mater. Interfaces 2019, 11, 6483.

[11] F. Güder, A. Ainla, J. Redston, B. Mosadegh, A. Glavan, T. J. Martin, G. M. Whitesides, Angewandte Chemie International Edition 2016, 55, 5727.

[12] V. V. Tipparaju, D. Wang, J. Yu, F. Chen, F. Tsow, E. Forzani, N. Tao, X. Xian, Biosensors and Bioelectronics 2020, 169, 112590.

[13] Y. Chen, F. Liu, B. Lu, Y. Zhang, X. Feng, Advanced Electronic Materials 2020, 6, 2000145.

[14] A. Aliverti, Breathe 2017, 13, e27.

[15] Y. Song, H. Chen, Z. Su, X. Chen, L. Miao, J. Zhang, X. Cheng, H. Zhang, Small 2017, 13, 1702091.

[16] L. Guo, L. Berglin, U. Wiklund, H. Mattila, Textile Research Journal 2013, 83, 499.

[17] E. Helfenbein, R. Firoozabadi, S. Chien, E. Carlson, S. Babaeizadeh, Journal of

Electrocardiology 2014, 47, 819.
[18] P. Sharma, X. Hui, J. Zhou, T. B. Conroy, E. C. Kan, npj Digit. Med. 2020, 3, 98.
[19] K. S. Tan, R. Saatchi, H. Elphick, D. Burke, in 2010 7th International Symposium on Communication Systems, Networks & Digital Signal Processing (CSNDSP 2010), 2010, pp. 770–774.
[20] J. D. Kim, W. H. Lee, Y. Lee, H. J. Lee, T. Cha, S. H. Kim, K.-M. Song, Y.-H. Lim, S. H. Cho, S. H. Cho, H.-K. Park, R. Soc. open sci. 2019, 6, 190149.
[21] C. Massaroni, A. Nicolò, D. Lo Presti, M. Sacchetti, S. Silvestri, E. Schena, Sensors 2019, 19, 908.
[22] R. Pirich, K. D'Ambrosio, in 2011 IEEE Long Island Systems, Applications and Technology Conference, 2011, pp. 1–4.
[23] Q. Chai, Y. Luo, Opt. Eng. 2019, 58, 1.
[24] B. M. Quandt, L. J. Scherer, L. F. Boesel, M. Wolf, G.-L. Bona, R. M. Rossi, Advanced healthcare materials 2015, 4, 330.
[25] T. L. Yeo, T. Sun, K. T. V. Grattan, Sensors and Actuators A: Physical 2008, 144, 280.
[26] H. Souri, H. Banerjee, A. Jusufi, N. Radacsi, A. A. Stokes, I. Park, M. Sitti, M. Amjadi, Advanced Intelligent Systems 2020, 2, 2000039.
[27] Ł. Dziuda, M. Krej, F. W. Skibniewski, IEEE Sensors Journal 2013, 13, 4986.
[28] W.-J. Yoo, K.-W. Jang, J.-K. Seo, J.-Y. Heo, J.-S. Moon, J.-Y. Park, B.-S. Lee, Journal of the Optical Society of Korea 2010, 14, 235.
[29] S. A. Nehmeh, Y. E. Erdi, Seminars in Nuclear Medicine 2008, 38, 167.
[30] Z. Gong, Z. Xiang, X. OuYang, J. Zhang, N. Lau, J. Zhou, C. C. Chan, Materials 2019, 12, 3311.
[31] C. K. Harnett, H. Zhao, R. F. Shepherd, Advanced Materials Technologies 2017, 2, 1700087.
[32] J. Witt, F. Narbonneau, M. Schukar, K. Krebber, J. D. Jonckheere, M. Jeanne, D. Kinet, B. Paquet, A. Depré, L. T. D'Angelo, T. Thiel, R. Logier, IEEE SENSORS JOURNAL 2012, 12, 10.
[33] L. Presti, C. Massaroni, P. Saccomandi, M. A. Caponero, D. Formica, E. Schena,

in Conference Proceedings:... Annual International Conference of the IEEE Engineering in Medicine and Biology Society. IEEE Engineering in Medicine and Biology Society. Annual Conference, 2017, pp. 4423–4426.
[34] J. Li, J. Chen, F. Xu, Advanced Materials Technologies 2018, 3, 1800296.
[35] B. Najafi, H. Mohseni, G. S. Grewal, T. K. Talal, R. A. Menzies, D. G. Armstrong, J Diabetes Sci Technol 2017, 11, 668.
[36] A. Leal-Junior, L. Avellar, A. Frizera, C. Marques, Scientific Reports 2020, 10, 13867.
[37] E. Agostoni, P. Mognoni, G. Torri, F. Saracino, Journal of Applied Physiology 1965, 20, 1179.
[38] A. P. Binks, R. B. Banzett, C. Duvivier, Physiol. Meas. 2007, 28, 149.
[39] "Size USA Data | Made-To-Measure Garments And Design Software," can be found under http://www.tc2.com/size-usa.html, n.d.
[40] H. Bai, S. Li, J. Barreiros, Y. Tu, C. R. Pollock, R. F. Shepherd, Science 2020, 370, 848.
[41] C. To, T. L. Hellebrekers, Y.-L. Park, in 2015 IEEE/RSJ International Conference on Intelligent Robots and Systems (IROS), IEEE, Hamburg, Germany, 2015, pp. 5898–5903.
[42] J. Jo, A. Xu, A. K. Mishra, H. Bai, A. Derkevorkian, J. Rabinovitch, H. Park, R. F. Shepherd, Adv Materials Technologies 2022, 7, 2200437.
[43] H. Zhao, K. O'Brien, S. Li, R. F. Shepherd, Science robotics 2016, 1.
[44] W. Zheng, X. Tao, B. Zhu, G. Wang, C. Hui, Textile Research Journal 2014, 84, 1791.
[45] M. Chu, T. Nguyen, V. Pandey, Y. Zhou, H. N. Pham, R. Bar-Yoseph, S. Radom-Aizik, R. Jain, D. M. Cooper, M. Khine, npj Digital Med 2019, 2, 8.
[46] R. I. Ramos-Garcia, F. Da Silva, Y. Kondi, E. Sazonov, L. E. Dunne, in 2016 10th International Conference on Sensing Technology (ICST), 2016, pp. 1–6.
[47] R. Ravichandran, E. Saba, K.-Y. Chen, M. Goel, S. Gupta, S. N. Patel, in 2015 IEEE International Conference on Pervasive Computing and Communications (PerCom), 2015, pp. 131–139.

[48] M. Amjadi, Y. J. Yoon, I. Park, Nanotechnology 2015, 26, 375501.
[49] T. Yamada, Y. Hayamizu, Y. Yamamoto, Y. Yomogida, A. Izadi-Najafabadi, D. N. Futaba, K. Hata, Nature Nanotech 2011, 6, 296.
[50] D. J. Cohen, D. Mitra, K. Peterson, M. M. Maharbiz, Nano Lett. 2012, 12, 1821.
[51] N. Lu, C. Lu, S. Yang, J. Rogers, Adv. Funct. Mater. 2012, 22, 4044.
[52] C. Mattmann, F. Clemens, G. Tröster, Sensors (Basel) 2008, 8, 3719.
[53] Y. R. Jeong, H. Park, S. W. Jin, S. Y. Hong, S.-S. Lee, J. S. Ha, Advanced Functional Materials 2015, 25, 4228.
[54] C. S. Boland, U. Khan, C. Backes, A. O'Neill, J. McCauley, S. Duane, R. Shanker, Y. Liu, I. Jurewicz, A. B. Dalton, J. N. Coleman, ACS Nano 2014, 8, 8819.
[55] S. Gong, D. T. H. Lai, Y. Wang, L. W. Yap, K. J. Si, Q. Shi, N. N. Jason, T. Sridhar, H. Uddin, W. Cheng, ACS Appl. Mater. Interfaces 2015, 7, 19700.
[56] B.-U. Hwang, J.-H. Lee, T. Q. Trung, E. Roh, D.-I. Kim, S.-W. Kim, N.-E. Lee, ACS Nano 2015, 9, 8801.
[57] Y.-G. Park, G.-Y. Lee, J. Jang, S. M. Yun, E. Kim, J.-U. Park, Advanced Healthcare Materials 2021, 10, 2002280.
[58] O. Atalay, A. Atalay, J. Gafford, C. Walsh, Advanced materials technologies 2018, 3, 1700237.
[59] M. Amjadi, M. Turan, C. P. Clementson, M. Sitti, ACS Appl. Mater. Interfaces 2016, 8, 5618.
[60] T. Dinh, T. Nguyen, H.-P. Phan, N.-T. Nguyen, D. V. Dao, J. Bell, Biosensors and Bioelectronics 2020, 166, 112460.
[61] Y. Zhang, X. Li, J. Kim, Y. Tong, E. G. Thompson, S. Jiang, Z. Feng, L. Yu, J. Wang, D. S. Ha, H. Sontheimer, B. N. Johnson, X. Jia, Advanced Optical Materials 2021, 9, 2001815.
[62] F. Jülich, L. Aulbach, A. Wilfert, P. Kratzer, R. Kuttler, J. Roths, Meas. Sci. Technol. 2013, 24.
[63] V. G. Schukar, N. Kusche, W. R. Habel, IEEE Sensors Journal 2012, 12, 128.
[64] K. Alemdar, S. Likoglu, K. Fidanboylu, O. Toker, in 2013 8th International Conference on Electrical and Electronics Engineering (ELECO), 2013, pp. 467–471.

[65] “Breath holding spell Information | Mount Sinai - New York,” can be found under https://www.mountsinai.org/health-library/diseases-conditions/breath-holding-spell, n.d.
[66] ASTM D5035-11, Standard Test Method for Breaking Force and Elongation of Textile Fabrics (Strip Method), ASTM International, West Conshohocken, PA, 2015.
[67] “MIR Reusable FlowMIR Turbine for MIR Spirometers With 100 PFT Filters,” can be found under https://www.spirometershop.com/p-1398-mir-reusable-turbine-100-pft-filters.aspx, n.d.
[68] “Use of Hydrogen Peroxide for Coronavirus Disinfection | MTAS,” can be found under https://www.mtas.tennessee.edu/knowledgebase/use-hydrogen-peroxide-coronavirus-disinfection, n.d.
[69] “sklearn.neural_network.MLPRegressor,” can be found under https://scikit-learn/stable/modules/generated/sklearn.neural_network.MLPRegressor.html, n.d.
[70] N. M. Norwawi, Data Science for COVID-19 2021, 547.
[71] ASTM Standard D4966 − 12, Test Method for Abrasion Resistance of Textile Fabrics (Martindale Abrasion Tester Method), ASTM International, West Conshohocken, PA, 2016.

CHAPTER 4

STRETCHABLE FIBER OPTIC-EMBEDDED GAIT MONITORING INSOLE

4.1 Introduction

Demand for daily gait pattern monitoring sensors is rapidly growing. The size of the global smart shoes market was about $226.92 million in 2021, and is expected to expand 16.5% every year between 2022-2027 [1], thanks to rising awareness on fitness and home healthcare through wearable technologies. Consumers also can take advantage of gait monitoring devices to improve physical activity performance, posture, or experiences in virtual/augmented reality. Monitoring over- and under-pronation can attribute to the correction of the wearer's walking/running/loading posture and prevention of ankle injuries [2]. Furthermore, gait monitoring devices can enhance the safety and quality of life of those suffering from gait abnormality issues, such as children with developmental disorders such as cerebral palsy [3], one third of the individuals older than 70 years [4], and 20% of people who survived from a stroke [5]. For example, approximately 20% of children with Autism Spectrum Disorder (ASD) display toe walking, which is a bilateral walking only using forefoot or toes without heel strike at the initiation of a stance [6,7]. Persistent toe walking can tighten the heel cords, restrict ankle dorsiflexion, lead to compensatory abnormal gaits [8]. In case of the elderly, abnormality in postural balance and gait is significantly related to severe injury and even to death [4].

Gait analysis is crucial for an effective treatment and evaluation [3]. Yet, it has been mostly available in lab settings with trained clinicians and expensive medical-level facilities though the collected data is often far from the real-world cases [9]. It could be much less meaningful if a sensor system cannot track the gait pattern of a sport player during a game, the rapidly decreasing mobility of an elderly, or the effect of

daily practice of a child with a developmental disorder when the child has limited time to get an effective intervention [10]. Inertial measurement unit (IMU) sensor has been widely explored for wearable gait tracking systems thanks to the compact size and light weight. However, it often requires to be placed on multiple locations of the body such as ankle, knee, thigh, and trunk and is susceptible to noises [11]. Plantar pressure sensor, on the other hand, is relatively more portable and comfortable for daily-basis gait tracking if it is part of a shoe, an insole, or a sock. Most plantar pressure sensors with high resolution and accuracy are not affordable for the general public ($5,000 – 15,000) and cumbersome due to heavy and rigid components and cords [12]. Other products in an approachable price range (~$300) in the market only provide limited information based on few sensing nodes with repeatability issues [13]. Also, most products in the market adopt resistive or capacitive sensors which need to be insulated to prevent any short or sensor mis-readings in the circuit by sweat or heat generated from the body. Thin dielectric insulation films introduce a slippery, unbreathable, and stiff interface, which is not favorable for the user comfort and safety.

Fiber optics has been introduced as an alternative wearable sensor based on the immunity of light to environmental changes such as humidity, temperature, chemical conditions, and electromagnetic interference [14,15]. While conventional glass- or plastic-based fiber optics with effective light transmittance are too fragile and not resilient to the dynamic movements of the body and textiles, polymer-based elastic optical fibers are suitable for the wearable applications maintaining the advantages of the optical sensors [16]. Furthermore, the thin and lightweight formfactor is suitable to be integrated to textiles for wearables, like weaving, knitting, embroidery, and/or threading [17]. Methods to measure varied aspects of light can track the changes around the human body like Fiber Bragg Gratings (FBGs) using a large and bulky tools, but collecting only one or a few measurands such as light intensity or color is

efficient to keep the system lightweight and small and effective to monitor strain, pressure, and bend of the body and textiles [18–20].

The present study utilized stretchable fiber optics to create a cost-effective plantar pressure sensor suitable for individuals in the general population who engage in moderate levels of activity and require regular monitoring of possible gait abnormalities. Local foot pressure deformed the elastomeric optical fiber, decreasing the light transmittance through the fiber (Figure 4.1), based on the elastomeric fiber optic's resilience against mechanical loads such as pressure and bending and immunity against humidity and temperature changes. The current study investigated the feasibility of stretchable fiber optics for gait monitoring devices through lab and human participant tests. More specifically, the experiments aimed to examine whether the sensor can measure the plantar pressure and center of force of the foot at the level of clinical commercial sensors. Lastly, the paper demonstrated the stretchable fiber optic-based insole device was capable of identifying the distinctive features of an abnormal gait pattern, toe walking. As the fiber optic sensor is durable and cost-efficient, it is promising that those with gait abnormalities or general interest in lower body mobility can benefit from this current device. Additional applications to explore the pressure sensing capability were also discussed.

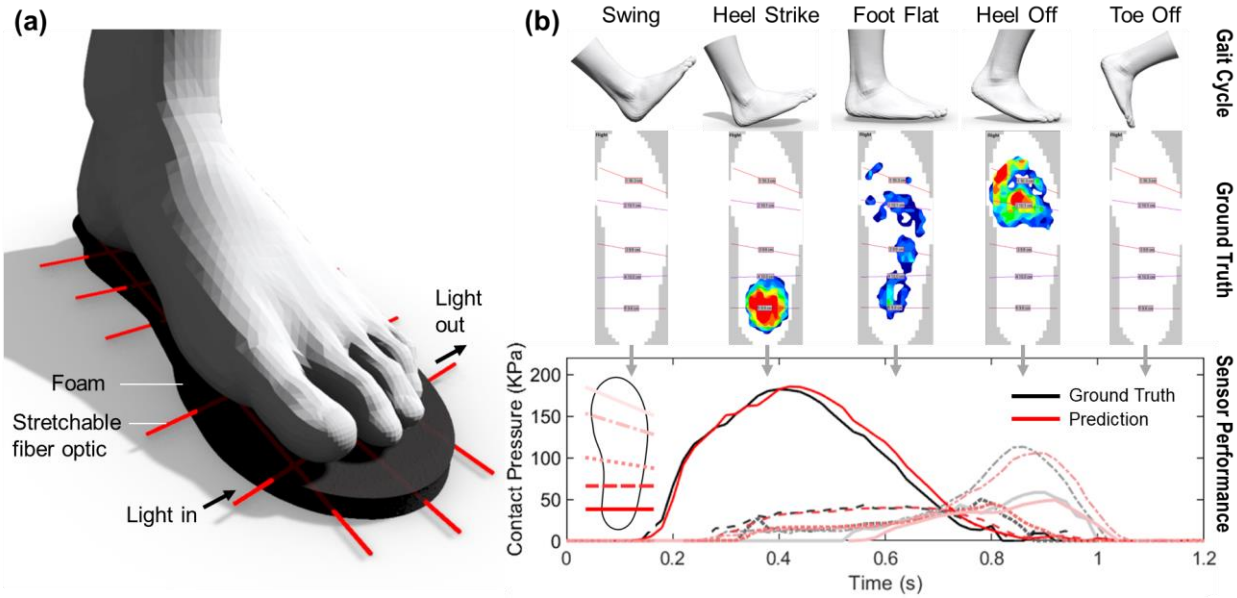

Figure 4.1 Stretchable fiber optic-based pressure sensing insole. (a) Design of the device, (b) a local foot pressure measurement during a stance.

4.2 Design and Prototype

Sensing principle

The gait sensor tracking foot pressure in this study adopted stretchable fiber optics as the main sensing material. Instead of the conventional fiber optics made of fragile materials such as glass, a soft, elastic, lightweight, thin, and transparent polyurethane string (Stretch Magic, Pepperell Braiding Co., Pepperell, MA) was used as the lightguide to be embedded into EVA foam-based footwears. The fiber was connected to a light source on one end and a photodiode (SFH 229, ams OSRAM, Austria) on the other end. A red LED (light emitting diode, Kingbright, Walnet, CA) provided the light with the wavelength of 625 nm into the fiber, considering the low absorption of the near infrared light [19]. When the foot pressure during the stance phase in the gait cycle compressed not only the insoles but also the embedded soft fibers, the transmittance of the light decreases because the cross section of the fiber is deformed

from circular to elliptical (Figure 4.2). While the cross-sectional deformation was the main source of the signal changes, the curvature change of the fiber from the straight line to curves by deformed insole was the secondary reason why the light intensity responded to the foot pressures.

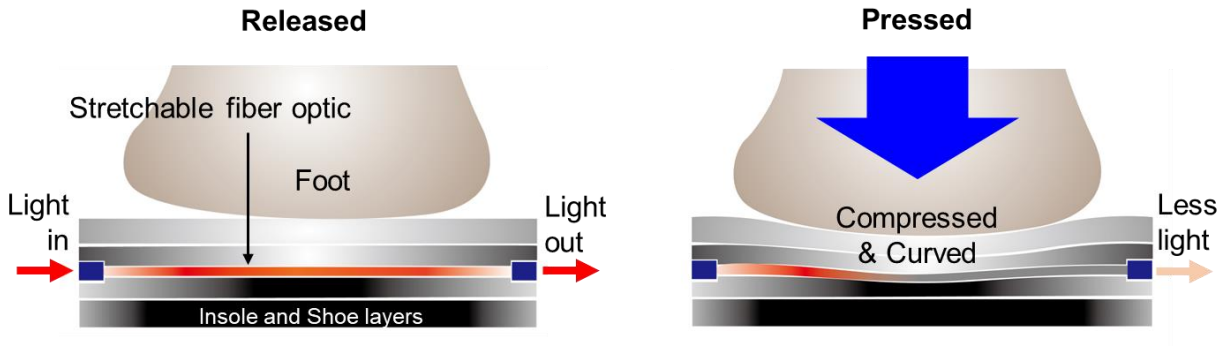

Figure 4.2 Sensing principle.

2.2. Design factor exploration

Lots of factors should be considered in the design process for the best performance of the sensor from the fiber diameter to compressibility of the EVA foam. To examine the effects of the factors and find the best design for the fiber optic gait sensor, 1-3 stretchable fiber optics were installed into an EVA foam cube in the size of 3*3*2 cm. The sensor-embedded foam was placed on the bed of a compression/tensile tester (Instron 5566, Instron, Norwood, MA), and 0, 1, 3, 5, 7, and 9 kg were loaded onto the sample for three seconds respectively.

The diameter of the fiber affects light transmissibility up to ~30 cm and embeddability within <1 cm thick insoles, so fibers too narrow or too thick are not feasible to be part of the gait sensor. The results showed that when the fiber diameter was between 1-1.8 mm, there was no significant difference in pressure sensing capability between the fibers with different diameters (Figure 4.3a). As the fiber itself absorbs the light [19], the thicker fiber with 1.8 mm diameter was chosen to guarantee enough light transmittance on the photo-detecting side.

The plantar pressure is two dimensional: during a stance, the center of pressure proceeds from the rear side of the foot to the forefoot, while it moves between the lateral and medial side of the foot according to the arch shape and gait style. Therefore, multiple parallel fibers in one array may not be able to monitor the two-dimensional movements on the plantar pressure plane. Figure 4.3b shows that when 1-3 fibers were installed into a foam together, they showed almost identical signal changes to the given pressures. It means that the signal response of the two or multiple arrays of fibers to the pressure changes will be the same when they are covering two-dimensional foot pressure plane.

Meanwhile, if two fiber arrays are so close that they create a dent to each other under pressures, then the light leaks more than enough at every intersections of the fibers [20]. Therefore, the buffer layer between the arrays is necessary, which will increase the overall thickness of the insole device. The current prototype embedded only two arrays of fibers to keep the comfortable thickness of the device while covering the two-dimensional foot pressure plane. The two fiber arrays represent the gait movements between anterior/posterior and right/left sides respectively. Figure 4.3c and 4.3d were the explorations to decide the material and its dimension for the prototype. Figure 4.3c shows that when the foam is too thin, the fiber may bear the load from the foot directly and the light loss will significantly increase due to the accelerated fiber deformations. It is possible to calibrate such signal changes, but it is still unfavorable because the user may be able to feel the fiber on the bottom of the foot. In the same sense, if the foam compressibility is too high (i.e., the foam is too soft), the required thickness of the foam would increase, which may make the insole not practical or convenient as a part of a shoe. On the other hand, if the foam is too hard, the comfort that the ergonomic device can give may decrease. Finding a semi-firm foam that performs well as a sensor but also provides enough comfort to the user

would be one of the major issues for the performance footwear development. Figure 4.3d demonstrated the differences in sensitivity by the compressibility of the foam.

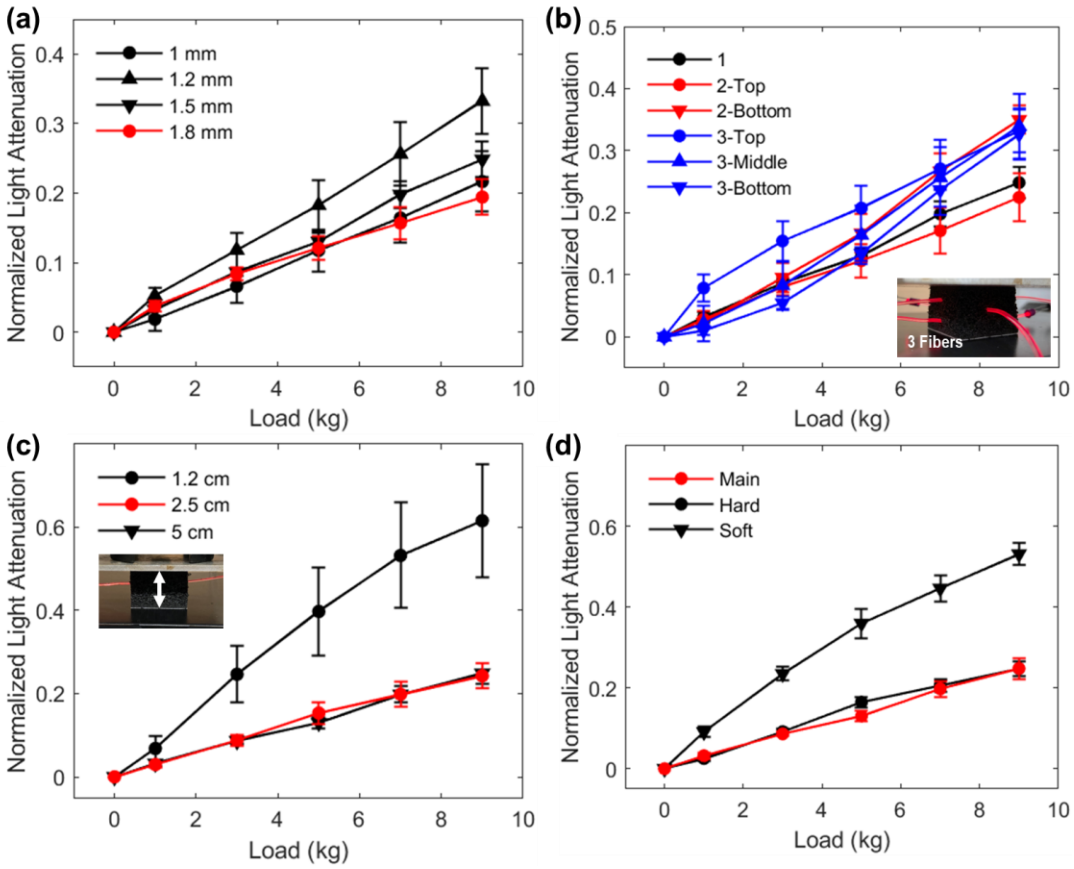

Figure 4.3 Design factors. (a) Fiber diameter, (b) Number of accumulated fibers, (c) Foam thickness, (d) Foam compressibility. Red line plot indicates the materials used in the final prototype.

Prototyping

Based on the explorations on the design factors, the gait monitoring insole using stretchable fiber optics was designed and prototyped (Figure 4.4). The mold for ergonomic insole casting was 3D printed in three different foot length-based sizes. After connecting the LED and the photodiode to each end of the fiber optic, the eight fiber optics (5 for anterior/posterior movements and 3 for right/left) were arranges into

the mold to crucial points on the foot pressure plane, which can be used to infer a foot pressure map in a higher resolution [21]. The two arrays of fibers had a distance from each other so that they were not touching each other nor creating any dents. A polyurethane flexible foam (FlexFoam-iT!™ IV Tuff Stuff, Smooth-On, Inc., Macungie, PA) were poured and cured in the mold. After curing, the electrodes of the light source/detector were soldered onto the custom-designed flexible PCB (printed circuit board). The PCB has resistors to protect the LEDs and potentiometers to adjust the initial amount of the light to prevent complete loss or plateau in light intensity. The flexible PCB was connected to a hard PCB with a microcontroller with wireless communication capability (Arduino Nano 33 BLE) and additional circuits converting currents generated from the photodiodes to voltage changes for analog pins of the microcontroller.

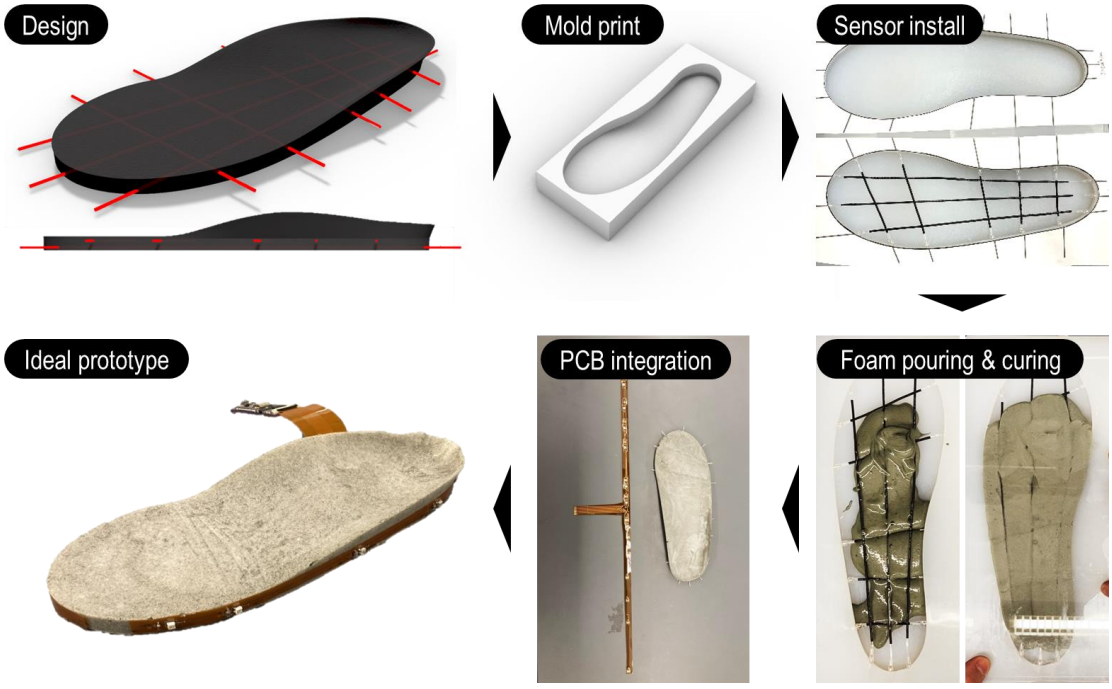

Figure 4.4 Prototyping procedure.

4.3 User Evaluation

Setting

The ideal prototype has a 3D ergonomic shape with arch supports. Yet, it was not compatible with the thin film-style clinical commercial sensor (F-Scan System, Tekscan, Norwood, MA) that this study used to get the ground truth foot pressures. Therefore, the same fiber optics were installed into a flat EVA foam sandal with a similar compressibility to the ideal prototype. Right-side sandals in three different lengthwise sizes were used to embedded to cover different foot lengths of the human participants. The commercial sensor was placed between the foot and the sensor-embedded sole.

Total 11 healthy adults (sex: 8 females and 3 males, age: 36.5 ± 12.1 years, height: 168.9 ± 9.0 cm, weight: 66.4 ± 21.2 kg, BMI: 23.4 ± 7.9, foot length: 248.2 ± 16.6 mm) joined the study upon the agreement on the protocol approved by the Institutional Review Board (IRB). The participants wore the given prototype according to their foot length size along with the commercial sensor. The current device aimed to assist daily and affordable gait monitoring needs among the general population. Therefore, the participants were asked to walk (60 seconds * 3 sessions), run (60 seconds * 3 sessions), stand still with closed eyes (30 seconds * 3 sessions), squat (5 times * 3 sessions), and tiptoe walk (60 seconds * 3 sessions) on the treadmill in an indoor lab environment, to assess the sensor capability to provide a comprehensive daily evaluation of their gait patterns. All the participants could adjust the walking/running speed as they wished. For the tiptoe walking, they randomly mixed normal walking (heel to toe) and tiptoe walking (forefoot only) for the 60 seconds. The task to stand still with closed eyes was included as one of the simplest balance tests, as well as for the purpose to see the residual force when the person is not moving.

Data acquisition and processing

Before every human participant test, the commercial sensor was calibrated by following the instructions recommended by the manufacturer. The commercial sensor collected the two-dimensional foot pressure data in a high resolution at 50 Hz. As the proposed sensor has the array in two directions, it is possible to retract a two-dimensional pressure map, but the common practices in gait analysis usually group the individual point pressures in longitudinal/transverse direction. Therefore, only the pressures on the linear area where the fiber optic was were retracted and compared to the signal from the proposed sensor, so that the sensor readings can be directly used for gait analysis. The microcontroller collected the light intensity through the analog pin at 100 Hz. Before the participants began the tasks, they were asked to raise their legs to measure the residual force not created by their body weight. The sensor readings from each fiber optic sensor were normalized respectively. After joining the two datasets (the commercial sensor and the prototype) in terms of time, the dataset of randomly selected three participants trained a neural network MLP (multilayer perceptron) Regressor model of the Scikit-learn library [22]. The input was the signals from the eight fiber optic sensors, and the expected output was the ground truth value of the target location from the commercial sensor. The model was trained until convergence or maximum 1,000 iterations with the Adam optimizer. The hidden layer size was 64*64*64 and the activation function was ReLU. The test result with the dataset of the other eight participants was described in this paper, with the label of 'Prediction'.

Foot pressure monitoring

The raw light intensity signals and the prediction through the MLP corresponded to the ground truth foot pressure trends. Figure 4.5 displays the foot pressure changes at each sensor location of a stance. Five sensors monitored the anterior/posterior

movements (H1-5), and while three sensors the right/left movements (V1-3). Figure 4.5 shows the sample signal trends from each location: five sensors for the anterior/posterior movements (H1-5) and three sensors for left/right movements (V1-3) of the foot pressure. While the rise, the peak, and the end of the raw signals (blue dotted lines) are well aligned with the plantar pressure trend from the commercial sensor, the MLP model trained by all eight sensors predicted the characteristic changes in trend at each location satisfactorily.

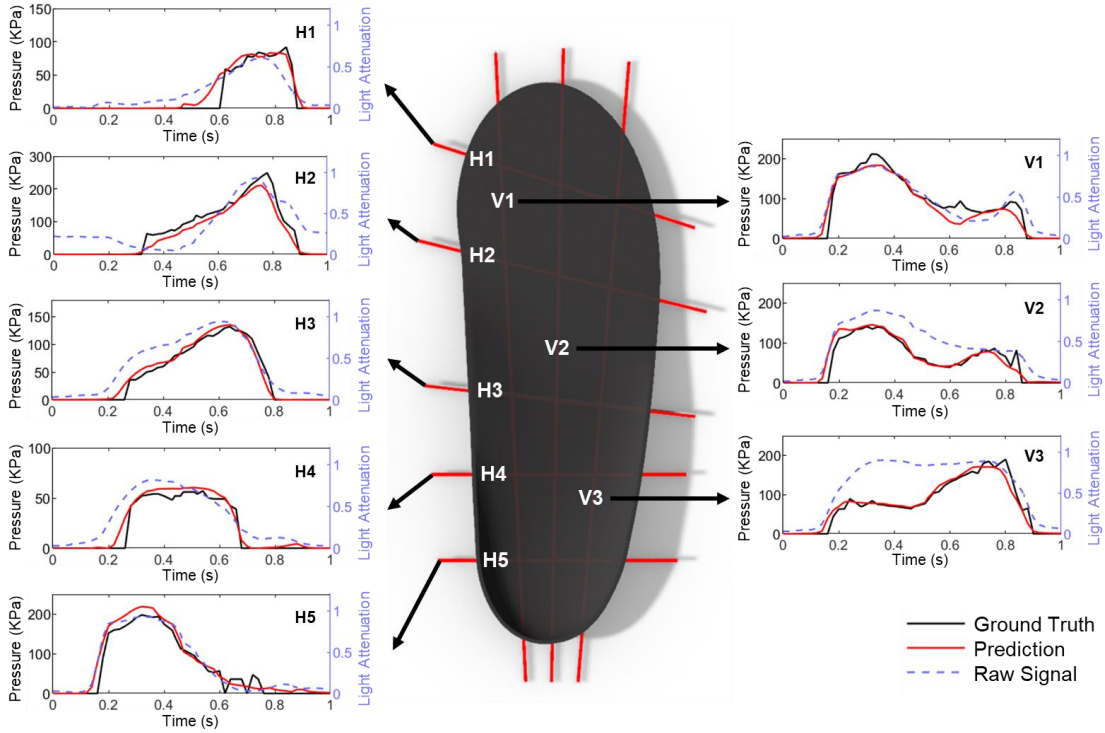

Figure 4.5 Ground truth from the commercial sensor, predicted foot pressure through the MLP, and the raw signal from the sensor of a walk stance.

Overall, the prediction from the MLP model showed a high correlation with the foot pressure values from the commercial sensor (Figure 4.6). The correlation coefficient (r^2) of the eight locations for the walking tasks was high (walk: $r^2 = 0.945 \pm 0.019$). The correlation coefficients (r^2) of the raw signal with the commercial sensor data

were also satisfactory ($Mean_{walk}$ = 0.84, SD_{walk} = 0.06). The foot pressure prediction displayed the root-mean-square error (RMSE) of 14.48 KPa on average (SD = 10.92 KPa).

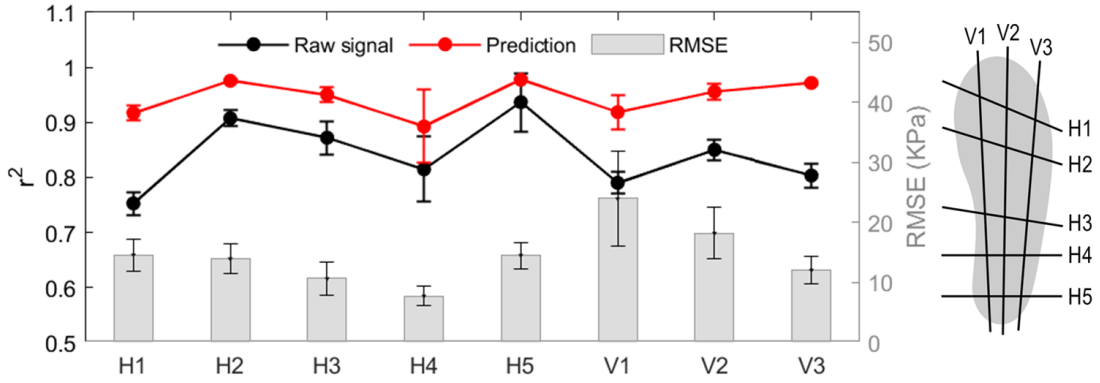

Figure 4.6 Correlation between the results of the fiber optic sensor and the commercial sensor. Bar plot represents RMSE (root mean square error) of the MLP prediction in terms of the ground truth at each location. The error bars represent standard errors.

In addition to walking, the sensor with MLP model could accurately predict other lower body movements such as running (r^2 = 0.919 ± 0.024) and squat (r^2 = 0.709 ± 0.069) as depicted in Figure 4.7. While the H4 sensor showed the lowest correlation during walking (r^2 = 0.892), the H5 showed the lowest (r^2 = 0.819) as some participants preferred forefoot running. The RMSE of the MLP model for running and squat was 15.70 ± 10.96 KPa and 10.53 ± 8.61 KPa respectively.

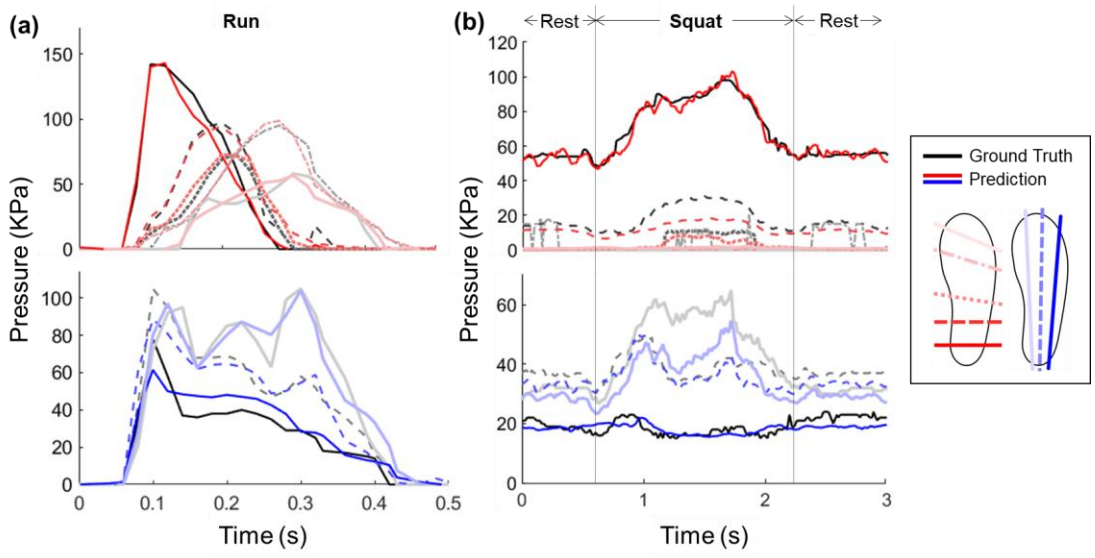

Figure 4.7 Ground truth and prediction from MLP model for running and squats.

Standing still with closed eyes is a widely known diagnostic tool called Romberg Test to identify a neurologic impairment [23]. The result for this task showed the fiber optic-based insole's sensitivity to static posture. The commercial sensor used in the current study filtered out the forces smaller than 10% of the expected maximum value to remove the residual force unrelated to the gait patterns. It resulted in failing to catch subtle foot pressure changes especially when the user is static, unlike the newly developed sensor of this study (Figure 4.8). The filtering policy of the commercial sensor partially influenced the lower correlation between the fiber optic insole and the ground truth both in standing still ($r^2 = 0.467 \pm 0.116$) and squat.

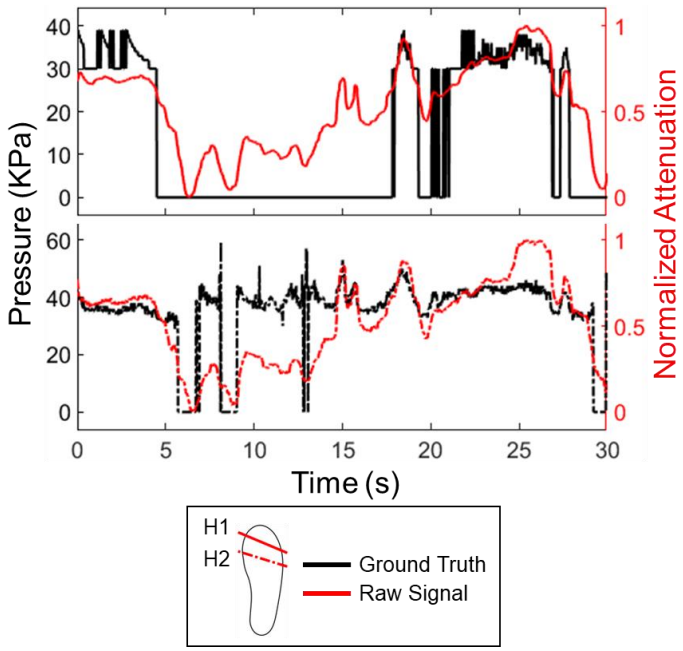

Figure 4.8 Ground truth and the raw signals for locations H1 and H2 for standing still.

Because foot morphology is different by sex in general [24], the correlations between the ground truth and the raw signal were analyzed through a nonparametric method, the Wilcoxon rank sum test (Figure 4.9a). The p value at H1, H3, and V3 were below 0.01, indicating the sensor performance may be significantly better in male users. The low performance in V3 might be related to the slimmer foot shape of the females. However, the current study did not collect the foot measurements but the foot length, and only recruited the low number of the participants, so the sensor performance by sex should be examined with a larger population in the future.

In the same sense, the correlation coefficient between the two sensors at H1, H3, and V3 showed a significant relation with weight (H1: r^2=0.44, p=0.01, H3: r^2=0.45, p<0.01, V3: r^2=0.47, p<0.01). Foot length was also related to the sensor performance at H4 (r^2=-0.54, p<0.01) and V3 (r^2=0.45, p<0.01). Yet, the scatter plots of the coefficients by weight or foot length imply that the significance might came from some of the outliers (Figure 4.9b and 4.9c), so the causal effect of the weight or the

foot length of the user on the sensor accuracy should be examined through testing with a larger scale.

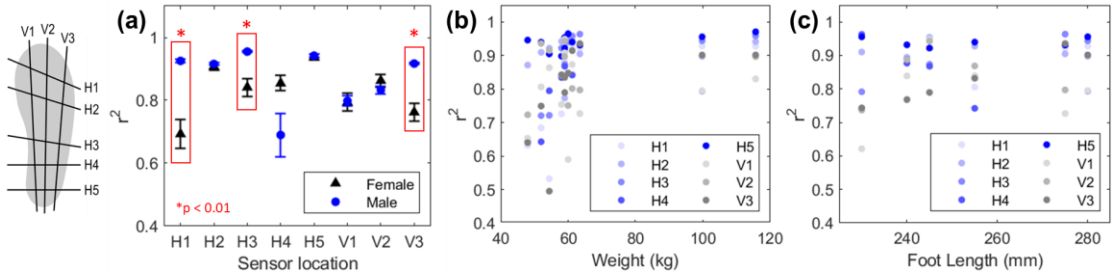

Figure 4.9 Correlation coefficients between the ground truth and the raw signal by sex, weight, and foot length.

Center of Force

Center of force (COF), one of the major measurands for gait analysis, is the centroid of all forces applied on the plantar surface of the foot [25]. COF and its trajectory provide valuable information regarding the balance and velocity of gait and foot morphology [26]. Following the formulae used in the commercial sensor[27], the signals less than 10% of the maximum value from the fiber optic sensors were filtered out as the residual pressure, and processed to get $X_{cof} = \sum_{k=1}^{3} k * V_k / (\sum_{k=1}^{3} V_k)$, and $Y_{cof} = \sum_{k=1}^{5} k * H_k / (\sum_{k=1}^{5} H_k)$ where V_k and H_k are the normalized signal values representing the light attenuation of kth vertical/horizontal sensor (e.g., when k=1, the normalized light attenuation at V1 or H1) respectively. The results calculated following the formulae with the raw signal showed a fair performance (r^2_y=0.82, r^2_x=0.78) for the walk tests, whilethe prediction by the MLP model outperformed with high correlation coefficients (r^2_y=0.96, $RMSE_y$=2.63 cm, r^2_x =0.96, RMSEx=0.85 cm) as described in Figure 4.10.

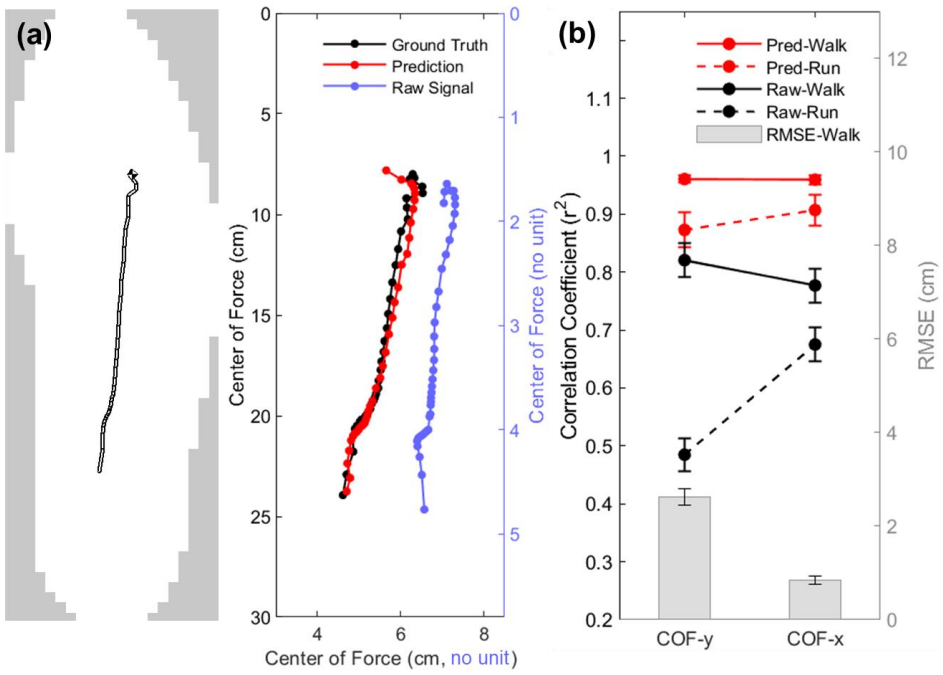

Figure 4.10 Center of Force (COF) prediction. (a) Ground truth from the commercial sensor, the MLP prediction, and the calculated COF using the raw signals, (b) correlation coefficients between the fiber optic sensor (raw signal and MLP prediction) and the commercial sensor, and RMSE of the MLP prediction results compared to the ground truth.

Case study: Toe walking

One of the major symptoms of the children with ASD is toe walking, which uses only forefoot area when walking. To address their needs for daily gait monitoring and to verify the capability of the sensor to identify abnormal gait patterns, this study asked the recruited healthy adults to mix normal walking and toe walking randomly as one of the tasks. The result showed that when the participant toe-walked, there was no response from the horizontal sensors around the rearfoot (Figure 4.11). The three vertical sensors covering the whole foot also showed different pressure trends with a single peak, compared to the normal walking with double peaks generated at heel and ball of the foot. The COFy clearly stayed within the forefoot area during the toe

walking. The result also demonstrated a high correlation between the two sensors ($r^2_{pressure}$ = 0.933 ± 0.02, r^2_{COF} = 0.944 ± 0.009).

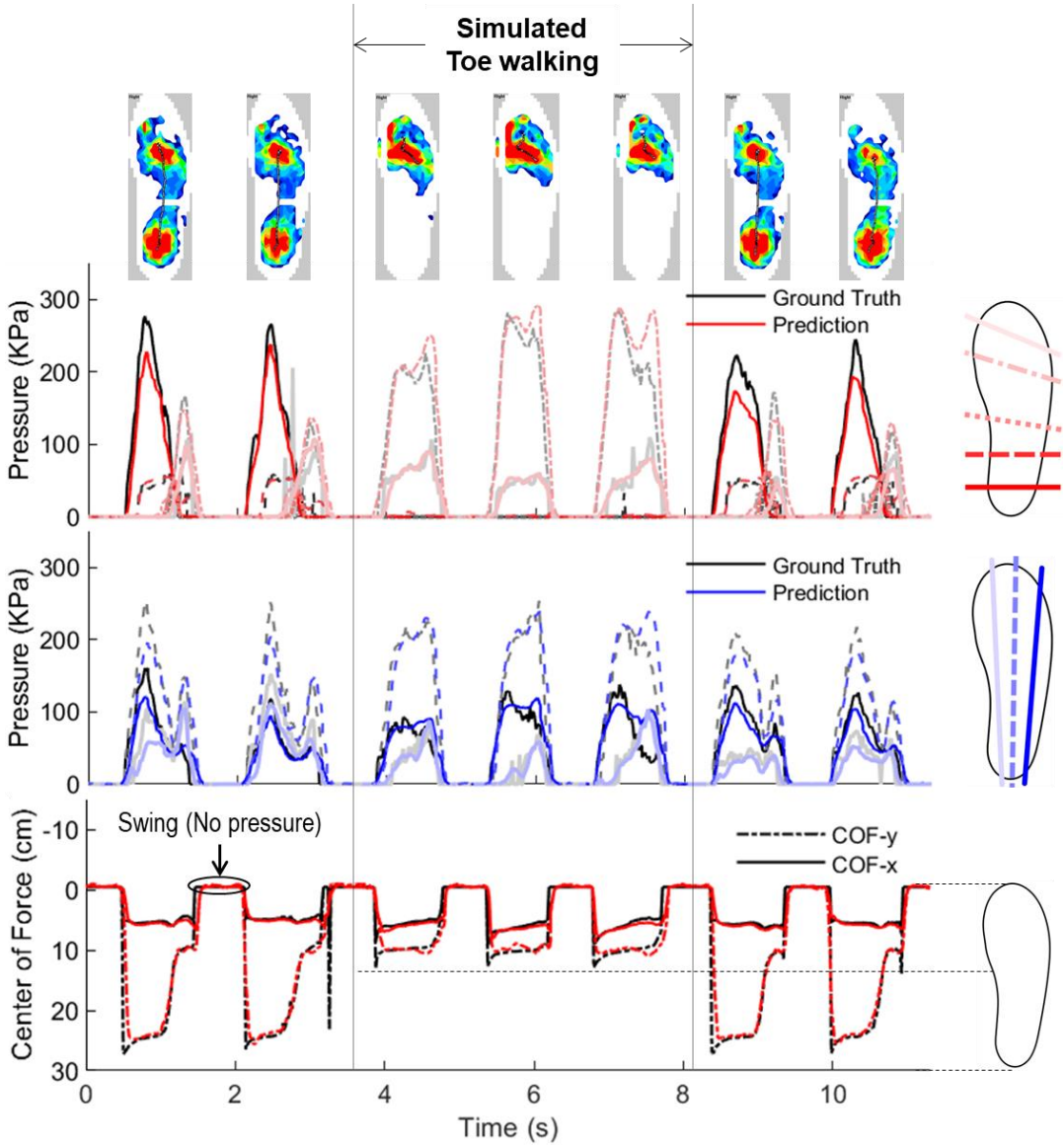

Figure 4.11 Toe walking. (Top) Anterior/posterior movement, (Middle) Right/left movement, (Bottom) COF changes by axis.

4.4 Discussion and Conclusion

In this study, stretchable fiber optic arrays embedded into flexible foam-based footwear tracked the plantar pressure of the wearer. When the foot presses down the

insole, the elastomeric fiber optics were compressed, which decreased the transmittance of the light. The light intensity measured on the other side of the light source showed high correlations with the data from a clinical device in the market. The two arrays could infer the trajectory of the center of force (COF) of each stance, which will enable advanced gait analysis to detect under/over-pronation. Furthermore, a deep learning model trained by the data of two 1-minute sessions of each participant could predict the last 1-minute session accurately. The sensor demonstrated its capability to identify toe waking, one of the characteristic abnormal gait patterns of children with autism spectrum disorder (ASD), with individual foot pressure trends and center of force trajectory. The study also investigated the effect of design factors such as fiber diameter or foam compressibility.

As demonstrated, the sensor was focusing on younger populations with developmental disorders suffering from gait abnormality, with an intention to provide an option for affordable, accurate, and convenient plantar pressure monitoring devices. With increasing needs in daily-basis home healthcare, the children, their families, and medical professionals can benefit from the device to track the progress in the gait abnormalities and provide instant and continuous feedback for better corrections. The other populations with gait issues such as stroke patients, the elderly, or those in rehabilitation can use the product for the fall risk management and improvement process for the lower body performance. Also, patients with diabetes often have serious issues on the foot when the shoe does not fit, and the fiber optic sensors installed not only on the sole but also around the upper side of a shoe will be able to identify unnecessary pressures from the ill-fitting footwear. Lastly, the device can also assist athletes and the general public to enhance their lower body performance by providing insights about their gait trends.

The foot pressure sensing and abnormal gait identifying capability of the current

sensor can support the safety of those working in harsh environments such as fireground, underwater, or a high electromagnetic field, by assisting localization, fall detection, or fatigue tracking. Moreover, unlike the weak and inextensible electric connections in most commercial sensors, the current sensor allows stretchability and resilience against external bending or tensile loads, allowing durability and versatility for dynamic activities. Meanwhile, infrared (IR) light therapy can relieve muscle pain and accelerate recovery after workout [28]. Though it was not investigated in the current study, the user of IR light LED as a light source may be able to provide muscle relief functionality in addition to the foot pressure measurement.

The current study introduced the fabrication process for the ideal prototype as an ergonomic insole, but used another sandal-style prototype for the user evaluation to have the flat surface compatible with the commercial sensor. The ideal prototype may generate a bit different result because of the ergonomic shape with arch supports, but the sensors are expected to behave in the same way as the sensor used in the evaluation process. Another weakness of the ideal prototype was the flexible PCB that contains LEDs and photodiodes which are indispensable for fiber optic sensors. When the insole device is in a shoe, the foot sometimes moves unexpectedly and steps on the flexible PCB. As the PCB is attached on the side, the foot pressure can fold the PCB and break the electrical connections, which should be carefully protected in further development. While the current study collected the data at a limited sampling rate of 100 Hz, which is generally sufficient for normal walking patterns and higher than the rate of the commercial device used in this study. However, a higher sampling rate should be achieved for the vigorous sensing of fast sports activities or slip/fall detection.

The current study embedded fiber optic into a flexible foam, one of the most common materials for footwear. However, the fibrous formfactor of the optical fiber has

extensive possibility to be embedded into other materials. For example, optical fibers can be woven/knitted/embroidered to a textile to create gait monitoring socks or local pressure sensing garments or gloves Also, other types of agents such as animals or robots will be welcomed to adopt the fiber optic pressure sensor to evaluate their mobility and dexterity. Lastly, the current sensor does not have to be limited to wearable applications but also is open to the varied situations to monitor pressures. Considering the stability against environmental changes and stretchability of the current sensor, the pressures around the unconventional, uneven, or dynamic surfaces should be able to suitable to maximize the pressure sensing capabilities of the stretchable fiber optics.

REFERENCES

[1] IMARC Group, “Smart Shoes Market: Global Industry Trends, Share, Size, Growth, Opportunity and Forecast 2022-2027,” can be found under https://www.researchandmarkets.com/reports/5562587/smart-shoes-market-global-industry-trends, n.d.

[2] L. E. Cain, L. L. Nicholson, R. D. Adams, J. Burns, Journal of Science and Medicine in Sport 2007, 10, 311.

[3] S. Armand, G. Decoulon, A. Bonnefoy-Mazure, EFORT Open Reviews 2016, 1, 448.

[4] J. Verghese, A. LeValley, C. B. Hall, M. J. Katz, A. F. Ambrose, R. B. Lipton, Journal of the American Geriatrics Society 2006, 54, 255.

[5] G. E. Gresham, T. E. Fitzpatrick, P. A. Wolf, P. M. McNamara, W. B. Kannel, T. R. Dawber, New England Journal of Medicine 1975, 293, 954.

[6] X. Ming, M. Brimacombe, G. C. Wagner, Brain and Development 2007, 29, 565.

[7] J. J. Ruzbarsky, D. Scher, E. Dodwell, Current Opinion in Pediatrics 2016, 28, 40.

[8] W. J. Barrow, M. Jaworski, P. J. Accardo, J Child Neurol 2011, 26, 619.

[9] L. C. Benson, C. A. Clermont, E. Bošnjak, R. Ferber, Gait & Posture 2018, 63, 124.

[10] E. A. Fuller, A. P. Kaiser, J Autism Dev Disord 2020, 50, 1683.

[11] P. B. Shull, W. Jirattigalachote, M. A. Hunt, M. R. Cutkosky, S. L. Delp, Gait & Posture 2014, 40, 11.

[12] “F-Scan System,” can be found under https://www.tekscan.com/products-solutions/systems/f-scan-system, n.d.

[13] S. Karki, J. Lekkala, 18th IMEKO World Congress 2006: Metrology for a Sustainable Development 2006, 3.

[14] B. Lee, Optical Fiber Technology 2003, 9, 57.

[15] V. Sanchez, C. J. Walsh, R. J. Wood, Advanced Functional Materials 2021, 31, 2008278.

[16] H. Ma, A. k.-Y. Jen, L. r. Dalton, Advanced Materials 2002, 14, 1339.

[17] Z. Gong, Z. Xiang, X. OuYang, J. Zhang, N. Lau, J. Zhou, C. C. Chan, Materials

2019, 12, 3311.
[18] H. Bai, S. Li, J. Barreiros, Y. Tu, C. R. Pollock, R. F. Shepherd, Science 2020, 370, 848.
[19] C. K. Harnett, H. Zhao, R. F. Shepherd, Advanced Materials Technologies 2017, 2, 1700087.
[20] J. Jo, A. Xu, A. K. Mishra, H. Bai, A. Derkevorkian, J. Rabinovitch, H. Park, R. F. Shepherd, Advanced Materials Technologies n.d., n/a, 2200437.
[21] F. Mun, A. Choi, J NeuroEngineering Rehabil 2022, 19, 4.
[22] "sklearn.neural_network.MLPRegressor," can be found under https://scikit-learn/stable/modules/generated/sklearn.neural_network.MLPRegressor.html, n.d.
[23] J. Forbes, S. Munakomi, H. Cronovich, in StatPearls, StatPearls Publishing, Treasure Island (FL), 2023.
[24] J. Jo, S. Sokolowski, M. McQuerry, L. Griffin, H. Park, Applied Ergonomics 2022, 102, 103753.
[25] V. Lugade, K. Kaufman, Gait & Posture 2014, 40, 719.
[26] C. Mizelle, M. Rodgers, L. Forrester, Gait & Posture 2006, 24, 356.
[27] "FAQs | Tekscan," can be found under https://www.tekscan.com/support/faqs?search_api_fulltext=calculate&antibot_key=wtdtThYdH6bRfpa_oEGbDB9xgJlElAKyLYX8KTKuh-M, n.d.
[28] B. Selm, M. Rothmaier, M. Camenzind, T. N. Khan, H. Walt, Journal of biomedical optics 2007, 12, 034024.

CHAPTER 5

BATTERY-FREE HEAD ORIENTATION MEASUREMENT USING PASSIVE RFID TAGS FOR LATERAL GLANCE DETECTION FOR CHILDREN WITH AUTISM SPECTRUM DISORDER

5.1 Introduction

Children with developmental disorders such as autism spectrum disorder (ASD) often display characteristic visual symptoms such as toe walking, gaze aversion, or hand flapping [1]. Among them, lateral glance, looking at objects out of the eye corners, is the atypical visual behavior observed most frequently among children with ASD [2]. The reason why the children with ASD prefer to use peripheral vision instead of the central is still under investigation, but it is known that the behavior responds to moving stimuli and be related to the reduced sensitivity in peripheral field of their vision [3–5]. One of the biggest consequences of the lateral glance is a challenge in social interactions, as maintaining the appropriate eye-to-eye contact is an essential skill in building relationships [6]. Lateral glance correlates with interpersonal relationships negatively [7], which eventually affects the low employment rate of the individuals with ASD along with other deficits in social interaction skills [8,9]. When communicating, children with ASD showed a significantly lower and shorter visual attention on the other person, while extensively exploring the lateral field of their vision and looking downwards, compared to the children without developmental challenges [10]. Tracking the gaze along with the lateral vision is important in diagnosing of the ASD, as well as optimizing the interventions that potentially improve the social skills of those with ASD [8,11,12].

Thanks to the recent advances in computer vision, the eye pupil or gaze tracking using cameras is achievable [13]. However, the currently available eye trackers often require

the users to wear either head-mounted or glasses-type devices with rigid and fragile cameras near the eyes [14], which may not be ideal in terms of the safety of the children with ASD considering their behavioral unpredictability in healthcare environments [15]. Camera-based systems with a distance is another main stream of gaze trackers [16], but continuously capturing the whole face cannot completely avoid with the privacy concerns [17,18]. Expensive cost for accurate systems (hundreds of dollars) and low feasibility (mean error of ~10 degree) of the affordable options [19] are also major concerns in the view of the patient and their families. On the other hand, monitoring of the eye movement without using vision-based sensors is challenging due to vulnerability of the eyeball and subtle movement of the eye muscles [20].

As eye gaze is a coordinated output of eye and head movements [21–23], head orientation often serves to estimate the gaze or the accompanied social attention [24,25]. The usability difference between head-gaze and eye-gaze has been a popular topic in virtual reality (VR) research, for the head orientation decides the field of view and often represented the eye gaze alternatively as an easier and affordable method [26–28]. Systems connecting the head pose and the attention provide seamless interactions between the users and the robot agents [29,30] or make the vehicles ready for upcoming direction changes for the drivers or wheelchair users [31,32]. Mouse cursor control through head movements for individuals with tetraplegia or cerebral palsy can be an alternative interaction technique to gaze-based mouses [33,34]. Furthermore, head motion sensors also contribute as medical applications for diagnosis or rehabilitation of those with motor disorders [35–37]. In case of the children with developmental disorders, the head motor impairments are important signals in diagnosis and progress of the diseases including ASD and cerebral palsy [38–40]. Inertial measurement unit (IMU) or cameras are the widely explored

approaches, and radiooculogram, LiDAR, electromyography (EMG), or microphone has been adopted to identify the head motion as well [18,41–45].

Yet, even non-vision-based wearable head orientation sensors mostly consist of rigid electronic parts including batteries and microcontrollers, which is not preferred in case of the active children with developmental disorders. Among wearable battery-free sensors, passive RFID (radiofrequency identification) tags are suitable for creation of soft, comfortable, lightweight, and low-cost wearable head motion sensor with wireless communication capability [46,47]. Passive RFID tag sensors are capable of tracking of temperature, pressure, humidity, motion, and/or bending by harvesting the radio wave from an RFID reader [48,49]. Design of a wearable RFID-based sensor should consider the radio wave absorbance by body location, distance from the reader, and accompanied body motions [50].

The current study introduces a wearable sensor system for children with ASD to monitor their head orientation to detect the lateral glance behavior. Pairs of passive RFID tags embedded into eye glasses, head pieces, and/or a face mask track the head movements of the wearer when the user is sitting in front of a screen with an RFID reader (Figure 5.1a). The sensor response corresponded to the head motions when the user rotated the head randomly, with high mean correlation coefficient $r^2 = 0.88 \pm 0.11$ (Figure 5.1b). This paper also demonstrated that a pair of RFID tags attached at each end of the frontal side of eyeglasses worked ideally in the scenario where the user is using an RFID reader-embedded laptop.

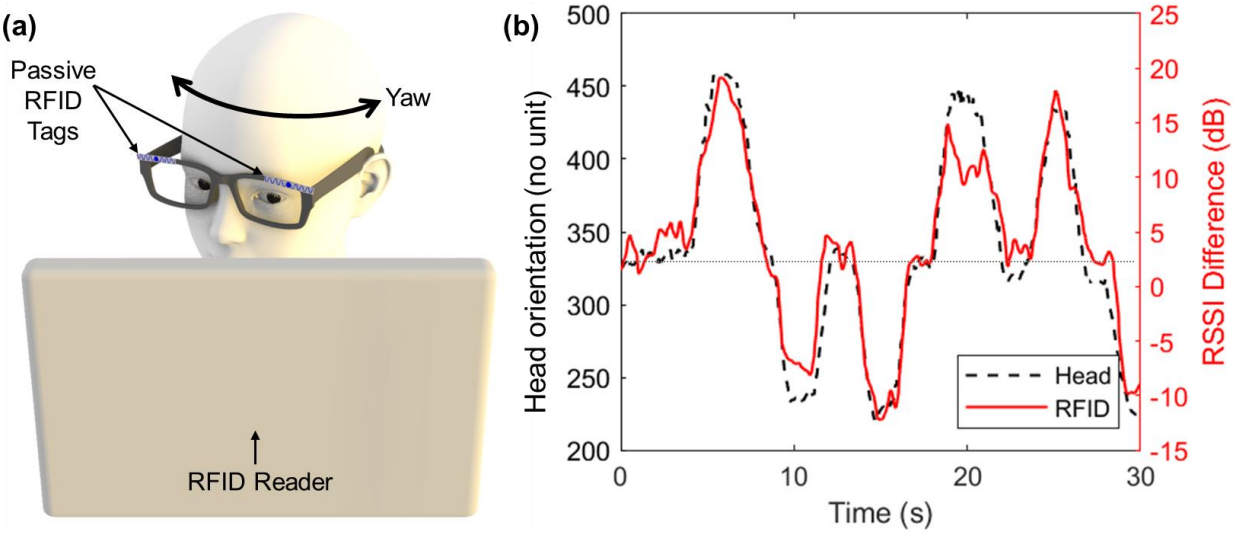

Figure 5.1 Passive RFID tag-based head orientation sensor. (a) Sensor design, (b) Random head orientation and the sensor response. The yaw angle of the head orientation is represented by the x-coordinates of the direction of the head pose projected onto a 2D plane. The range of values for yaw is 0 to 720. The horizontal gray dotted line at the center of the plane represents the direction of looking straight ahead on the screen.

5.2 Sensing Principle and Design

Sensing principle

The strength of the backscattered signals depends on the distance between the radio wave source and the tags according to the Frii's free space loss: $P_R = P_T \left(\frac{\lambda}{4\pi r}\right)^2 \Psi_T \Psi_R$, where P_R and P_T are the strength of the signal of the receiver and transmitter respectively, r is the distance between the transmitter and the receiver, λ is the signal wavelength, and Ψ_R and Ψ_T are gains of the antenna of the receiver and transmitter respectively [51]. The current system located a pair of passive tags on each side of the forehead (e.g., each end of the foreside of the eyeglasses, Fig. 1a) to track the head rotation in the transverse plane (yaw). When the wearer turns the head left, the RFID tag on the left side becomes far from the reader, while the distance on the

other side gets closer. It results in a decrease in the received signal strength indicator (RSSI) of the left tag, and an increase of the right tag signal strength (Figure 5.2). As this system supposes a scenario where the user is continuously looking at the screen of an RFID reader-embedded device, the rotated head means the child is using the peripheral vision instead of the central one.

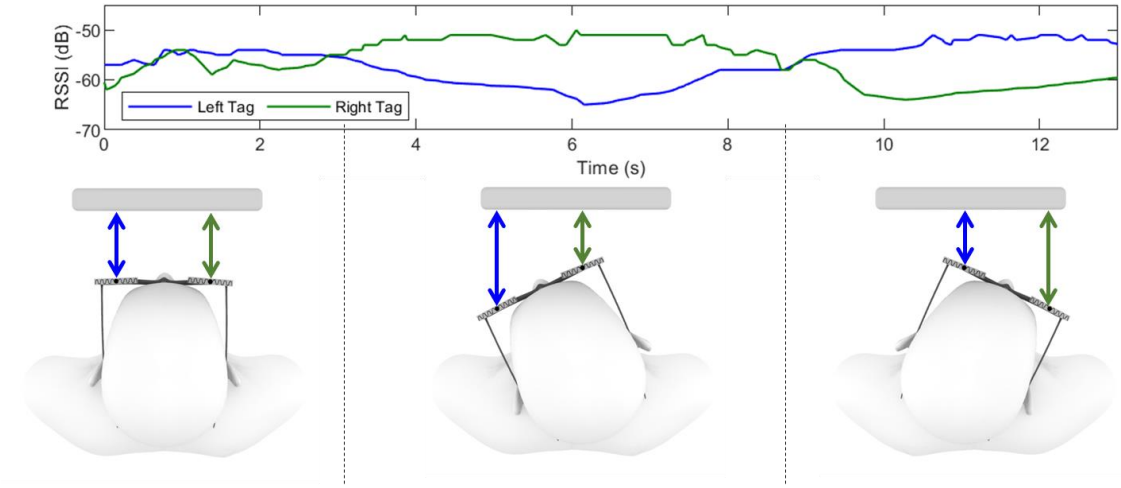

Figure 5.2 Sensing principle. The color of the lines in the plot matches the arrow color in the illustrations.

Sensitivity by distance from the RFID reader

Consumer electronics with a screen can embed an RFID reader, but the distance between the device and the user's head is typically different by the type of the devices. For example, smartphones will be closer to the eyes of the user compared to televisions. To examine the effect of the distance between the RFID reader and the tags, the sensor-worn manikin head rotated from -60^{o} to 60^{o} at 25, 50, 75, 100, and 150 cm distance, with considerations on different scenarios including smartphone, tablet, laptop, or television. The system showed the biggest difference between the tags on each side when they are 50 cm apart from the reader (Figure 5.3a). As expected, the sensitivity represented by the RSSI difference decreased when the

distance from the RFID reader became far. The sensor was still capable of responding to the angular changes at 100 and 150 cm distances, but the low mean RSSI implies that it may not be an ideal setting for stable and continuous sensing (Figure 5.3b).

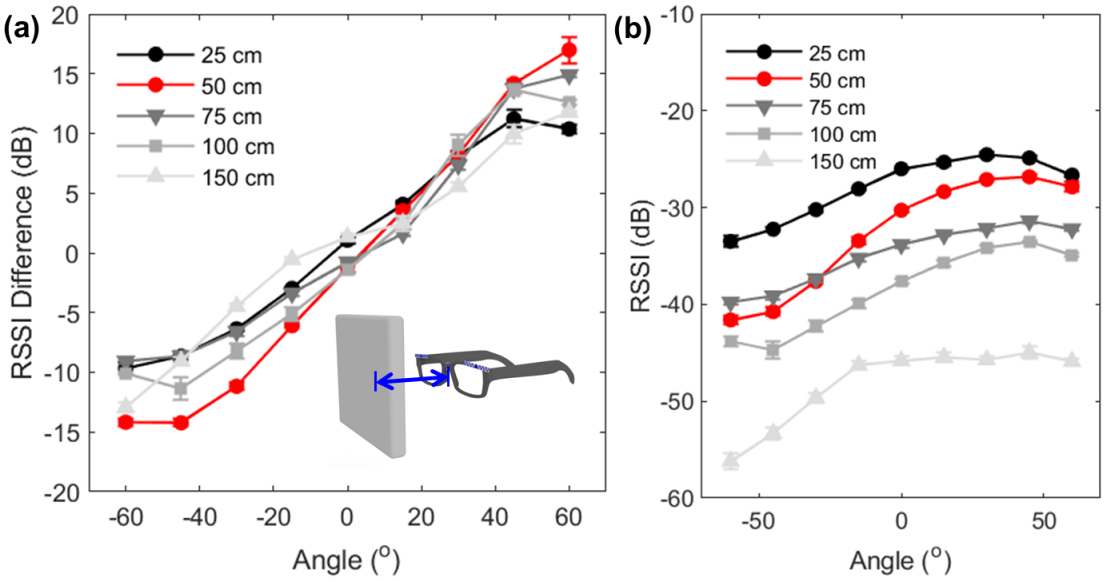

Figure 5.3 Sensor performance by distance from the RFID reader. (a) RSSI difference by distance from the reader, (b) Mean RSSI of the left tag by the distance from the RFID reader. Error bar indicates standard error and red line plot represents the selected setting for the user evaluation study.

Sensitivity by distance between the tags

Distance between the two tags can affect the sensitivity, as it decides the changes in the distance of each tag from the reader. The results of the exploratory experiment indicated that when the center-to-center distance of the two tags were 13 cm, the RSSI difference was the biggest within the -60° ~ 60° angle range in terms of the reader (Figure 5.4). The longest distance (20 cm, not linear measurement but on the surface), achieved by placing the tags on each leg of the glasses, did not generate a better performance. Closer distances, resulting in smaller differences in distance from the reader, also reduced the sensitivity. This corresponded to the failure of vertically

arranged tags to track the pitch head movements on the sagittal plane (Figure 5.8). The distance between the vertically arranged tags was only 25 mm, and the correlation coefficient r^2 between the RSSI difference of the tags and the head movement was unsatisfactory (< 0.5).

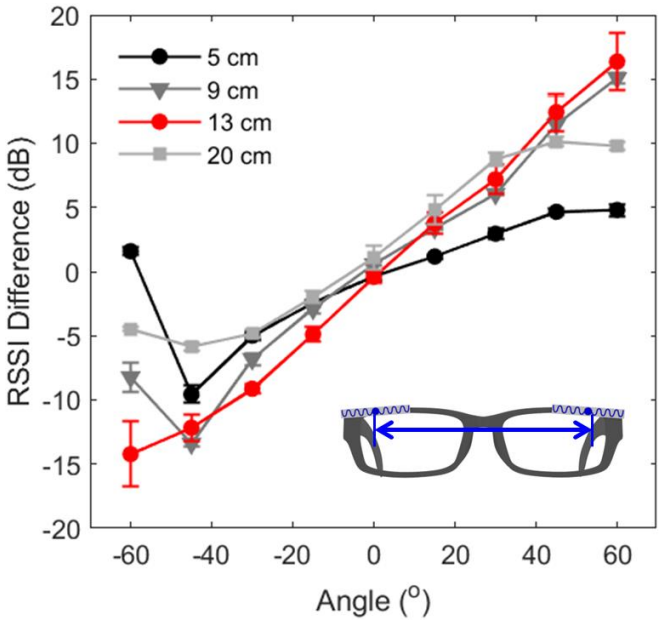

Figure 5.4 Sensor performance by distance between the tags. Error bar indicates standard error and red line plot represents the selected setting for the user evaluation study.

Sensitivity by RFID tag type

As signal strength of passive RFID tags relies on the dimension, shape, and material of the antenna, the current study examined five different types of off-the-shelf RFID tags for the system: three made of PET (polyethylene terephthalate), one textile, and the other ceramic (Figure 5.5a). The tag C consisting of a canvas textile and a conductive thread antenna showed the biggest RSSI difference between the two tags overall (Figure 5.5b). Meanwhile, inlay-style tags made of PET, which is the most common in the market, showed better performances in tag counts and RSSI than the textile tag

(Figure 5.5c and 5.5d). The tag E encased by ceramic did not show any favorable results. The tag A showed the highest RSSI and tag count thanks to the biggest dimension, but the sensitivity was moderate, and the large dimension may not be suitable to be part of eyeglasses or headpieces. For the user evaluation, the tag B with a fair sensitivity, signal strength, and appropriate dimension was implemented.

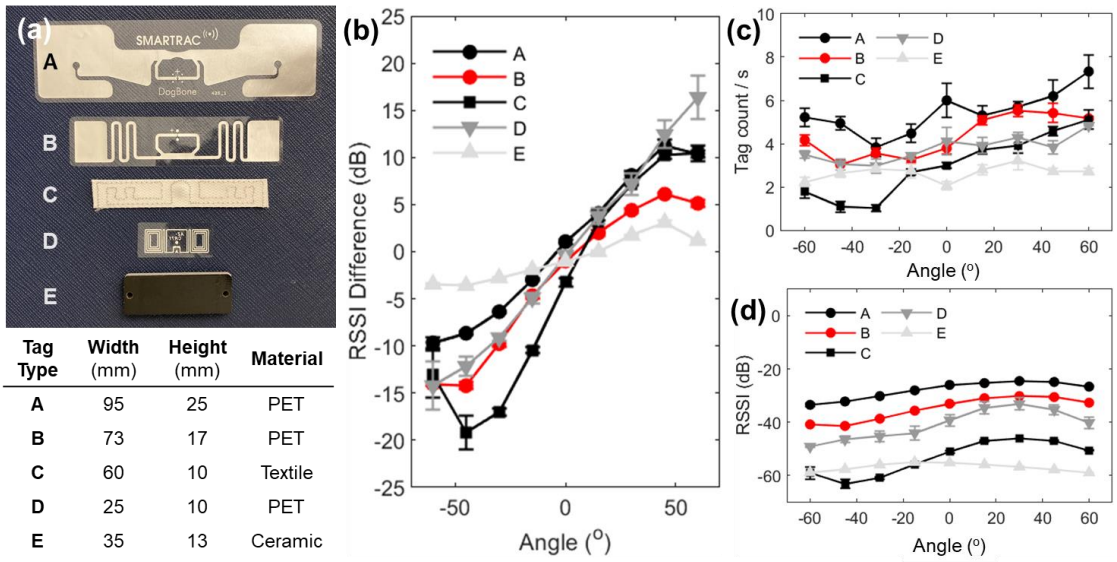

Tag Type	Width (mm)	Height (mm)	Material
A	95	25	PET
B	73	17	PET
C	60	10	Textile
D	25	10	PET
E	35	13	Ceramic

Figure 5.5 Sensor performance by type of passive RFID tag. (a) Information of the tags used in this study, (b) Sensor performance by tag, (c) Mean tag counts per second by tag, (d) Mean RSSI by tag, (e) Laundry tag example. Error bar indicates standard error and red line plot represents the selected setting for the user evaluation study.

5.3 User evaluation

Setting

10 healthy adults (7 females and 3 males, age: 25.5 ± 5.5 years, height: 168.3 ± 9.5 cm) participated based on the agreement with the experiment protocol approved by the Institutional Review Board (IRB). The participants wore safety glasses where two pairs of RFID tags were attached and sat on a chair in front of a desk. An RFID antenna (S9028PCR, Rfmax, NJ, USA), connected to an RFID reader (Speedway

Revolution R220, Impinj, WA, USA), was right above the screen of a laptop on the desk. The built-in webcam of the laptop was on top of the screen, right below the RFID antenna. The distance between the antenna/laptop screen and the face of the user was 50 cm. As the first task, the participants randomly rotated their head for 1 minute, while fixating their gaze anywhere on the laptop screen. After three sessions of the first task, the participants used the laptop without any instructions as they usually do for five minutes.

Data acquisition and processing

The laptop camera captured the user face at 30 Hz during the tasks. A computer vision python library finding landmarks from a face, MediaPipe [52], collected x and y coordinates of the head orientation, eye pupil, and corner of the eyes (near the center) captured on the screen [53]. The distance between the eye pupil and the eye corner represented the discrepancy of the head orientation and the gaze (i.e., lateral glance), labeled as 'Pupil – Eye Corner' in the following figures in this paper. The current method requires RSSI from the tags on both sides to draw the difference. However, the RFID reader used in this study cannot read multiple tags simultaneously but randomly chooses only one tag at a time, which means when the RSSI of a tag was reported, the value from the other tag was missing. Therefore, the missing values were filled through linear interpolation in Matlab by using the adjacent data. The RSSI differences from the two pairs of the tags were averaged and smoothed through the moving-average method (window = 5). Lastly, the obtained vision data through the camera and MediaPipe was joined with the backscattered signal dataset of the passive RFID tags to calculate the correlation between the two datasets.

Sensor performance

The passive RFID tag-based sensor showed a high correlation with the head and eye pupil movements respectively when the user rotated the head randomly (Figure 5.6a). The correlation coefficient (r^2) of the sensor was 0.88 with the head pose, and 0.83 with the left eye pupil. The distance between the pupil and the eye corner showed a relatively lower coefficient ($r^2 = 0.50$). It may reveal the limitation of the current sensor system tracking not the gaze itself but the head pose. However, considering most eye trackers in the market use multiple cameras, the current experiment setting with a single webcam might not be ideal to accurately track the gaze movements. Meanwhile, the sensor performance during the free laptop usage was not as impressive as the case of the random, slow, and continuous head rotations. Correlation coefficient r^2 between the sensor and the head, left eye pupil, and the distance between the pupil and the eye corner was 0.59, 0.49, and 0.30 respectively. The free laptop usage with no specific instructions involved less head movement compared to the intended and continuous head movement, while the noises became more distinguishable (Figure 5.6b). Lower signal-noise-ratio (SNR) during the free laptop usage (-1.32 ± 6.32 dB) compared to the intended movements (9.90 ± 6.81 dB) confirms the higher influence of the noises.

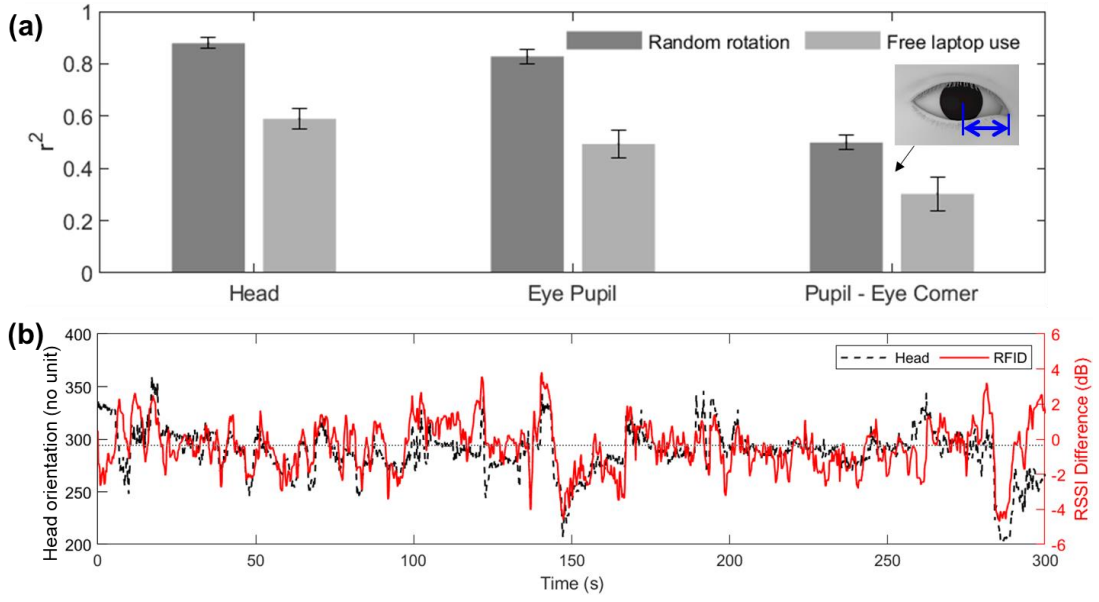

Figure 5.6 User evaluation results. (a) Mean correlation coefficient between the sensor and the head, eye pupil, and distance between the eye pupil and the eye corner during random head rotations. Error bars represent the standard error. (b) Head orientation from the vision and the sensor during 5-minute free laptop usage. The yaw angle of the head orientation is represented by the x-coordinates of the direction of the head pose projected onto a 2D plane. The range of values for yaw is 0 to 720. The horizontal gray dotted line at the center of the plane represents the direction of looking straight ahead on the screen.

The demographic factors, including sex, age, and height, did not show any significant influence or relations to the performance of the current sensor (Figure 5.7). Wilcoxon rank sum test, a nonparametric method, did not find any significant difference ($p > 0.05$) between the two sexes, as well as the correlation tests of the height and age with the correlation coefficients of the sensor ($p > 0.05$, respectively).

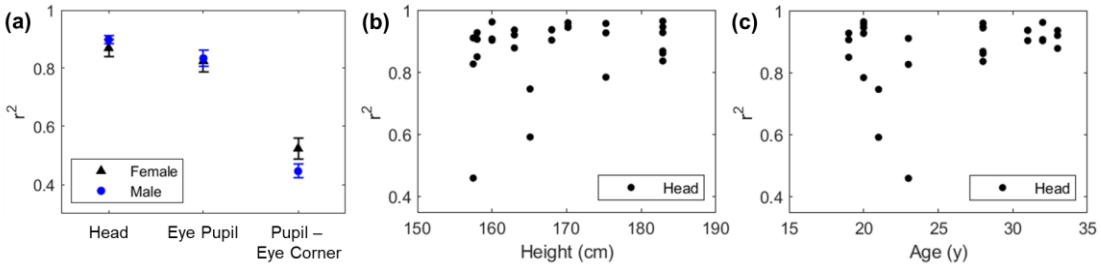

Figure 5.7 Correlation coefficient between the sensor and the ground truth by (a) sex, (b) height, and (c) age of the participants.

The current glasses-type sensor contained two pairs of RFID tags to reduce the vulnerability of RSSI of the passive tags against the multipath effect, as well as to explore the application of the same rotation sensing capability to measure head rotation in the pitch direction. This is particularly relevant for children with ASD who tend to look downwards [10]. However, as previously shown in Figure 5.4, the distance between the vertically arranged RFID tags was only 25 mm (Figure 5.8a),

which turned out to be too small to create a noticeable difference in the distance from the reader caused by head pitch rotation. Although the experiment detected a significant RSSI difference (Figure 5.8b), the experiments could not confirm that it originated from head motions due to the low correlation between the RSSI readings and the random and continuous head rotation ($r^2 = 0.35$). Moreover, the correlation between the sensor readings and the head movements during free laptop usage was even lower ($r^2 = 0.24$).

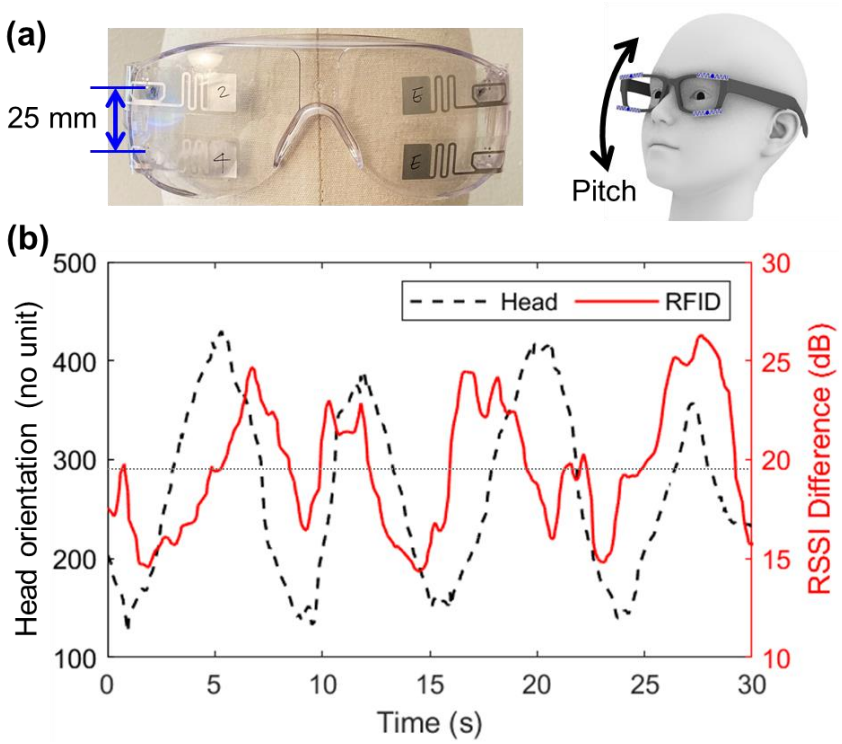

Figure 5.8 Pitch rotation measurement. (a) The prototype with vertically arranged tags and head rotation in pitch. (b) Head movements in pitch and the RSSI difference between the vertically arranged tags. The pitch angle of the head orientation is represented by the y-coordinates of the direction of the head pose projected onto a 2D plane. The range of values for pitch is 0 to 480. The horizontal gray dotted line at the center of the plane represents the direction of looking straight ahead on the screen.

5.4 Discussion and Conclusion

This study introduced a battery-free wearable head orientation sensor for detection of the lateral glance behavior of children with ASD by using passive RFID tags. The higher sensing capability of the system at a distance of 50 cm from the reader (Figure 5.3) implies that it is best suited for tablet or laptop usage rather than for smartphones or televisions. Though the current study installed PET film-based tags to eyeglasses, textile tags may be an alternative option when implementing the system into other types of accessories such as a headpiece, or cap, thanks to their advantages in wearability and maintenance. Devices covering the larger area of the face, such as mask or VR headset, may be able to provide enough distance for pitch direction sensing, which was not successful with the vertically arranged tags in the current prototype (Figure 5.4 and 5.8). Head circumference of the children with ASD also should be carefully considered for the final product design, as their head size tends to be smaller than the adults but bigger than the typically developing children [54].

The other populations with needs to monitor their above-neck mobility, such as those with neck disk or in rehabilitation, will be able to benefit from the current sensor to optimize the treatments. Sleeping mask will be another application by providing the evaluations of sleeping quality based on head pose and movements [55]. Head rotation measurement capability of the current sensor can be part of entertainment systems for VR or AR experiences, to enhance the user interaction with physical environments. For example, cardboard 3D glasses can maximize the battery-free motion sensing capability of the current system for enhanced interactions. As one RFID reader can detect limitless tags within a detectable range, it will be possible to provide such experience to multiple users looking at the same direction (e.g., museum, theater, and/or classroom) [25].

The rotation sensing capability without a battery can be adopted to not only wearable devices but also other applications related to human-computer interaction. For

example, an interactive screen with an RFID reader can respond to a product with a pair of RFID tags when the customer rotates or shakes the product in retail stores. This may allow the screen to track the orientation of the product and display it on the screen like a magic mirror, without using a camera. In an educational setting, RFID tag-embedded toys or materials can create interactive and immersive learning experiences with an RFID reader-embedded table or display. Additionally, RFID technology has been researched for indoor localization of robot agents, and the current method can help identify the direction in which the agent is heading, improving overall agent localization [56].

The primary objective of this paper was to develop an application for children with ASD. However, due to the challenges in conducting controlled research experiments with this vulnerable population, the current study recruited a small sample of healthy adults to validate the concept. While the results showed equivalent sensor performance across demographic factors, further investigation is required to assess feasibility in the target population of younger children with smaller body/head size. The dependence of the RF signal strength on the surrounding environment remains a significant challenge for achieving stable sensitivity of the passive RFID tag sensors. The study assumed a short distance between the reader and tag to eliminate weak signals coming through multi-paths and to exclude interference from obstacles, other RFID tags, or metal. However, the presence of these factors can significantly impact sensor functionality. Furthermore, currently available portable devices such as smartphones or laptops only have an RFID reader functioning at a lower frequency (HF, NFC). For larger detection distances and the potential of UHF RF waves, RFID readers operating at UHF are promising to be embedded in future devices.

REFERENCES

[1] R. A. Coulter, Optometry and Vision Development 2009, 40, 164.

[2] L. Mottron, S. Mineau, G. Martel, C. S.-C. Bernier, C. Berthiaume, M. Dawson, M. Lemay, S. Palardy, T. Charman, J. Faubert, Develop. Psychopathol. 2007, 19, DOI 10.1017/S0954579407070022.

[3] T. Nakano, K. Tanaka, Y. Endo, Y. Yamane, T. Yamamoto, Y. Nakano, H. Ohta, N. Kato, S. Kitazawa, Proceedings of the Royal Society B: Biological Sciences 2010, 277, 2935.

[4] E. Milne, A. Scope, H. Griffiths, C. Codina, D. Buckley, J Autism Dev Disord 2013, 43, 1976.

[5] H.-P. Frey, S. Molholm, E. C. Lalor, N. N. Russo, J. J. Foxe, European Journal of Neuroscience 2013, 38, 2125.

[6] K. M. Hustyi, A. H. Ryan, S. S. Hall, Research in Autism Spectrum Disorders 2023, 100, 102074.

[7] A. Hellendoorn, I. Langstraat, L. Wijnroks, J. K. Buitelaar, E. van Daalen, P. P. M. Leseman, Research in Developmental Disabilities 2014, 35, 423.

[8] D. C. Strickland, C. D. Coles, L. B. Southern, J Autism Dev Disord 2013, 43, 2472.

[9] C. Sung, A. Connor, J. Chen, C.-C. Lin, H.-J. Kuo, J. Chun, Autism 2019, 23, 1542.

[10] B. Noris, J. Nadel, M. Barker, N. Hadjikhani, A. Billard, PLoS ONE 2012, 7, e44144.

[11] D. Fabiano, S. Canavan, H. Agazzi, S. Hinduja, D. Goldgof, Pattern Recognition Letters 2020, 135, 204.

[12] E. M. Benssassi, J.-C. Gomez, L. E. Boyd, G. R. Hayes, J. Ye, IEEE Pervasive Comput. 2018, 17, 11.

[13] Z. Chang, J. M. Di Martino, R. Aiello, J. Baker, K. Carpenter, S. Compton, N. Davis, B. Eichner, S. Espinosa, J. Flowers, L. Franz, A. Harris, J. Howard, S. Perochon, E. M. Perrin, P. R. Krishnappa Babu, M. Spanos, C. Sullivan, B. K. Walter, S. H. Kollins, G. Dawson, G. Sapiro, JAMA Pediatrics 2021, 175, 827.

[14] J. Daniels, N. Haber, C. Voss, J. Schwartz, S. Tamura, A. Fazel, A. Kline, P. Washington, J. Phillips, T. Winograd, C. Feinstein, D. P. Wall, Appl Clin Inform 2018, 09, 129.
[15] E. Pettersson, B. M. Christensen, I. G. Berglund, K. Huus, Child: Care, Health and Development n.d., n/a, DOI 10.1111/cch.13119.
[16] Tobii, "Tobii: Global leader in eye tracking for over 20 years," can be found under https://www.tobii.com/, 2023.
[17] K. W. Bowyer, IEEE Technology and Society Magazine 2004, 23, 9.
[18] O. N. Tepencelik, W. Wei, L. Chukoskie, P. C. Cosman, S. Dey, in 2021 29th European Signal Processing Conference (EUSIPCO), 2021, pp. 766–770.
[19] S. Hutt, A. E. B. Stewart, J. Gregg, S. Mattingly, S. K. D'Mello, Proc. ACM Hum.-Comput. Interact. 2022, 6, 1.
[20] R. D. Findling, T. Quddus, S. Sigg, in Proceedings of the 17th International Conference on Advances in Mobile Computing & Multimedia, ACM, Munich Germany, 2019, pp. 107–116.
[21] E. Bizzi, Scientific American 1974, 231, 100.
[22] S. R. H. Langton, The Quarterly Journal of Experimental Psychology Section A 2000, 53, 825.
[23] L. Sidenmark, H. Gellersen, in Proceedings of the 32nd Annual ACM Symposium on User Interface Software and Technology, ACM, New Orleans LA USA, 2019, pp. 1161–1174.
[24] S. J. Lee, J. Jo, H. G. Jung, K. R. Park, J. Kim, IEEE Transactions on Intelligent Transportation Systems 2011, 12, 254.
[25] B. Jiang, W. Xu, C. Guo, W. Liu, W. Cheng, in Proceedings of the ACM Turing Celebration Conference - China, ACM, Chengdu China, 2019, pp. 1–6.
[26] J. Blattgerste, P. Renner, T. Pfeiffer, in Proceedings of the Workshop on Communication by Gaze Interaction, ACM, Warsaw Poland, 2018, pp. 1–9.
[27] P. Renner, T. Pfeiffer, in 2017 IEEE International Symposium on Mixed and Augmented Reality (ISMAR-Adjunct), 2017, pp. 176–181.
[28] O. Špakov, H. Istance, K.-J. Räihä, T. Viitanen, H. Siirtola, in Proceedings of the

11th ACM Symposium on Eye Tracking Research & Applications, ACM, Denver Colorado, 2019, pp. 1–9.
[29] Y. Tamaru, Y. Ozaki, Y. Okafuji, J. Nakanishi, Y. Yoshikawa, J. Baba, in 2022 17th ACM/IEEE International Conference on Human-Robot Interaction (HRI), IEEE, Sapporo, Japan, 2022, pp. 1064–1068.
[30] B. Zhang, Y.-H. Chen, C. Tuna, A. Dave, Y. Li, E. Lee, B. Hartmann, in Proceedings of the 2nd ACM Symposium on Spatial User Interaction, ACM, Honolulu Hawaii USA, 2014, pp. 17–25.
[31] Y. Zhao, L. Görne, I.-M. Yuen, D. Cao, M. Sullman, D. Auger, C. Lv, H. Wang, R. Matthias, L. Skrypchuk, A. Mouzakitis, Sensors 2017, 17, 2692.
[32] K. Takahashi, H. Kadone, K. Suzuki, in Proceedings of the 2nd Augmented Human International Conference on - AH '11, ACM Press, Tokyo, Japan, 2011, pp. 1–4.
[33] M. R. Williams, R. F. Kirsch, J Rehabil Res Dev 2016, 53, 519.
[34] M. A. Velasco, A. Clemotte, R. Raya, R. Ceres, E. Rocon, International Journal of Human-Computer Studies 2017, 106, 1.
[35] Z. Mihajlovic, S. Popovic, K. Brkic, K. Cosic, Multimed Tools Appl 2018, 77, 19113.
[36] Y. Yamanobe, M. Fujioka, M. Ohashi, H. Ozawa, J Med Syst 2022, 46, 80.
[37] M. R. Ali, T. Sen, Q. Li, R. Langevin, T. Myers, E. R. Dorsey, S. Sharma, E. Hoque, ACM Trans. Comput. Healthcare 2021, 2, 1.
[38] J. E. Flanagan, R. Landa, A. Bhat, M. Bauman, The American Journal of Occupational Therapy 2012, 66, 577.
[39] S. Saavedra, M. Woollacott, P. van Donkelaar, Exp Brain Res 2010, 201, 13.
[40] R. Raya, E. Rocon, R. Ceres, J. Harlaar, J. Geytenbeek, in 2011 IEEE International Conference on Rehabilitation Robotics, 2011, pp. 1–6.
[41] R. Kamoshida, K. Takemura, in Adjunct Proceedings of the 31st Annual ACM Symposium on User Interface Software and Technology, ACM, Berlin Germany, 2018, pp. 39–41.
[42] M. R. Williams, R. F. Kirsch, IEEE Transactions on Neural Systems and

Rehabilitation Engineering 2008, 16, 485.
[43] I.-C. Severin, in 2020 International Conference on E-Health and Bioengineering (EHB), 2020, pp. 1–4.
[44] I. Salinas-Bueno, M. F. Roig-Maimó, P. Martínez-Bueso, K. San-Sebastián-Fernández, J. Varona, R. Mas-Sansó, Sensors 2021, 21, 2237.
[45] Z. Zhang, E. C. Kan, in 2022 IEEE Sensors, 2022, pp. 1–4.
[46] A. Kiourti, IEEE Antennas and Propagation Magazine 2018, 60, 14.
[47] C. Luo, I. Gil, R. Fernández-García, Materials 2020, 13, 3292.
[48] Z. Meng, Z. Li, Measurement Science Review 2016, 16, 305.
[49] B. Nath, F. Reynolds, R. Want, IEEE Pervasive Comput. 2006, 5, 22.
[50] S. Manzari, C. Occhiuzzi, G. Marrocco, IEEE Antennas and Propagation Magazine 2012, 54, 49.
[51] M. Bolic, D. Simplot-Ryl, I. Stojmenovic, 2010.
[52] "MediaPipe," can be found under https://developers.google.com/mediapipe, n.d.
[53] "GitHub - amitt1236/Gaze_estimation: Gaze tracking," can be found under https://github.com/amitt1236/Gaze_estimation, n.d.
[54] R. Sacco, S. Gabriele, A. M. Persico, Psychiatry Research: Neuroimaging 2015, 234, 239.
[55] P. Sharma, E. C. Kan, in 2018 IEEE/MTT-S International Microwave Symposium - IMS, 2018, pp. 1419–1422.
[56] Z. Zhang, G. Xu, E. C. Kan, IEEE Journal of Radio Frequency Identification 2023, 7, 12.

CHAPTER 6

CONCLUSION

6.1 Summary

This dissertation provides an overview of textile-based wearable sensors and proposes three advances in on-body soft sensors monitoring bio-signals and human motions. Stretchable fiber optic and passive RFID tag performed as the key technologies with sensing capabilities as well as outperforming advantages over the existing wearable electronics. The sensors demonstrated the monitoring of respiration, gait, and head orientation respectively. The summary of the principal findings are as follows:

Chapter 2. Textile interface for wearable sensors

i. Fibers, yarns, and textiles as wearable sensors measure mechanical, electrical, electromagnetic, chemical changes around the body, while the other textile structures accommodate the sensors and supporting components.
ii. Textile-based sensors should endure moisture and laundry while securing electric connections and preventing burn injuries.

Chapter 3. Machine embroidery enclosure for stretchable fiber optic respiration sensor

i. Zigzag-based embroidery provided a stretchable enclosure allowing the optical fiber transitions between a serpentine and a straight shape by strain.

ii. The embroidery parameters, enclosure shape, density, and tension adjusted by the water-soluble stabilizers influenced the strain sensing capability.

iii. The system functioned after 100,000 abrasions and 10 machine washes.

Chapter 4. Stretchable fiber optic embedded gait monitoring sensor

i. The light transmissibility of the stretchable fiber optic array embedded within flexible foam responded to the local foot pressures.

ii. The sensor performed differently by fiber diameter, foam compressibility and foam thickness.

iii. The human participant tests confirmed that the system predicted the plantar pressure and center of force satisfactorily.

Chapter 5. Battery-free head orientation measurement using passive RFID tags for lateral glance detection for children with autism spectrum disorder

i. The RSSI difference within a pair of passive RFID tags attached on eyeglasses correlated to the head orientation of the wearer.

ii. The sensor performance depended on the type of RFID tag, the distance between the tag, and the distance from the RFID reader.

iii. The system performed better during the continuous head rotations, compared to the free laptop usage.

6.2 Challenges

The wearable sensors explored in the present dissertation are soft, flexible, washable,

and/or stretchable, yet still need conventional rigid components on/near the body. Each stretchable fiber optic requires to be connected to small hardware (i.e., light source, photodetector, microcontroller, etc.) with wires, like the passive RFID tags needs an RFID reader for the wireless communications. Furthermore, the signal strength through both sensors became weak when they are far from the light/microwave source. Therefore, to maintain the advantages of the sensor systems introduced in this dissertation, miniatured light sources/photodetectors, stretchable wirings, strategic distribution of the electronics, as well as RF-abundant environments are essential [1–3].

Securing a stable connection between the sensors and the signal sources was often challenging. Multipath effect is a widely known limitation in the RSSI-based approaches in RFID sensors, a stable connection can be achieved by complex signal processing techniques or a fixed and close distance from the reader, which is hard to expect in wearable applications [4,5]. Furthermore, the human body, a conductor, often blocks the electromagnetic waves for the passive tags, so strategic placement of the RF source in the room to secure the wireless connection remains as a task[6]. In the case of fiber optics, maintaining a mechanical contact between the cross section of the thin polyurethane fiber and small LEDs and photodiodes was tricky and often became the source of significant noises [7]. The fiber optic systems introduced in this dissertation used heat-shrink tubing as a connector to the light source/detector, but tubing made of polyolefin may not be ideal because it does not preserve the light as cladding and is not suitable for surface-mounted smaller components [8]. Permanently bonding the fiber optic onto the electronics can reduce the noise but will generate discomfort to the wearer, as well as the issues in durability and electric connections when the system goes through maintenance such as washing.

Lastly, the current sensor applications are capable of detecting patterns of biometric

data (e.g., breathing in and out) but rely on calibration to provide accurate absolute values to the users. The sensors used ground truth values acquired by commercial sensors to convert the raw readings to meaningful bio-signals. It means, at the beginning of the product use and also time to time, the user needs to have access to another sensor to calibrate the sensor. Furthermore, some of the applications in this dissertation showed a satisfactory result only with supervised deep learning techniques (e.g., respiration monitoring during running), so initial collection of datasets using both the current sensors and any reliable commercial sensor is almost unavoidable[9]. One of the best scenarios for user convenience will be to use their smartphones for calibration [10,11]. The sensors embedded in smartphones such as camera, microphone, and/or accelerometers and apps based on machine intelligence may be able to help collect the initial datasets as well as time-to-time calibrations.

6.3 Opportunities

The sensing capabilities of the current sensors in this dissertation – stain, pressure, and rotation – can be applied to other wearable/non-wearable applications to monitor such as joint movement, posture, robot/animal mobility, built structure stability, and/or human-computer interactions. The topics to make further advances beyond the current technologies through the future works may include local strain sensing, three-dimensional rotation sensing, and 3D printing of the sensors. The current strain sensor arranged the embroidery enclosure all at a place on the center of the front bodice and aimed to measure the circumference changes. However, the enclosure rooms accommodating the fiber can be distributed throughout the body surface to cover multiple locations of interest with one fiber optic. The signal will change when a strain occurs at any of the locations, though identifying the location of strain will need another technique such as color [12]. It may contribute to the convenience in hardware

design and user comfort, because if one fiber can cover multiple areas, the location and the size of the hardware for light source/detector can be optimized accordingly. The paired passive RFID tags were capable of tracking the rotation changes in the current dissertation, especially in yaw (leftward/rightward). Though the sensor could not monitor pitch rotations (upward/downward) satisfactorily, it would be promising if another wearable application (e.g., face shield) could achieve a longer distance between the two tags. However, monitoring of the roll rotation on the frontal plane (tilting toward the shoulders) is a different issue, as the distance of each tag from the reader will not change in the current setting even if the head tilts where the RFID reader is right in front of the user. Another RFID reader on the ceiling or the side of the user will be able to detect the changes following the roll movements of the head. Also, an RFID reader located in a diagonal direction will be able to detect the distance changes following all three-dimensional rotations, while the RSSI difference would be subtle.

For the fabrication of the insole device, arranging the fiber optics in the middle of the mole for the casting of flexible foam was challenging, because the foam fluid movement sometimes affected the fiber arrangement. 3D printing of a thermoplastic polymer to fabricate stretchable optical waveguides has been explored, which may allow more accurate, controlled, and unmanned fabrications [13]. 3D printing of an insole is not common for mass manufacturing but can meet the needs of customization of orthotic insoles, where tracking the plantar pressure distribution and gait patterns is necessary [14]. Not only for the insoles, but also for the other applications introduced in this dissertation can involve the additive manufacturing techniques. RFID tags are being mass-produced using fully automated printing/embroidery facilities and 3D printing has shown the fabrication capability of stretchable tags [15], so incorporating them with the garment or accessory manufacturing will make the process faster and

efficient. 3D printing will be useful to create a soft fiber optic that has a serpentine or in a more complex shape in resting without enclosures, which may contribute to more convenient control of the fiber movement by strains [16].

REFERENCES

[1] K. Huang, Md. T. Islam Molla, K. Roberts, P.-S. Ku, A. Galada, C. H.-L. Kao, Delocalizing Strain in Interconnected Joints of On-Skin Interfaces, 2021.

[2] J. Lee, B. Llerena Zambrano, J. Woo, K. Yoon, T. Lee, Advanced Materials 2020, 32, 1902532.

[3] B. Wang, A. Facchetti, Advanced Materials 2019, 31, 1901408.

[4] C.-C. Pu, W.-Y. Chung, IEEE Sensors Journal 2008, 8, 1884.

[5] J. Wisanmongkol, L. Klinkusoom, T. Sanpechuda, L. Kovavisaruch, K. Kaemarungsi, in 2019 19th International Symposium on Communications and Information Technologies (ISCIT), 2019, pp. 47–51.

[6] U. T. Virk, K. Haneda, IEEE Transactions on Antennas and Propagation 2020, 68, 2256.

[7] T. Li, Y. Su, F. Chen, H. Zheng, W. Meng, Z. Liu, Q. Ai, Q. Liu, Y. Tan, Z. Zhou, ACS Appl. Mater. Interfaces 2022, 14, 22666.

[8] "FEP Heat Shrink Tubing Technical Information | Nordson MEDICAL," can be found under https://www.nordsonmedical.com/Components-and-Technologies/Heat-Shrink-Tubing/FEP-Heat-Shrink-Tubing/Technical-Information/, n.d.

[9] Y. Feng, X. Chen, Q. Wu, G. Cao, D. McCoul, B. Huang, J. Zhao, IEEE Sensors Journal 2021, 21, 20943.

[10] H. Aly, M. Youssef, in IEEE INFOCOM 2016 - The 35th Annual IEEE International Conference on Computer Communications, 2016, pp. 1–9.

[11] Y. Nam, B. A. Reyes, K. H. Chon, IEEE Journal of Biomedical and Health Informatics 2016, 20, 1493.

[12] H. Bai, S. Li, J. Barreiros, Y. Tu, C. R. Pollock, R. F. Shepherd, Science 2020, 370, 848.

[13] E. Nseowo Udofia, W. Zhou, Additive Manufacturing 2020, 31, 100912.

[14] R. Xu, Z. Wang, Z. Ren, T. Ma, Z. Jia, S. Fang, H. Jin, Med Sci Monit 2019, 25, 3510.

[15] M. Rizwan, M. w. a. Khan, H. He, J. Virkki, L. Sydänheimo, L. Ukkonen, Electronics Letters 2017, 53, 1054.

[16] Y. Zhu, T. Tang, S. Zhao, D. Joralmon, Z. Poit, B. Ahire, S. Keshav, A. R. Raje, J. Blair, Z. Zhang, X. Li, Additive Manufacturing 2022, 52, 10